UNIVERSITY OF CALIFORNIA, MERCED

Advancements in Varnish Removal Chemical Flush Testing

By: Monica Ferrera

A thesis submitted in partial satisfaction of the requirements of the degree of

Master of Science in Mechanical Engineering

Committee in charge:

Professor Ashlie Martini, Chair (Advisor)
Po-YaAbel Chuang
Mehmet Z. Baykara

The Thesis of Monica Ferrera is approved:

_____

Ashlie Martini, Adviser Date

_____

Po-Ya Abel Chuang Date

_____

Mehmet Z. Baykara Date

University of California, Merced

Table of Contents

Table of Figures/Tables

1 Background and Motivation

2 Test Methods

3 Testing Anomaly Investigation

4 Varnish Removal of Commercial Cleaners

5 New Test Cell Modifications

ACKNOWLEDGMENTS

I owe an immense thank you and likely my career to Professor Ashlie Martini for affording me amazing opportunities in both my undergraduate and graduate experience and for having faith in me to accomplish everything thus far. To the engineering faculty of University of California, Merced for giving me the tools and confidence to work on complex engineering problems. To my family for providing the support and inspiration before I even knew I needed it. I would like to dedicate this thesis to my grandfather and his lifelong passion for the partnership between engineering and the human experience.

ABSTRACT

Lubricants in mechanical systems are currently being designed to have greater efficiency and longer run time between maintenances. In lubricated systems involving high heat processes and tight tolerances, one impediment to this goal is oil degradation which leads to the accumulation of a thin, hydrocarbon-based film, known as varnish. Varnish can have adverse effects on a system ranging from loss of efficiency to total shutdown and replacement of costly key parts. There are several ways to address varnish and its precursors within a system, but, in the event of severe accumulation, the method typically used is a high flow rate chemical flush. Although many chemical cleaners exist in the commercial market today, there is no standardized method of directly comparing the removal abilities of these fluids. In this study, we used our lab's existing varnish removal test rig, which allows *in situ* imaging of the varnish removal process. The rig pairs real-time imaging with a post processing algorithm to measure varnish removal. Both quantitative and qualitative methods were used to evaluate not only the effectiveness of the cleaner fluids at removing the varnish layer, but also the mechanism by which each fluid removes varnish. The rig was used here to evaluate a set of 13 commercial cleaners. A wide range of removal capabilities was observed from the fluids included in the study, from barely any removal to nearly complete removal after 8 hours of testing. In the process of the research, we improved the testing methodology and approach for analysis of varnish removal. In addition, we designed a new test cell to accommodate more realistic test objects. This study demonstrates the importance of comprehensive characterization when selecting the appropriate chemical cleaner for a given system plagued by varnish accumulation.

Chapter 1: Background and Motivation

1.1 Lubricants

Lubricants play a key role in the operation of mechanical systems, keeping moving parts separated, as a coolant at surface contact points to remove heat generated by friction, cleaning surfaces within systems, acting as a vehicle for essential additives, and assisting with maintaining efficiency during power transfer mechanisms such as hydraulics, transmissions, and breaks. Lubricants operate under the principals associated with the Stribeck curve shown in Figure 1.1.

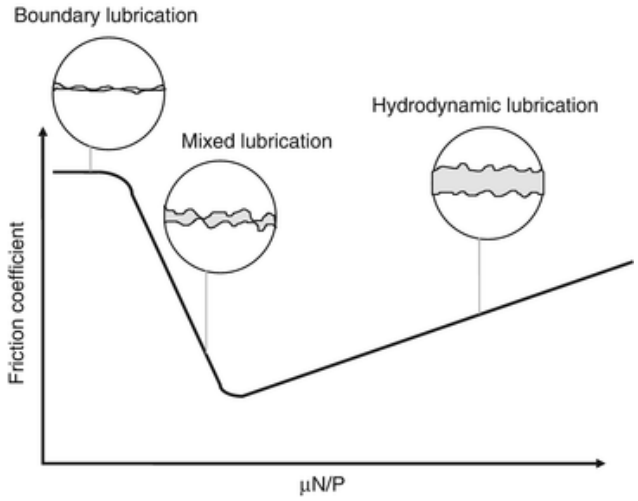

Figure 1.1: The Stribeck Curve & associated lubrication regimes is used to evaluate friction coefficient vs. a fluid property ratio. [1]

The Stribeck curve defines the lubrication regimes in terms of operating conditions using the Hershey Number.[2] The Hershey Number, refers to the ratio of viscosity (η) and rotational speed (N) to average pressure (P).[3] The various lubrication regimes are defined based on how much the two surfaces in contact are separated by the. Boundary lubrication is characterized as the point at which two substrates are close to full contact. This regime may have a very thin lubrication film and is characterized by many microscopic asperities in contact that impede the

movement of the two surfaces. In mixed lubrication, surface roughness is extremely important and is highly correlated to friction properties and sliding speed. In the hydrodynamic regime, surfaces are separated by lubricant and are therefore able to slide over each other with ease.

The Stribeck curve is a lubricant engineer's tool to evaluate which lubrication regime their fluid will fall under and therefore how much friction will be exhibited in lubricated contact given these parameters.[4] Lubricants comprise base oils and additives (molecular components that can be added to a lubricant to modify various oil properties). Changing the composition of base oils and additives can have a large impact on the effects of lubricating fluids.[5]

1.1.1 Base Oils

Lubricant base oil chemistries are directly correlated to the performance of the lubricant produced.[6] Base oils are placed in different categories based on chemical composition. Many base oils are hydrocarbons. Hydrocarbons are molecular structures that are exclusively made from Hydrogen and Carbon atoms. Ester oils are structures that contain Hydrogen, Carbon, and Oxygen as base atoms and can be derived from phosphoric acid esters. Polyglycols, on the other hand, are structures containing Hydrogen, Carbon, and Oxygen like Ester Oils, but have a different binding state than Esters, which tend to be weak organic acids.[5] Base oils are classified into five main groups and three additional subgroups that further the identification criteria of groups I, II, and III. One of the major criteria that separates base oil groups is Viscosity Index (VI), a unit-less measure of a fluid's change in viscosity with temperature. The lower the VI, the more temperature changes will affect viscosity.

Group I base oils consist of lubricants made from saturated hydrocarbons without alkenes, or hydrocarbon double bonds (>90%) and sulfur content amounting to > 0.3% with a VI

between 80 and 120. Group I+ is one of the previously identified subgroups which has the same properties listed in Group I, but a VI range of 103-108 instead. The Group II base oils comprise hydrogenated (saturated) hydrocarbons and the same sulfur content and viscosity range as Group I, but Group I oils are more prone to reactions yielding polar molecules and insoluble residue. Group II oils instead yield oxygenated products at the expense of saturate performance during degradation.[6] Group II+ base oils have a VI range of 113-119 and is manufactured by hydrocracking, solvent extraction, or catalytic dewaxing giving them a clearer/water-like appearance. Groups III, IV, and V are classified as synthesized hydrocarbons (SHC).[4] Group III oils have a saturation of $> 90\%$, a sulfur content of 0.03%, and a VI of > 120. They are produced by catalytic procedure with simultaneous rearrangement of the carbon skeleton during hydrogenation. Group III+ base oils are produced with a VI > 140. Group IV and V base oils do not have subcategories like the first 3 oils mentioned. Group IV oils are made using a base of Poly-α-Olefins (PAO). Because PAO based oils do not contain ring structures, alkenes, sulfur, nitrogen, or "waxy" hydrocarbons, they make for a highly non-polar solution with a high VI and good low-temperature flow and oxidation stability, which is important for preventing the accumulation of sludge and varnish.[7] Lastly, Group V contains all oils that do not fall into the categories above.[8]

VI, as described above, partially determines the use of these various lubricants. Figure 1.2 shows the importance of selecting the correct lubricant viscosity for a given operating temperature. Low molecular weight fluids start at a VI of ~ 2 to 15, which is water-like consistency and can be used for pneumatic spraying such as those utilized in machining. Oils with higher viscosities (~100+) are typically utilized as lubricants.

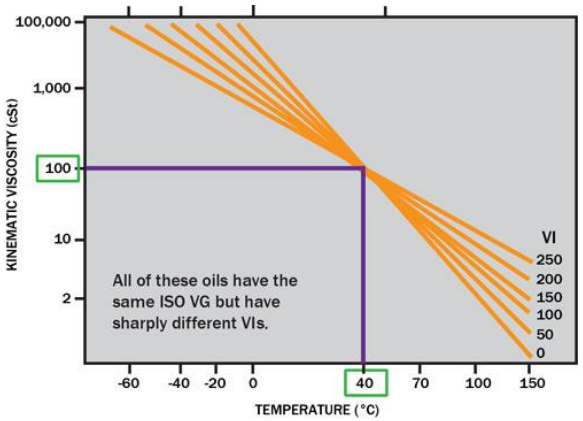

Figure 1.2: Oil viscosity vs. temperature plot for low and high viscosity base oils [9]

1.1.2 Additives

In a typical lubricant blend, base oil makes up only about 70-95% of the oil blend. The remainder of this volume is comprised of various oil additive components that are designed to modify the effects of oils under the range of operating conditions within different systems.[10] Different lubricant properties are required for different functions such as metalworking, which requires fluid that can easily remove cutting debris while also cooling the tool. Bearing lubricants, on the other hand, have cooling and cleaning as secondary functions rather than their primary function, to reduce friction. Given that base oils must be adaptable to changing conditions within complex systems, additives are included in a lubricant blend where they are carried by the base oil vehicle to provide sufficient lubrication within the contact.[11]

Although many additives are used to perform various functions, we will be differentiating components here by primary roles; viscosity index improvers, oxidation inhibitors, rust & corrosion inhibitors, detergents and dispersants, and antiwear additives.[12] These particular additives were selected because they target system characteristics that lead can lead to various types of lubricant degradation, such as oil viscosity increase, oxidation & conglomeration of

oxidative byproducts and wear of the metal components, all of which can contribute to varnish formation.

1.1.2.1 Viscosity Modifiers

As discussed previously, viscosity is an extremely important characteristic of a lubricant, especially due to its effect on film thickness.[14] Viscosity modifiers, also known as viscosity index improvers, are used to keep the viscosity of a given lubricant around the ideal lubrication regime, even during times of temperature fluctuation. Their quality is typically assessed by thickening efficiency, viscosity-temperature relationship, and shear stability.[15] Viscosity modifiers can be high weight polymers or, more recently, ionic liquids.[16][17] Figure 1.3 depicts how polymer additives affect lubricant viscosity.

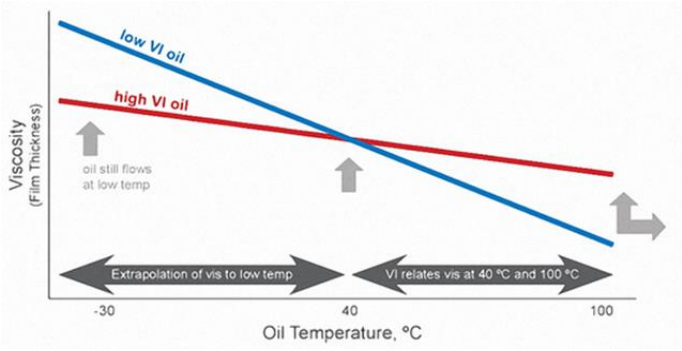

Figure 1.3: Graph of oil temperature vs. lubricant viscosity given differing amounts of viscosity modifying additives. [18]

Polymers are conventionally used in commercial additives and much research has been put into their performance, which mostly depends on their molecular chemistry and structure. [19] Although viscosity modifiers are designed to improve oil performance, they have both detrimental and beneficial qualities, depending on operating conditions and desired effect. An example of detrimental effect caused by VM is system clogging due to the conglomeration of additive molecules which can drastically lower efficiency. [20]

1.1.2.2 Rust & Corrosion Inhibitors

Rust and corrosion inhibitors provide corrosion protection for metals.[21] Corrosion, in this case refers to deposits of harmful contaminants, such as water, in a lubricated contact.[22] Many corrosion inhibitors are targeted towards the precursors of rust and corrosion.[23] The main mechanisms of corrosion prevention in industry are one or more of three methods of molecular surface protection. First, chemisorption, depicted in Figure 1.4, is a chemical reaction between the surface metal and the additive which can then repel contaminants that would otherwise bond with the surface. Second, additives initiate the formation of a thin film designed to prevent oxidation of the base metal. Lastly, the inhibitor chemically interacts with a corrosion precursor found in the lubricant.[24]

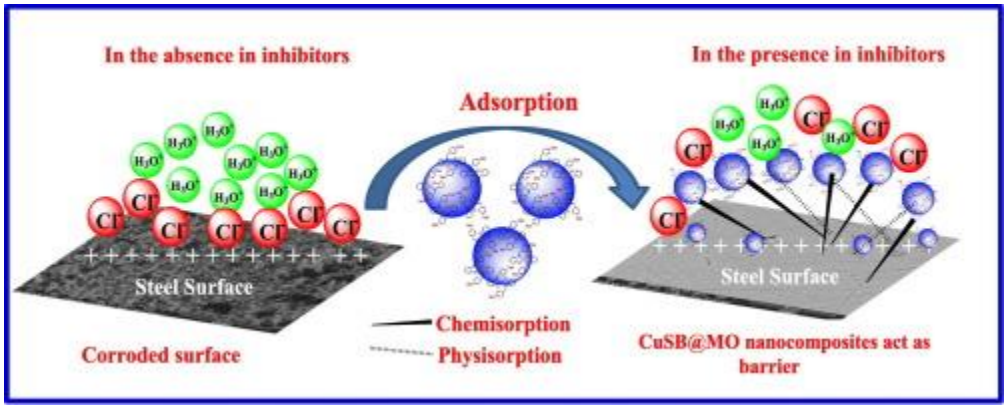

Figure 1.4: Illustration of chemisorption of a corroded surface vs. adsorbed barrier method of surface protection. [25]

Corrosion changes the friction properties of a surface and can impact overall efficiency as well as component lifetime and therefore is of great importance to lubricated systems.[26] Although rust and corrosion inhibitors both perform similar functions, there is one main difference between them. Corrosion inhibitors are typically anodic or cathodic to target specific environments, whereas rust inhibitors affect iron substrates and are typically film-forming or

"mixed" inhibitors that reduce both anodic and cathodic reactions such as phosphorus and silicon-based molecules.

1.1.2.3 Detergents & Dispersants

Detergents and dispersants target contaminants in oil blends to prevent the formation of larger agglomerations or adherence to the surface. They help to minimize friction by minimizing wear within tight tolerances and thereby extending the useful life of oils and machine maintenance costs.[27] Figure 1.5 shows how dispersants can impact oil within a system, providing space between contaminant particles that may have otherwise created congestion.

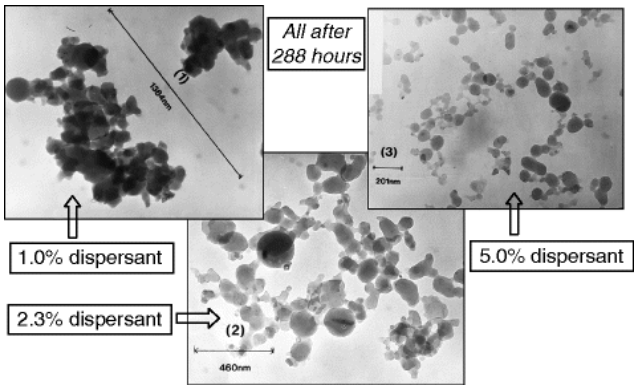

Figure 1.5: Dispersant additives and their impact on contaminants within oils. [28]*Figure* 1.5: Dispersant additives and their impact on contaminants within oils. [28]

Dispersants are able to perform this function because their heads are designed to attach themselves to the contaminant particle while their tails provide spacing, thereby repelling other contaminant particles from glomming onto it.[29] Detergents remove contaminants that fall out of solution from the metal surfaces.[30] Figure 1.6 depicts dispersant and detergent additives being used to preserve mechanical performance on a molecular level. Together detergents and dispersants mitigate effects of contaminants and improve lubrication performance and are

usually made of substances that are chemically basic, to neutralize the acidic contaminants within the system.[31]

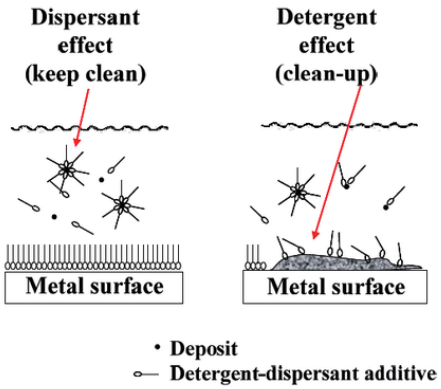

Figure 1.6: How dispersants & detergents work together to preserve mechanical performance on a molecular level. [32]

1.1.2.4 Oxidation Inhibitors

Oxidation inhibitors, or antioxidants prevent the oxidation of oil species which form products which can condense and form polymeric materials. Polymeric materials lead to the formation of sludge and then, as viscosity increases, varnish films. [33] Oxidation inhibitors are additives that are sacrificed to the byproducts of lubricant oxidation in order to delay oxidation of oil blends, thus protecting the base oil. [34]

1.1.2.5 Antiwear & Extreme Pressure Additives

Antiwear additives are used to prevent wear by forming a protective barrier on contacting surfaces. The most common types of antiwear additives are those containing phosphorus.[35] However, just like antioxidants, these additives are used up as they prevent wear and some cause surface corrosion themselves. Wear particles also contribute to varnish and sludge accumulation while some metals can also catalyze oxidation reactions within the system.

Extreme pressure additives are vital to protecting equipment from wear and enabling it to operate under large loads. While in the hydrodynamic lubrication regime, friction is low and allows for easy movement in contacts, but under high pressure, the system can enter boundary lubrication which increases friction and wear.[36] The most common types of additives in this category are those containing sulfur and/ or chlorine. [37] These molecules bond with the surface under high temperature conditions and create an anti-wear layer on the metal surface. [38] In absence of this film, severe wear and friction increase can occur. [39]

1.2 Oil Degradation

There are several types of oil degradation and different methods of measuring the severity of this degradation. Here degradation is grouped into three categories: water contamination, particle contamination, and oxidation.[40]

Water contamination refers to water content within a lubricating oil that exceeds the amount that the oil can tolerate given its base oil properties and additives. This form of contamination affects oil viscosity and may shorten the oil lifetime, performance, and damage machinery gradually with continued use.[41]

Particle contamination is a major source of failure and wear within mechanical systems as well, which affects oil viscosity, expected oil temperature under various conditions, and lubricity measures such as friction properties.[42] Depending on the type of particle, contaminants can increase contact area within small tolerances, have adverse chemical reactions with the lubricating oil and metal surface, and create clogging in small channels thereby decreasing system performance and lifetime. Common types of particle contaminants are minerals and dust, metal wear particles, and soot/products of combustion.[43]

Lastly, lubricant oxidation is a process by which components within a lubricant combine with oxygen to form compounds. Oxidation usually results in discoloration of the lubricating fluid. At high oxygen concentrations, compounds can combine to form polymers that become sludge and varnish. [44]. The flow chart is shown in Figure 1.7 illustrates oil degradation metrics.

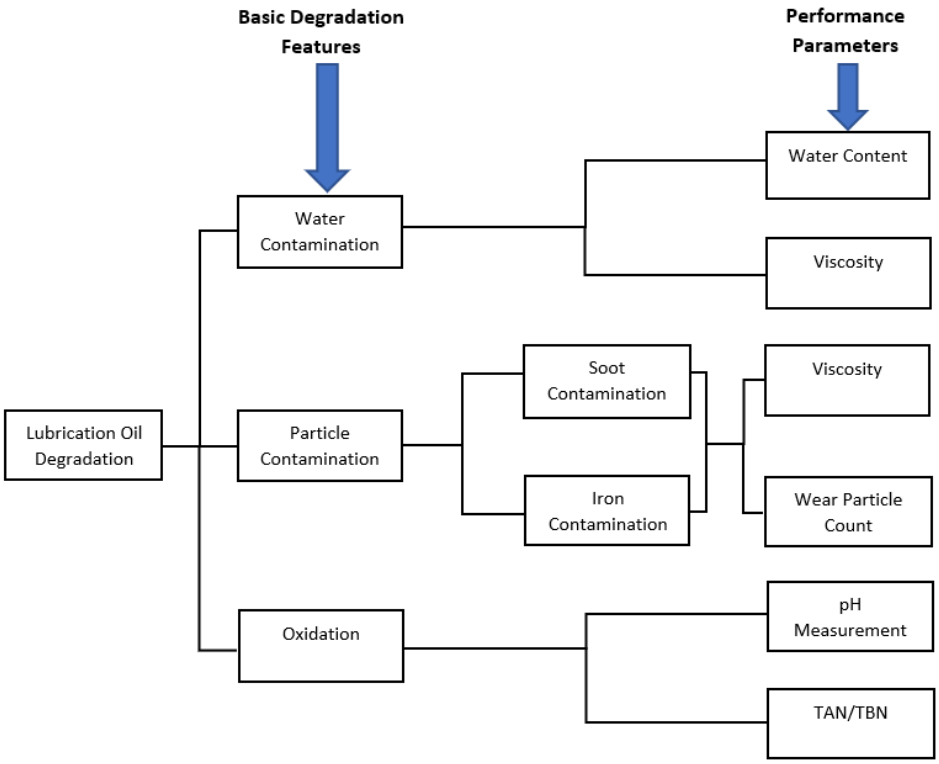

Figure 1.7: Lubrication oil degradation and detection flow chart. [45]

Oil degradation is a natural process that occurs in all lubricants over time. This process cannot be stopped, but additives, sensor monitoring, and careful use can improve an oil's useful lifetime.[46]

1.3. Varnish

1.3.1 Formation

Varnish is a detrimental combination of oxidative byproducts of lubricants and metallic wear particles created by high heat processes such as combustion in mechanical systems.[47] The main oxidative portion of varnish is formed by the breakdown of hydrocarbon chains during high temperature reactions that are common to many parts of mechanical systems.[48] As varnish accumulates within a system, it has a tendency to adhere to metal components, forming a polymeric film. This polymer layer has brown, yellow or red coloring depending on the percent composition of the various component elements, the base lubricant it is formed from, and the film thickness.[49]

The main focus of our discussion is on varnish accumulation in mechanical systems. The locations within a system where varnish is likely to accumulate and greatly affect performance often have tolerances of five to ten thousandths of an inch.[50] Any obstruction of these tolerances by varnish films can diminish efficiency since the thicknesses of varnish layers tend to be larger than the tolerances of the gaps in which they accumulate. So, these films can be detrimental to system performance.[51] Negative impacts from varnish accumulation can range from minor maintenance and efficiency losses, if oil is maintained properly and the system is run under normal operating conditions, to multi-million-dollar failures of major capital equipment.[52] The varnish formation process, depicted in Figure 1.8, begins with the oxidative

degradation of a lubricant combined with water contamination and catalyzed by metal particles.

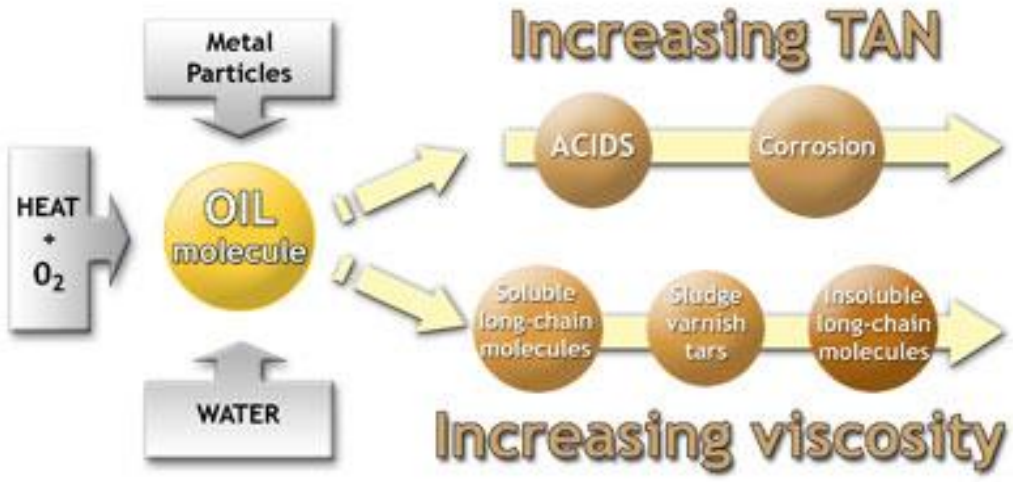

Figure 1.8: The varnish formation process is shown here with inputs, precursors, and outputs. [53]

This reaction leads to two things, increasing viscosity and increasing Total Acid Number, or TAN. TAN refers to an oil's acidity, which is caused by organic acidic components in solution such as naphthenic acids and phenols. Increasing acidity leads to corrosion/fouling within the system, which is detrimental to the lifetime of mechanical components.[54]

The second consequence of oil oxidation is the conversion of soluble, long-chain carbon-based molecules to layers comprised of insoluble long-chain of increasingly long, carbon-based monomers, otherwise known as varnish. This process occurs through a chemical process of carbon chain propagation in a heated environment and is catalyzed by metal wear particles in solution.[55] Precursors to varnish formation are esters, ketones, peroxides, alcohols and previously mentioned acids these polar, oxidized compounds are formed from free radicals, species with an unpaired electron which are highly reactive.[56] After formation, these chains adhere to metal substrates within a system and to each other, forming varnish layers.

1.3.2 Removal

There are several methods of varnish removal in practice today. Some methods aim to filter out loose pieces of varnish film and its precursors while still suspended in solution, and some aim to remove varnish deposits after they have been formed.[57]

Electrostatic absorption can be used to drag the polar molecules that contribute to varnish formation out of solution. This occurs as a subsidiary loop from the main track of the flow of lubricant and reduces the concentration of varnish and varnish precursors thus reducing overall varnish deposits within a given mechanical system. To remove these polar molecules, oil is passed through a filter with the opposing charge of the particles targeted for removal. This draws varnish particles toward the filter and allows the capture of these particles which can then be removed with the filter.[58]

Chemical cleaners and flushes remove varnish by replacing the primary lubricant in the system with a chemical flushing fluid that targets varnish deposits. These types of fluids are designed to remove the varnish from the metal to which it is adhered. Varnish can then be filtered out of the system using a downstream filter.[59] Chemical cleaners are typically a last resort for severe accumulation because they require machinery to be taken offline for the duration of the chemical flushing process. However, chemical flushing boosts the efficiency of the system, protects from rust & varnish build-up and increases the lifespan of mechanical systems. Our research is targeted towards improving varnish removing chemical cleaners and evaluating their removal characteristics.

1.4 Varnish Removal Test Rig

Our test rig was designed to provide a controlled environment for the testing of various varnish removal fluids. The environmental control in this case includes continuous flow through

the testing portion of the cell and temperature control throughout the rig with only slight variations from the target temperature. The current test rig is designed to test artificial varnish adhered to steel coupons formulated to mimic gas turbine engine varnish. The fluid reservoir for the test apparatus was built to minimize excess fluid but maintain a ratio of varnish to chemical cleaner as would be seen in flushing conditions. Figure 1.9 shows the test rig that was used throughout this study.

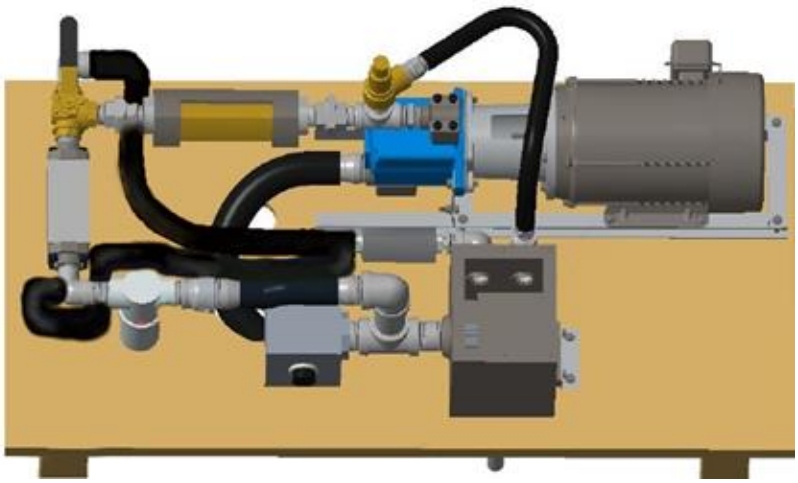

Figure 1.9 A model of the varnish removal test rig used in this study is shown above.

Figure 1.10 shows a test coupon and the dimensions of the adhered varnish as well as how the coupons are stored to prevent contamination and oxidation. Artificial varnish is adhered to the coupons, provided by an offsite lab, using a method called coking involving heating the oil and repeatedly splashing it against the steel surface used for the coupon.[60] These varnish coupons were tested in conditions that mimic the environment that this type of varnish would encounter in a gas turbine engine.

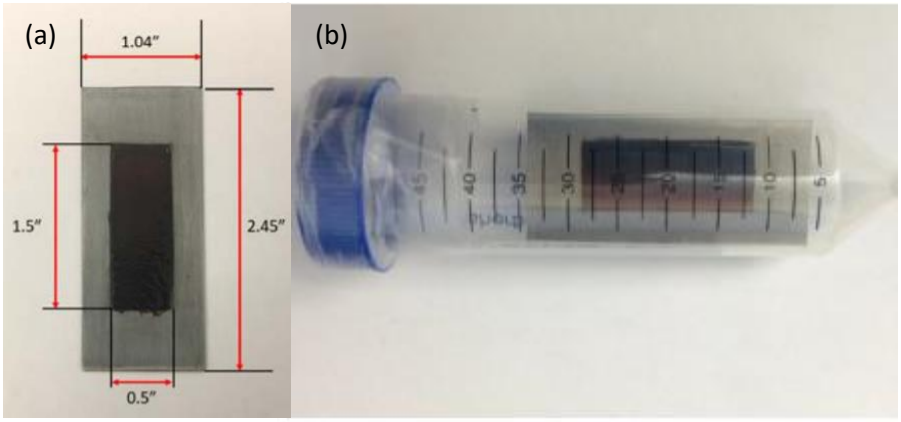

Figure 1.10: (a) Varnish covered test coupon and dimensioning. (b) Varnish coupon sealed within the test tube during storage.

1.5 Contents

This thesis research focused on characterization of varnish removal by chemical cleaners. To analyze results, we use a combination of physical results obtained by comparing varnish coupons before and after testing, and statistical results generated by our visual analysis software. Our visual analysis software imports the images taken from the system during testing and converts them to red-green-blue values that can then be evaluated to quantify the removal during testing. Modifications were made to an existing test rig and analysis code during this project. Notably, the test rig was improved to accommodate other types of test objects other than a flat coupon in order to give a more realistic picture of chemical cleaner performance in a real engineering system. Improvements were also made to the testing procedure as well as the visual analysis software to improve the accuracy of testing to ensure consistency of results. Chapter 2 contains a description of the test methods as well as improvements to the test procedure and the visual analysis code used in post-test analysis. Chapter 3 describes an investigation of testing anomalies found over the course of the lifetime of the test rig. Chapter 4 reports the main outcomes of this research based on a detailed comparison of the varnish removal characteristics

of 13 commercially available chemical cleaners. Chapter 5 describes design of a new test cell that will enable varnish removal to be measured on real mechanical components. Lastly, Chapter 6 contains a summary of the research and suggestions for future work on this topic.

Chapter 2: Test Methods

2.1 Testing Procedure

This section contains a description of our testing procedure, including the safety equipment, apparatus nomenclature, testing and flushing procedure, and visual analysis process. The test procedure and analyses method subsections emphasize improvements and modifications that have been made in this research.

2.1.1 Safety Equipment

Given the high testing temperature and dangers of various fluids being both skin and lung irritants some safety equipment is required when operating the varnish removal rig.

- Nitrile Gloves – used when handling anything that has come into contact with the varnish removal fluid
- Slip Resistant Insulted Thermal Gloves – used when handling filter housing and taking coupon in and out of the rig or when handling any heated portion of the rig
- Safety Goggles/ Glasses – used when handling oil or turning on or off the rig
- Filtering face mask – a mask that has filtering capability is required for tests where the fluid is listed as a lung irritant on the SDS sheet
- Flame /Oil Resistant Lab Coat –used at all times during testing

In addition, appropriate clothing is always be worn in laboratory setting, including closed-toe shoes and long pants that cover any exposed skin

2.1.2 Apparatus Nomenclature

The test rig is a system of pressurized piping and high-pressure valves where oil flow is driven by an external pump towards the coupon housing, allowing oil to flow over a test coupon. The flow then proceeds toward a downstream filter seated in the filter housing and then back to the reservoir. Images of the various components of the test rig are shown in Figure 2.1.

Figure 2.1: Relevant test rig nomenclature that will be used in this study.

A schematic of the test system is shown in Figure 2.2. (a) The primary test loop is marked in blue, the path through the high precision flow meter is marked in yellow and completes the loop by bypassing the test cell. The reservoir loop is in green. Power to the electronics is started by turning on the breaker. The electronic components include a battery powered flow meter and a heating element to keep the fluid at temperature. The GoPro camera and a set of three lamps for consistent lighting are on independent power supplies shown in Figure 2.2 (b).

(a)

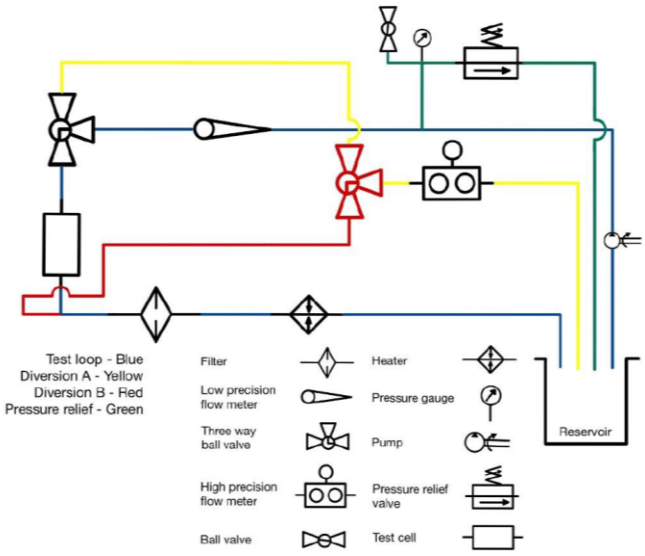

(b)

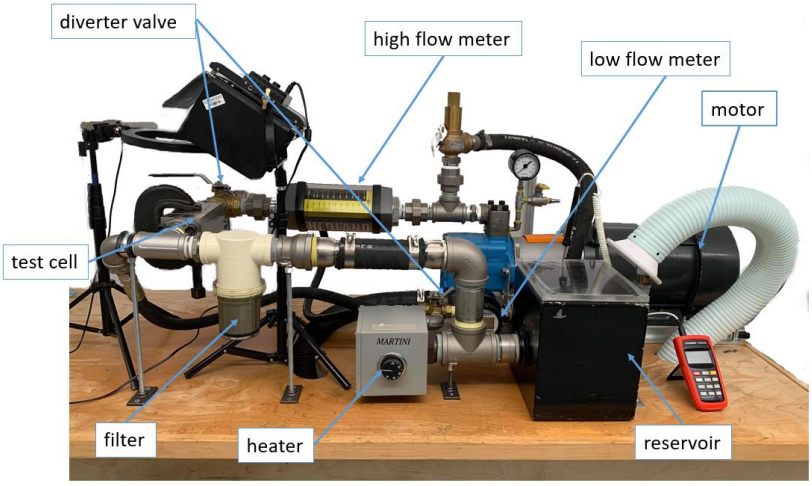

Figure 2.2: (a) A schematic of the test rig flow paths and (b) Image of the full test rig with labeling.

There are several valves in the system that enable switching between various flow paths through different section of the test rig. These valves are used to run the test in four different orientations:

A. Valve 1: open, Valve 2: open. Note: This orientation flows through the sensitive flow meter so DO NOT push a large amount of air through.
B. Valve 1: closed, Valve 2: open.
C. Valve 1: open, Valve 2: closed. Note: This orientation flows through the sensitive flow meter so DO NOT push a large amount of air through.
D. Valve 1: closed, Valve 2: closed.

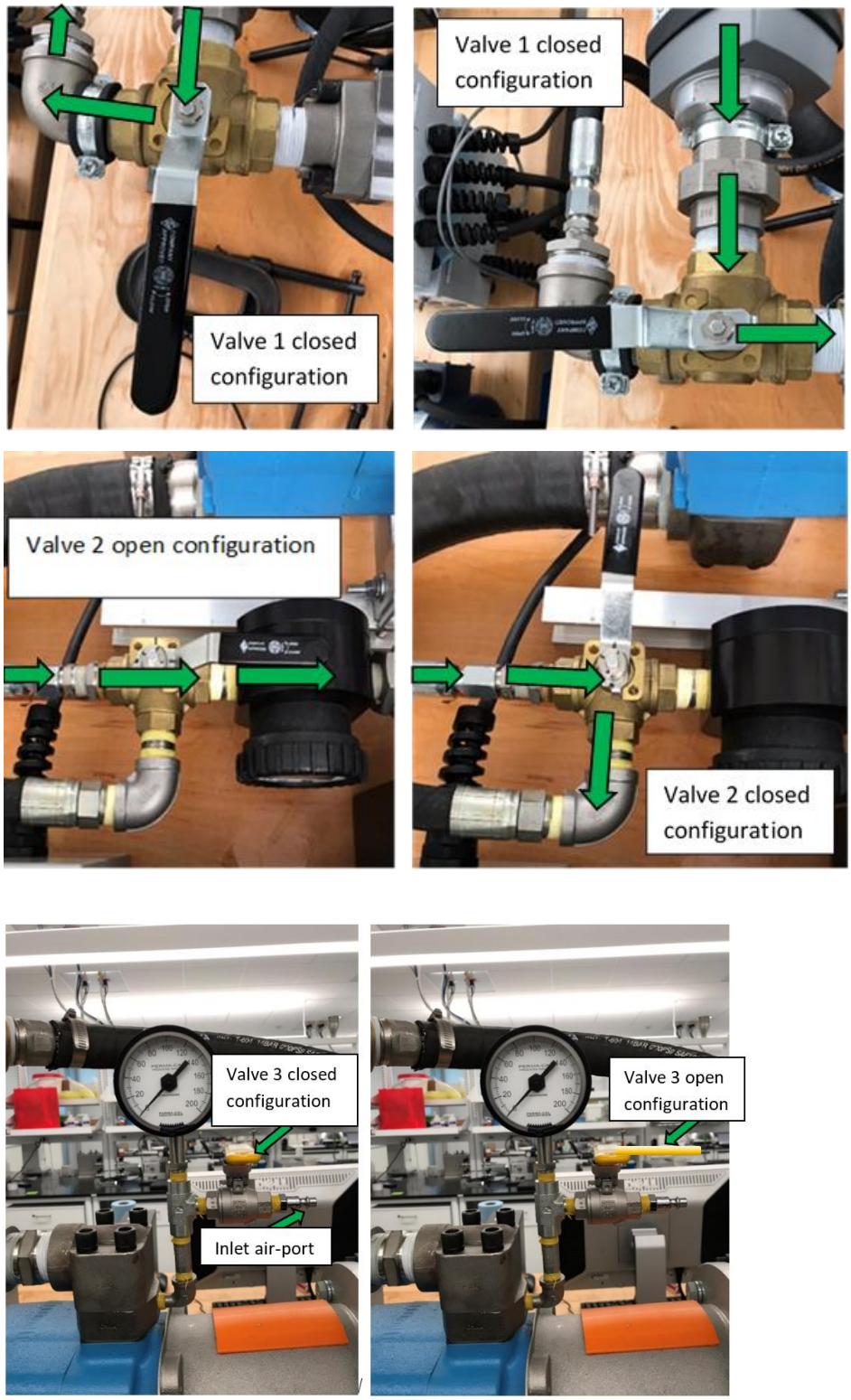

Figure 2.3: Relevant flow control valve orientations for the test rig.

2.1.3 Preparation: Filter Cutting

The process of preparing a filter for testing begins with obtaining a single sheet of clean, uncut filter from a package of new filter paper. Then, use the template provided in the bag as a size reference and place the template in the upper right corner of the clean filter. Use a permanent marker to trace the outline of the reference filter onto the clean filter sheet on the smoother side of the filter. Make as many outlines with the stencil as can be made on the clean filter, depending on filter sheet size. Either two or six test filters can be made from the standard sizes kept in the lab inventory. Once the outlines on the filter are finished, place the clean filter with the outlines on a cutting surface and weigh down the edges to prevent movement of the paper. Then, cut the outlines of the clean filter using a sharp blade to make each individual test filter. Place the spare test filters in a clean, oil-resistant bag and store for later use.

2.1.4 Pre-Test Procedure

Remove the polycarbonate lid on the reservoir. Fill reservoir with test oil slowly to allow the oil to distribute throughout the system. After ensuring the oil is distributed, the oil level should be just above the manifold in the reservoir. Replace reservoir lid and put valves in previously described orientation C. Turn on the breaker for the test rig. When ready, start the flow, press the green “GO” button on the controller switch. Turn on heater and set to testing temperature by turning the dial clockwise. Change the flow direction to orientation D. Turn on the thermometer by pressing the red power button and place the probe of the thermocouple through the small hole in the reservoir lid. Fill a beaker with approximately 100mL of testing oil and place it in front of a white background. Take a photo of the pre-test oil. An example of a pre-test fluid image is shown above in Figure 2.3.

Figure 2.3: An example of a beaker image of 1000 mL of testing fluid is pictured.

Obtain a clean pre-cut test filter. Write the coupon number, the fluid identification number, test number, flow rate, and the testing temperature on the rough side of the filter, being sure not to obscure the main part of the filter, as seen in Figure 2.4. The writing has been whited out for the confidentiality of our collaborators. Take a picture of the clean filter with the written values. An example of a clean, cut test filter.

Figure 2.4: Example image of a test filter before it has entered the system.

Remove a fresh test coupon from the batch. Turn on the analytical balance and tare. Take the coupon out of the packaging and place the coupon on the balance. Record the weight of the coupon. An image of the fresh coupon should be taken. Make sure to minimize glare from the light. An example of a good image, absent of glare, is shown in Figure 2.5.

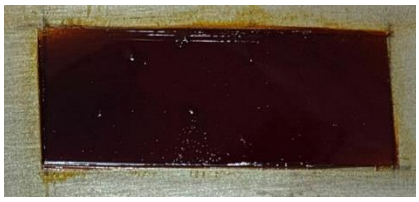

Figure 2.5: Example image of a new test coupon right after it has been removed from the packaging and weighed.

Turn off flow by pressing “STOP” on motor controller when the rig is heated to ~10 degrees below the testing temperature. Remove the clamp from coupon housing and remove the metal lid to expose the inside of the test cell. Remove the blank coupon from the housing and replace with the test coupon with the coupon number etched into the back of coupon facing the flow outlet.

Take the polycarbonate test lid shown in Figure 2.6 and secure it to the test cell by placing two thin metal strips on the outer area of the test lid such that half of the plank material is on the metal part of the test cell and half is on the clear test lid. The metal strips are designed to distribute the clamp load across the edges of the test cell to ensure proper seal and not cause the polycarbonate lid to crack. Place a clamp on each plank and tighten. A good fit is such that the clamps cannot be turned using finger strength and be sure not to over-tighten.

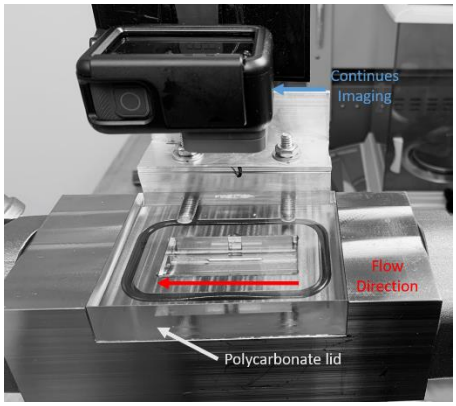

Figure 2.6: Shows a polycarbonate, optical quality test cell lid.

Put on the thermal protective gloves and flip the filter housing into the up position shown in Figure 2.1. Once the fluid has drained back into the system, unscrew the top and set aside. Roll test filter into a cylinder with the portion that has been written on facing inward. To secure the filter, use pliers and guide the bottom of the test filter towards the black ring located in the bottom of the filter housing to create a good seal and ensure the filter captures all varnish particles that are pushed downstream of the coupon. Replace the top of the filter housing and flip the housing back down.

Start the flow again. Mount the GoPro on the test cell and plug in the GoPro charger. Make sure GoPro is set to the "Time lapse" setting for every 10s. Turn on the lamps for even image lighting. Set locked exposure on GoPro by holding down a section of the touchscreen and dragging the locked exposure box to a portion of the screen where the image lighting is not expected to change unless the overall lighting in the frame changes.

Put the flow in orientation B. The oil should just be flowing through the flow meter. Now slowly open valve 1 to flow oil through the coupon housing. Keep opening valve 1 until the oil flow through test cell reaches 0.25 GPM and bubbles emerge in the oil stream. Keep oil flowing through the coupon housing until there are no visible bubbles in the stream. Close valve 1. Once oil has reached the operating temperature range, the test may be started.

2.1.5 Test Procedure

When ready to start testing, open valve 1 slowly until test flow rate is reached on the meter. Press the record button on top of the GoPro to start taking images. Set the thermocouple to record max/min temp as well as the real time temperature to ensure it stays within the testing range. Close valve 1 once the test duration has been reached. The time can be calculated from the number of images on GoPro. For example, a 4-hour test calculation is seen below:

$$4 \quad hours \; x \; 60 \frac{minutes}{hour} = 240 \; minutes \; x \; 6 \frac{images}{minute} = 1440 \; images \; on \; gopro \quad [1]$$

Once the test is finished, press the record button again to stop GoPro imaging. Record the maximum and minimum temperatures. Turn off the heater and flow

2.1.6 Post-Test Procedure

The whole system will be hot, so handle the rig carefully with thermal gloves. Remove the GoPro from the mount above the test cell and take off the clamps. Pull the SD card from the GoPro and turn off the camera. Remove the polycarbonate test lid. Once the test lid has been removed, get the pliers and remove the varnish test coupon and replace it with the blank steel coupon. Place the coupon on a clean white background and take an image. An example of a post-test coupon image is shown in Figure 2.7.

Figure 2.7: Image of a post-test coupon with oil still on the coupon.

Place the metal test cell lid back on the coupon housing and tighten with a clamp. Flip the filter housing upside down and unscrew the top. Take the pliers and remove the filter by pinching top of filter and pulling gently and the filter will slide out. Replace the top of the filter housing. Place the filter on a clean towel with the writing facing up. Weigh the corners of the filter down without obscuring the filter. Take an image of the varnish covered filter. An example is shown in Figure 2.8.

Figure 2.8: An example of a post-test filter that has captured varnish particles.

Use the beaker previously used for the clean fluid and place it under the test rig drain. Open the spigot and allow approximately 1000 mL to flow into the beaker. Place the beaker under the same lighting as the initial image with white background. Wait until the fluid in the beaker cools before taking a picture of the fluid.

During this time, the microscopy portion of the testing can be done. Images must be taken of both the filter and the coupon. In this case, we used a Nikon Microscope Eclipse Ci-L, with paired Leica Acquire software, but any light microscope capable of measuring 10x and 20x magnification will work for our purposes as long as the imaging is consistent throughout the comparison.

Turn the microscope on using the switch on the power box next to the microscope. Turn the associated computer on and open the microscope software. Place the post-test varnish coupon under microscope on top of a white background. Attempt to capture the level of varnish removal and properties by recording the part of the coupon where the varnish has been removed. Record coupon images at 10x and 20x magnification. An example of a post-test coupon image is shown in Figure 2.9.

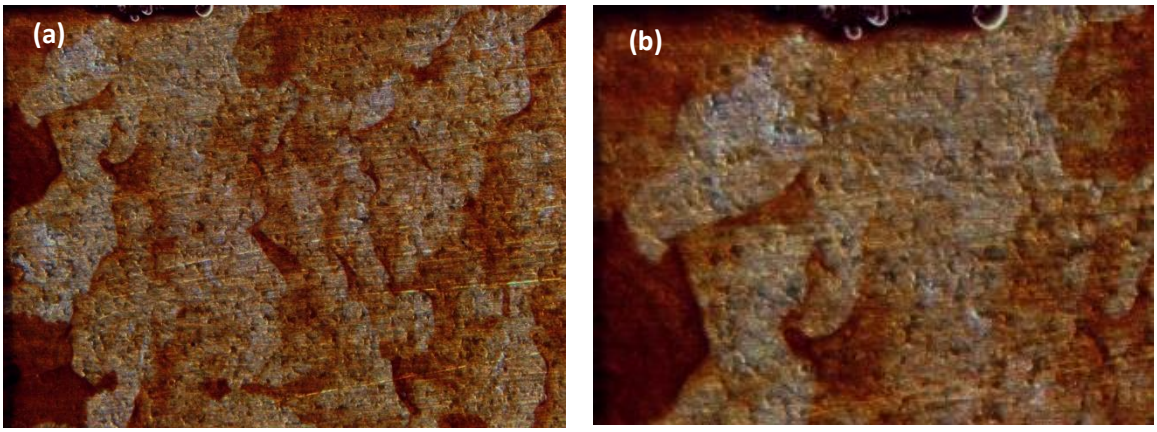

Figure 2.9: Two examples of (a) 10x and (b) 20x images are shown and were taken with an optical microscope.

Remove the coupon from the microscope. Then put a new clean background down on the microscope for the next sample. Now place the filter underneath microscope on the white background. Capture a filter image at 10x and 20x magnification. An example is shown in Figure 2.10.

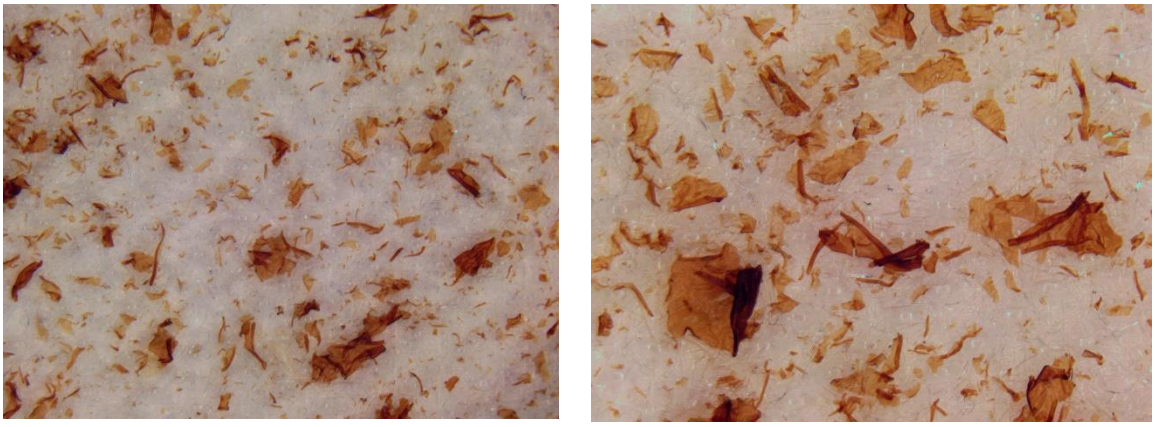

Figure 2.10: Examples of (a) 10x and (b) 20x images taken with an optical microscope.

Once all the pictures have been taken go to the "File" menu and click "Save As". Create a new folder for each test as a save location and select. Save all six pictures with naming convention: TestNumber_Filter or Coupon_Magnificationx.png

Wrap the filter in a fresh towel and write the test number on the outside of the towel. Place the filter in storage for future reference if needed. Fill a glass jar with~50 mL of heptane. Use the

pliers to rinse off the excess oil from the coupon into the jar of heptane. Swirl slowly and carefully to ensure that no varnish is removed. Firmly grip the coupon and remove it from the jar of heptane.

Use the air hose to dry the coupon gently on the lowest air flow setting. Once all oil and heptane has been removed from the coupon, place in the analytical balance. Record the weight of the coupon. Take the coupon out of the analytical balance and place on white background and take a post-heptane image. An example is shown in figure 2.11. The test is now complete.

Figure 2.11: An example of a post-test coupon after heptane has been applied to remove the excess oil.

2.1.7 Flushing

The system is flushed after each test. Unscrew the cap on the righthand size of the reservoir to allow air flow. Position the vacuum hose to cover the reservoir outlet created in order to capture all escaping fumes. The vacuum hose, reservoir and lid are shown in Figure 2.12.

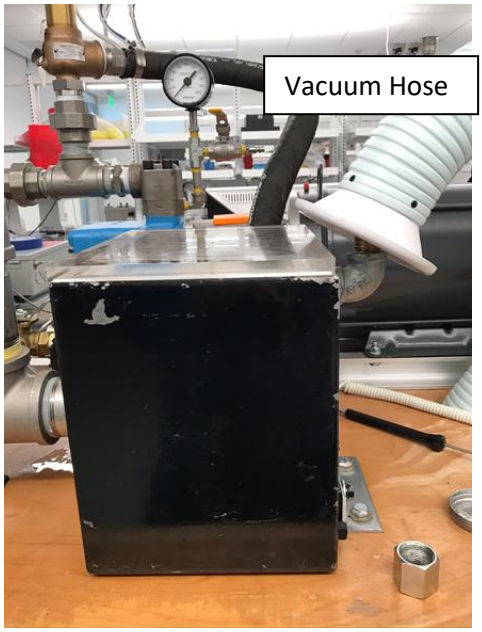

Figure 2.12: Image of the reservoir assembly with lid, cap, and vacuum hose.

Under the table there is a control box for the vacuum hose with a red on/off switch. Turn the vacuum hose on. Prepare an empty waste drum capable of housing approximately 4 gallons of oil. Place the drum underneath the drain spigot. Once the drum is beneath the table, open the spigot and allow oil to drain from the system for 5 minutes. Take the air hose and attach to the inlet air port on valve 3. Flip the filter housing up and allow the fluid to drain. Flow air through the system in each of the above configurations for 5 minutes each. Close the drain spigot. Now that the system has minimal amounts of testing fluid, remove the top of the reservoir and pour in the provided cleaning fluid. Fill to slightly above the metal manifold inside the reservoir. Put the resevoir lid back on.

Change flow to orientation B and turn on the breaker. Turn on flow by pressing the green “GO” button on the controller switch. Allow the cleaning fluid to flow in this configuration for 5 minutes. Let oil flow through each configuration above for 5 minutes each. Place the cleaning oil drum underneath the drain spigot and open the spigot to allow the fluid to leave the system. Once

the oil has reached an inch above the bottom of the reservoir, stop the flow by pressing the red "stop" button on motor controller. Turn off the breaker. Attach the air hose to the inlet air-port on valve 3. Flip the filter housing upside down and allow the fluid to drain. Flow air through the system in each of the above configurations for 5 minutes each. Close the drain spigot. Now the system is ready for the next test.

2.2 Visual Analysis

Images are taken by utilizing a GoPro mounted above the test rig. An imaging window is created in the test cell by use of an optical quality polycarbonate test lid that allows for a clear view of the coupon varnish from above. A time lapse images are taken at intervals of 10 seconds during the testing. These images need to be analyzed to quantify varnish removal.

2.2.1 Previously Established Varnish Removal Analysis Software

The previous varnish removal code used a normalizing method based on the darkness of the test coupon. Specifically, the amount of varnish was quantified using a CMKY color scale. As depicted in Figure 2.13 the CMYK color model refers to the four ink colors originally used in color printing and how they combine to form others. Here, C is Cyan, M is Magenta, and Y is Yellow, which all combine to form K, or Key. The K value was used to track varnish removal, assuming that varnish values can be correlated directly to darkness values through this color evaluation process seen in Figure 2.13.

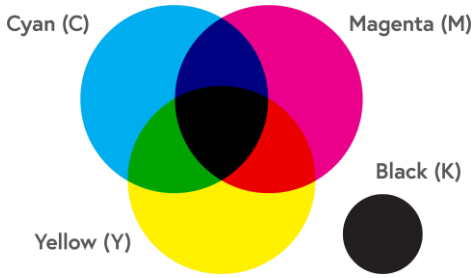

Figure 2.13: The CMKY color diagram which can be used to describe computerized color reading.[70]

Because the artificial varnish used in testing is a dark brown polymer and is semi-translucent, the steel coupon on which the varnish is deposited is revealed more and more as the varnish is removed throughout testing. The varnish removal code compensates for this by allowing the user to take crop of an area of the coupon where the varnish is located and of steel without varnish on the coupon. The program then averages the K (darkness) values over the steel and varnish crop regions and assigns them a K value of color intensity between 1 and 255. The K values are then divided by 255 to give an average percentage value. The first steel crop and the first varnish crop are saved as 100% for full removal (steel) and 0% for no removal (initial varnish color). This process is done for each image for the entire test and then K values are the plotted against time producing a varnish removal graph. These values are then used to compare different varnish removal conditions and removal efficiency. The issue with this method is that since we are using CMYK but only the K value we are not only considering intensity of combined color and not allowing for the program to account for the average values of each color in the spectrum.

2.2.2 New Varnish Removal Analysis Software

Two improvements were made to the analysis software. First, the image cropping process was improved. Second, the normalization algorithm was made more robust.

The varnish visual analysis code, located in appendix A.1, crops by first selecting “Run” on the Matlab program, which brings up an interactive window with the whole first image taken during the given test. The user is then prompted to select a smaller crop to get a closer image seen in Figure 2.14 (a). The older code automatically cropped the image to a pre-established place and size given precedent, but it was realized that if the camera was not perfectly aligned the user would have to exit the program and manually adjust crop values within the code. The new crop selected by the user, shown in Figure 2.14 (b), are then analyzed by use of a red-green-blue (RGB) code package within Matlab Figure 2.14 (c).

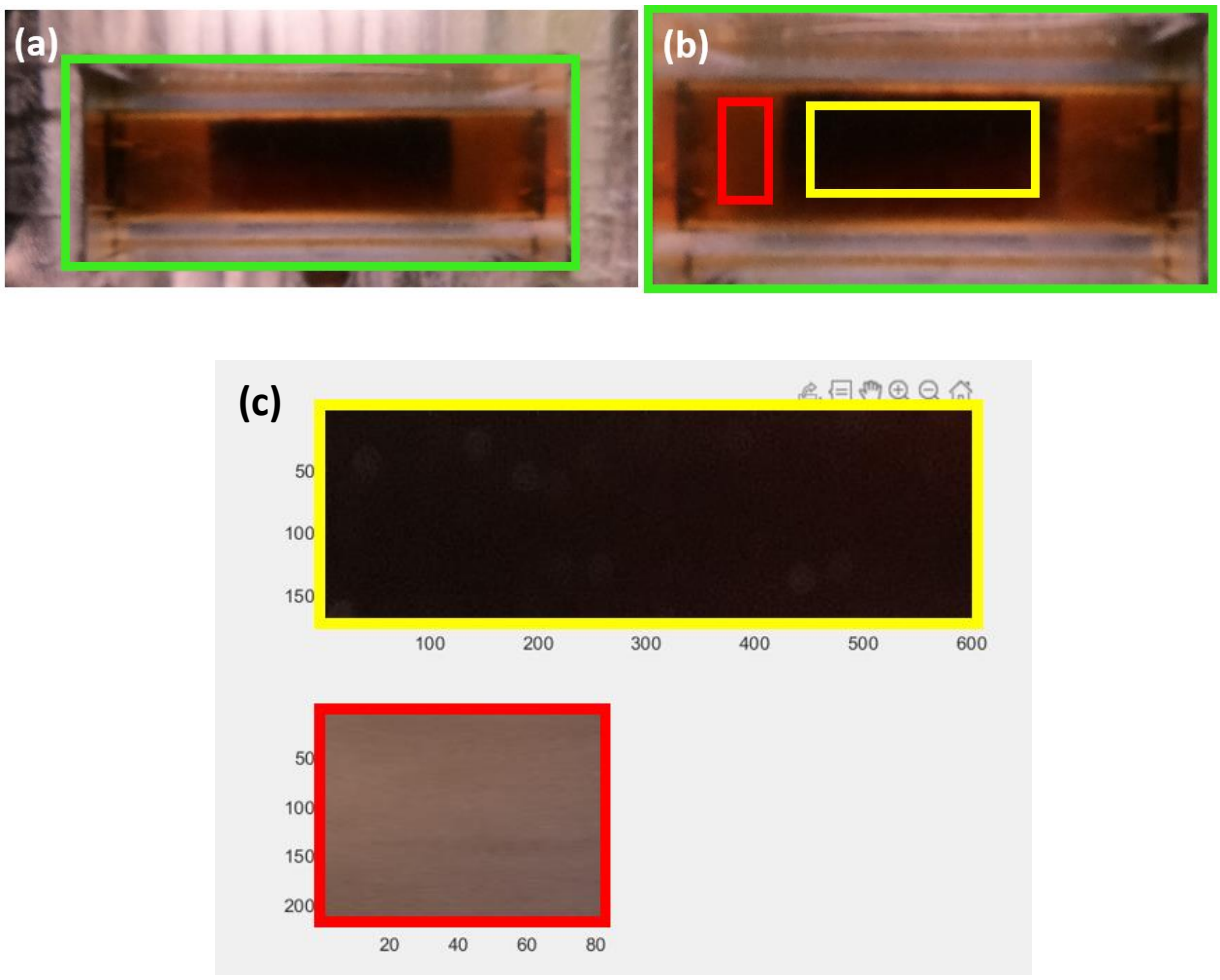

Figure 2.14: The test cell image that the viewer sees when utilizing the program is shown where the green box is the size the user selected to view, the yellow box is a varnish area crop, and the red box is a steel and fluid area crop.

The option is then offered to re-crop, quit the program, or continue with the crops selected. Previously, the code merely began to execute the program automatically after selecting the image crops. Each image is now analyzed for the maximum values of RGB intensity, red (R), green (G), and blue (B), instead of the CMYK method previously used, on a given area of the initial image. A visual representation of how Matlab evaluates images with RGB in Figure 2.15.

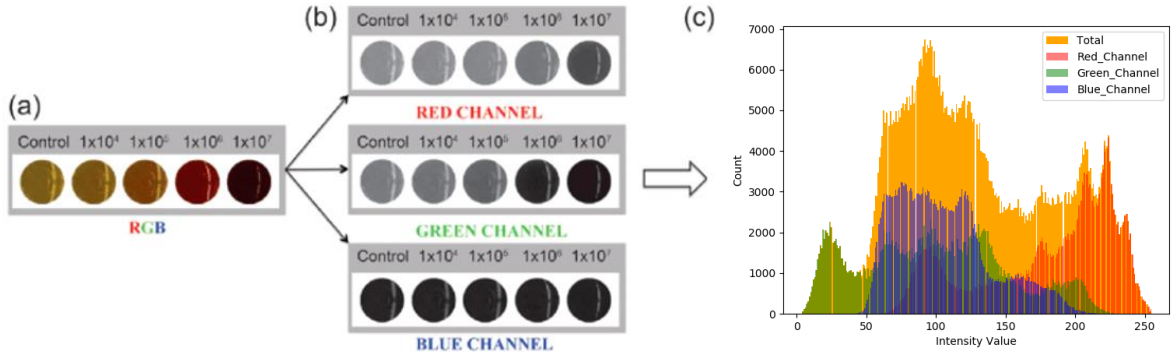

Figure 2.15: (a) Pixels are selected from pictures. (b) Pixels are separated by RGB intensity per photo. (c) Depicts an example color intensity in red, green, and blue as well as total intensity. [71]

Average color intensity values for each image per pixel for red, green, and blue are converted to vector form, as shown in Equation 2, and saved for further analysis. The new intent of the code is to analyze the steel and varnish regions and compare the average color of R, G, and B. The initial average color vector $(\hat{R}, \hat{B}, \hat{G})$ was calculated at the start of the test for both the region where varnish covers the test coupon and the region with exposed steel.

$$Ri + Gj + Bk \qquad [2]$$

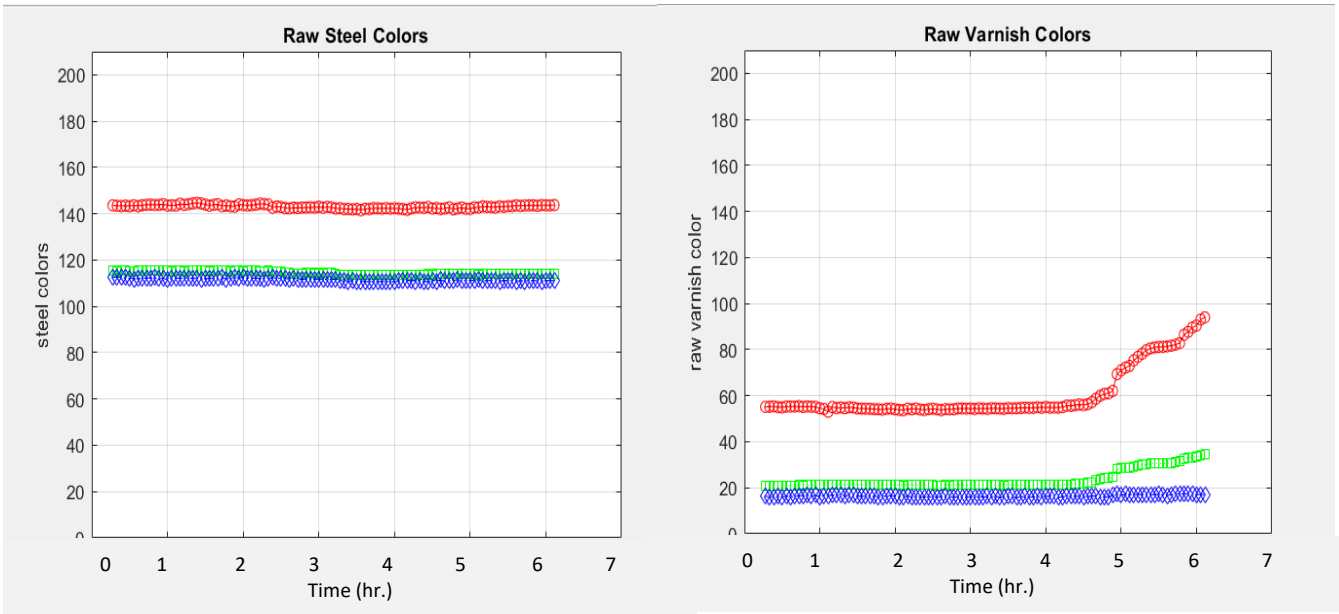

Figure 2.16: (a) An example graph showing raw RGB intensity data from a clean coupon or "steel" section of the image over the duration of a test. (b) A graph showing raw RGB data from the varnished section of the coupon.

Next, a dot product of the color vector for the steel and the color vector for the varnish region is calculated. This yields a small value for dissimilar vectors dotted together and larger values for similar vectors, so as the varnish is removed the steel and varnish vectors should converge and the dot product should increase. The comparison of the individual colors as opposed to the CMYK method that only includes the maximum color value of all the colors is a more accurate way to quantify varnish removal because it captures changes in any color.

After this, the dot product scalar values are rescaled using the value calculated from the steel portion of the coupon and the value calculated on the varnish for each image, such that the varnish removal ranges from 0 to 1. Here, a value of 1 means the coupon is fully varnished at the start of the test. Section two in the code in A.1 runs a simple additive calculation that creates a string of values starting at time zero and increases by increments of 0.00278 hours which equates to about 10 seconds per frame (the rate at which the time lapse takes pictures) for to the duration

of the test. We can use this to find and match all the values of time at which the images were taken during testing. Lastly, in section 6 of the program, the varnish removal percentages vs. test time are graphed, with 1 being a fully varnished test coupon and 0 being a fully cleaned test coupon. An example can be seen in Figure 2.18.

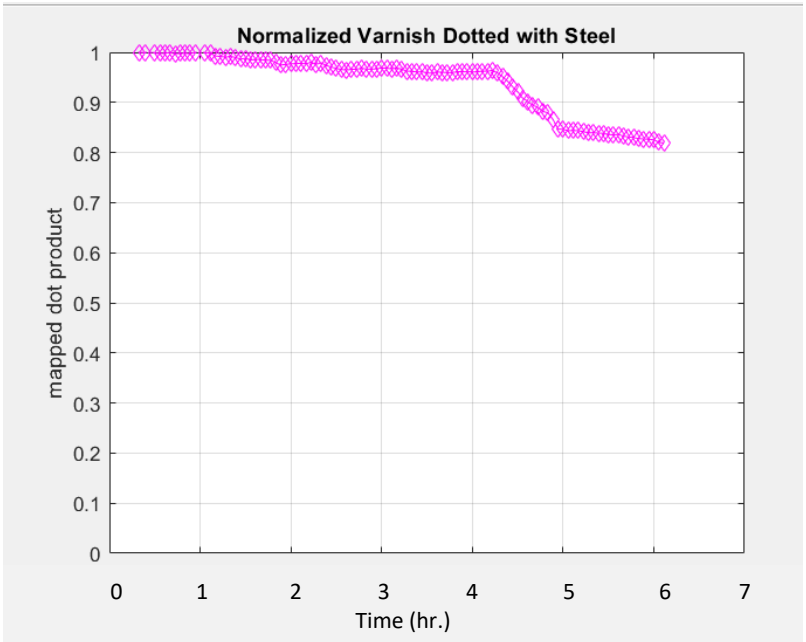

Figure 2.18: A graph showing an example of the normalized plot of the varnish dotted with steel values vs. testing time.

Chapter 3: Test Anomaly Investigation

During the preliminary testing, several unexpected results were obtained. To ensure consistent and reproducible testing, we performed a detailed study of two such anomalies, fluid degradation and varnish darkening.

3.1 Fluid Degradation Analysis

To obtain statistically comparable results and conserve fluid that is difficult to obtain, our testing required repeat testing with certain cleaners under given testing conditions. However, early testing results suggested diminishing return on performance quality of used fluid. Specifically, results showed less removal for all fluids tested when they were re-used for subsequent testing. In order to confirm this hypothesis a study to evaluate and quantify cleaner fluid degradation was performed. A commercial fluid with strong initial cleaning properties was used in this study.

For this testing, a flow rate of 2 GPM, testing temperature of 90 °C (this means temperature stays ± 5 °C from 90°C through the duration of each test), test duration of 4 hours, including setup and shut down. The varnish covered test coupon was weighed before and after testing as a physical comparison to keep the validity of our results. Post-test analysis also includes filter analysis. The filter is used to collect the varnish particles moving through the system which gives us a better view of the removal properties of the fluid because we can see both the amount of varnish and the size of particles removed.

The same fluid was used for four repeat tests at the same conditions. Snapshots of the test coupons from each test are shown in Figure 3.1. These images shown that less varnish is removed by the fluid in the test run with previously used fluid. This implies the effectiveness of

the cleaner fluid is deteriorating over time.

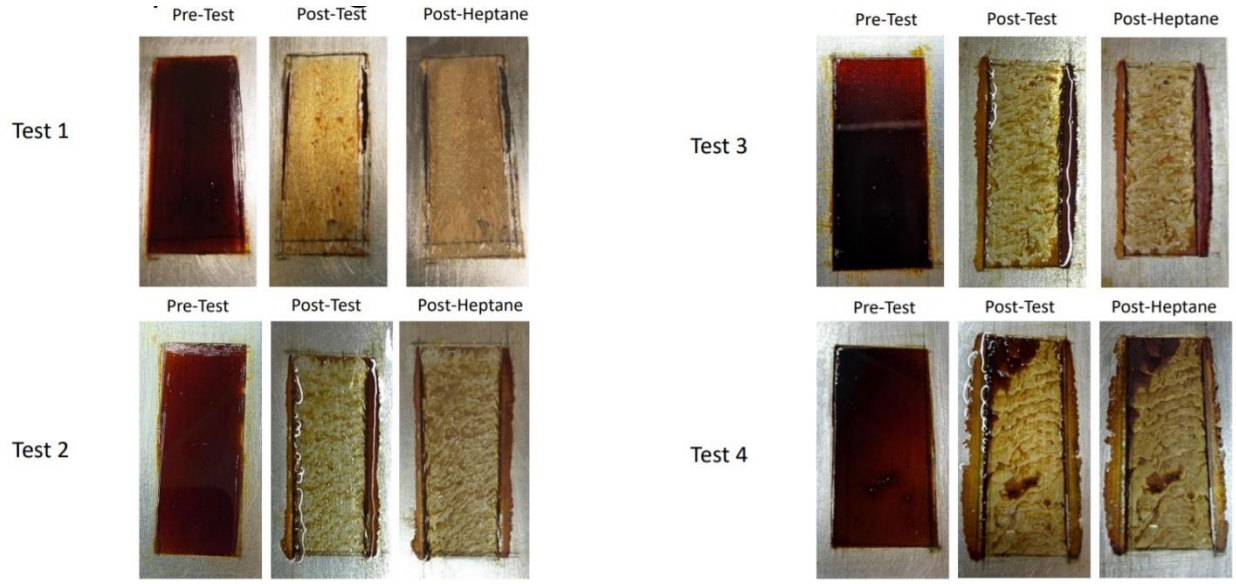

Figure 3.1: Images of the pre-test, post-test, and post-heptane images from four subsequent tests with the same fluid.

The effect of repeat testing on varnish removal can also be observed by analyzing the filters. As shown in Figure 3.2, varnish flakes on the filters increase in size with number of tests. This may be indicative of waning removal properties. Varnish removal fluid must be filtering and flushing when flakes are large and is usually preferred to use a fluid that removes varnish in the

form of small particles that do not need filtering.

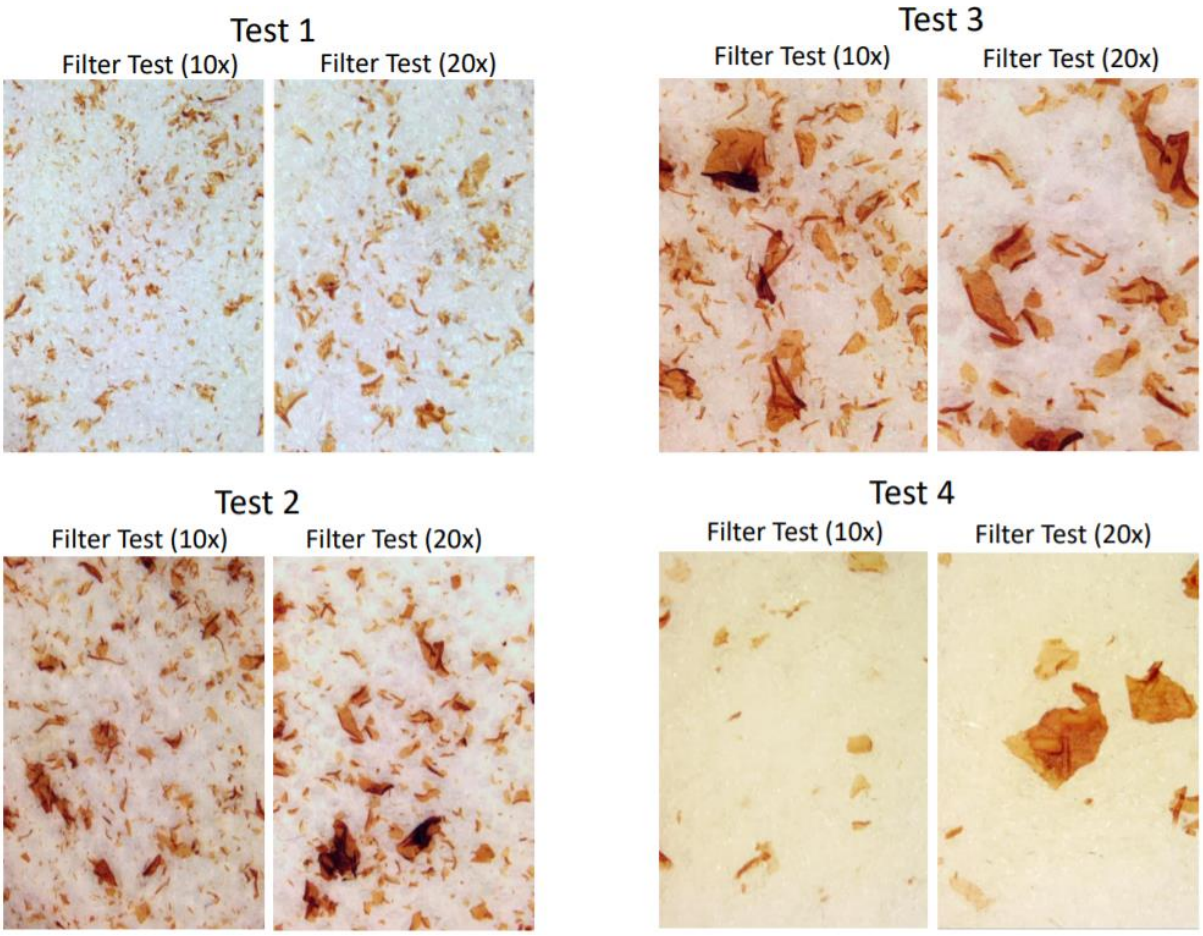

Figure 3.2: Images of the filter pot-test at 10x and 20x from four subsequent tests with the same fluid.

The results were also analyzed in terms of the visual varnish results, as shown in Figure 3.3. For the first and second test, the rate of varnish removal are similar and nearly all varnish is removed during both tests. However, the rate of varnish removal decreases rapidly in test 3 and then again in test 4. For test 4, only about half of the varnish was removed at the end of the four hour test.

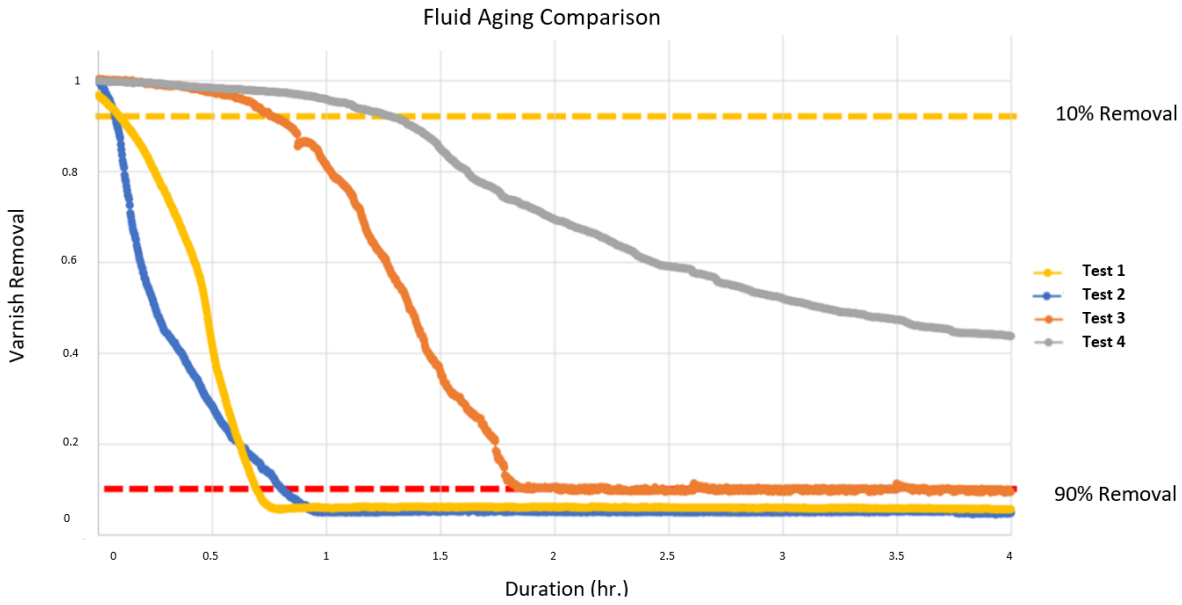

Figure 3.3: Percent varnish removal as a function of time for the subsequent 4-hour tests with the same fluid at 2.0 GPM. Varnish removal performance degrades after repeat testing.

The total amount of varnish removed was quantified using visual analysis and mass loss, as shown in Figure 3.4. Both results show that the total amount of varnish removed decreases with number of tests.

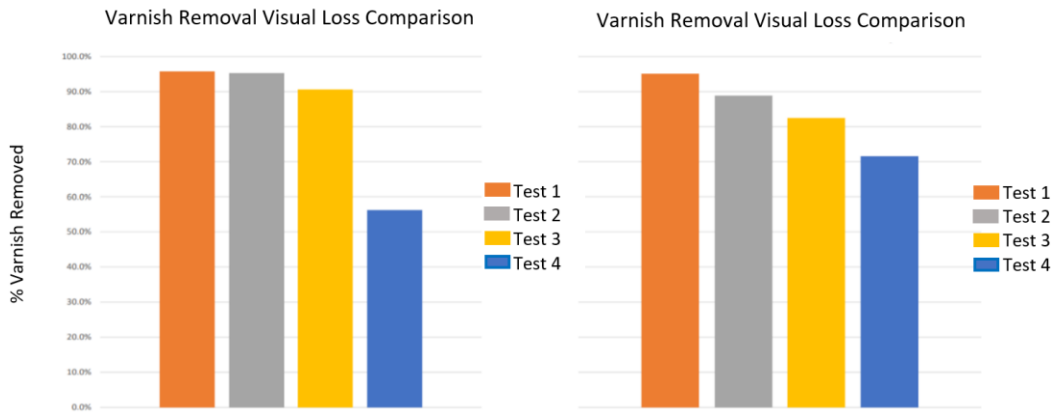

Figure 3.4: Varnish removal visual loss comparison by test for the repeat 4-hour testing with the same fluid. at 2.0 GPM. Varnish removal performance data reflects sign degradation in both actual loss and visual analysis-based loss.

The graphs above suggest that there is some form of degradation going on within the fluid. This is also represented in the post test statistics from all four tests. The first and second tests show significant removal. These first tests also show a faster removal rate, quantified by the time to 10% removal, which was 0.327 hours, and the time to 90% removal, which was 0.797 hours. Test #3 reaches only 10% removal by 0.834 hours which, compared with test #1 and test #2 that reach 90% removal before this time. As expected, by test #4, the fluid removal properties did not even reach the 90% removal during the four hours of testing and appears to plateau around 3.75 hrs. We can thereby assume that this chemical flushing fluid's efficiency is significantly reduced by the fourth test.

Test Number	1	2	3	4
Pre-Test Varnish Weight	88.2 mg	94.7 mg	91.4 mg	86.5 mg
Post-Test Varnish Weight	6.9 mg	10.6 mg	16.1 mg	24.6 mg
Varnish Removal Quantity	81.3 mg	84.1 mg	75.3 mg	61.9 mg
Time to 10% Removal	0.57 hr	0.084 hr	0.834 hr	1.375 hr
Time to 90% Removal	0.79 hr	0.804 hr	2.0 hrs	N/A

Table 3.1: Comparison of time taken for a fluid to reach 10% and 90% removal compared to pre- and post-test weight as well as overall varnish removal quantity.

3.1.1 Degradation Mechanisms

There are many potential reasons for the degradation of oil we have seen in our aging tests. In this next section we will be exploring reasons found in literature that may be potential causes for the diminished cleaner performance.

Thermal degradation can happen to oils, usually at temperatures greater than 400 degrees Fahrenheit (~ 200˚C). This is usually attributed to hot spots, micro-dieseling, or compression.[72] In this case, the likely cause of degradation from a thermal standpoint would be hot spots. In the test rig, there is one section of the rig tubing that is subjected to high heat from the heating coil used to heat the rest of the system. Although testing temperature is only 90˚C, which means that maximum temperature should be 95 ˚C. However, because the test rig thermocouple measures the fluid in the reservoir and not near the heater sometimes this temperature can be exceeded. Thermal degradation produces byproducts which are detectable using molecular light spectroscopy and can be measured and translated to a rate of accumulation of these products and depletion of antioxidants within the oil.

Another cause of degradation due to heat that is a likely contributor to the diminished performance of oil over multiple tests is the loss of base oil within the testing fluid due to evaporation.[72] Evaporating base oil can cause the varnish removal additives and viscosity modifiers within the oil to concentrate, which will then cause performance to be impacted over time. This could possibly be tested by weighing a portion of the fluid or by microscopy before and after each round of testing.

One other cause of diminishing return on fluid performance might be mechanical factors within our testing system. Additives within a fluid can be separated mechanically from the base oils that carry them through filtration and settling.[73] In our testing, we attempt to ensure that no additives are lost due to settling by making sure to remove the fluid from the system while it is still hot and flowing, but there are some additives that are prone to settling over time. In addition, we have a fine mesh filter in our fluid circuit that is used to filter varnish particles.

However, especially with blockage from varnish particles, essential additives may be removed from the fluid by filtration during the test.[74]

3.1.2 Discussion

Commercial cleaners are created from base oils and additives which both have finite lifetimes. Although different testing fluids may perform differently, the fluid evaluated here exhibits severe degradation by the third run with the same fluid batch. This analysis should be repeated for other common fluids to determine when their effectiveness is diminished.

3.2 Investigation of Fluid Darkening Phenomenon

During some of the tests, an anomaly was noticed for fluids that did not removal all of the varnish right away. We observe a graduate increase in the amount of varnish, as quantified by the visual analysis, during testing in which the coupon appears to be gaining varnish during the test. An example is shown in Figure 3.5.

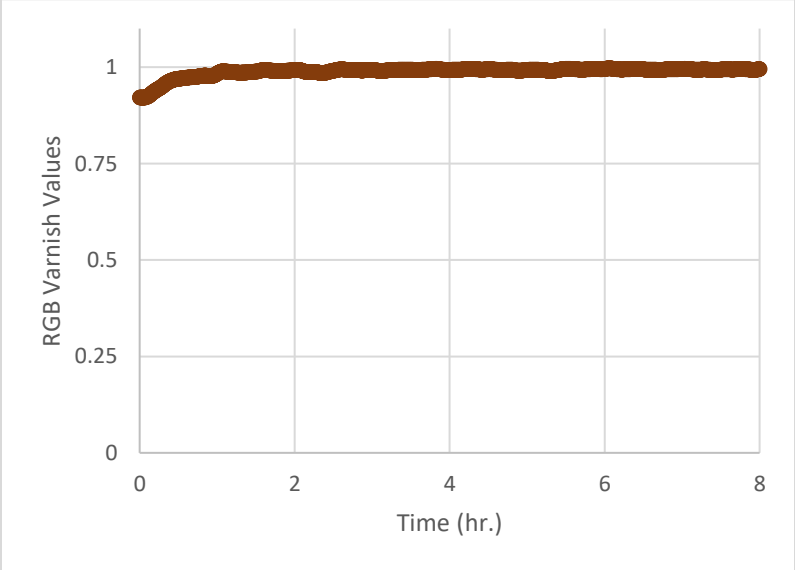

Figure 3.5: An example of poor varnish removal data vs. testing duration that shows a distinct anomaly in testing data.

As previously stated, the varnish removal quantity is generated by analyzing the varnish coloration using our visual analysis software. Knowing this, the first step was to ensure that what the camera was perceiving was in fact physically happening. We looked back at the images taken by our testing GoPro and, as seen in Fig.3.6, the varnish does appear to darken during testing from start to finish, despite the lack of change in weight.

Figure 3.6: Images taken from our test rig Go Pro at the start and end of testing.

This phenomenon was also observed for cleaners that removed moderate amounts of varnish. However, in the case of medium removers, there only appeared to be a darkening affect after the varnish that can be removed in this testing, here a little over half, had been cleaned from the coupon. This anomaly is seen in Figure 3.7.

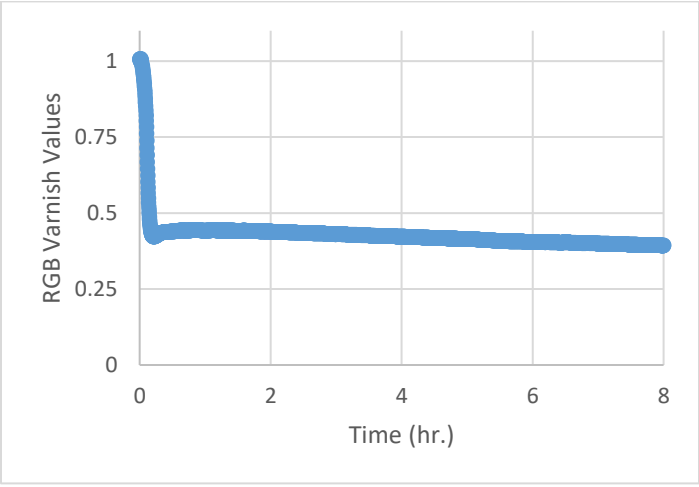

Figure 3.7: An example of medium varnish removal data vs. testing duration that shows a distinct anomaly in testing data.

Our team considered several hypotheses for the cause of the darkening phenomenon and tested them in the following manner. Varnish is made primarily from components of degraded lubricants and therefore we considered the idea that the oil-based varnish removal fluid or its components could be “absorbed” in some capacity by the varnish on the coupon.[75] Varnish is adhered to the steel test coupon through a process called coking which involves heating degraded oil and splashing it against a substrate which helps the varnish adhere itself into layers of film within various parts of mechanical systems.[77]

To explore the source of the darkening, the heat factor needed to be isolated from other possible sources of darkening. A simple test setup was established to mimic coupon heating during rig operation. A coupon in an isolated environment was heated. The test coupon was isolated from foreign contaminants by covering the coupon with a non-insulating clear plate. The testing assembly can be seen in Figure 3.8.

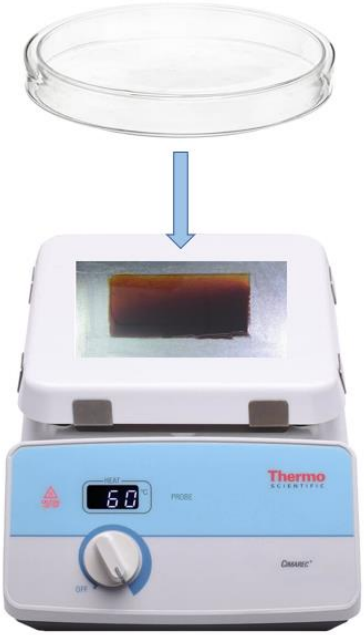

Figure 3.8: Pictured above is a hot plate testing assembly with a testing coupon in a stable environment with protective plate.

The coupon was then imaged at times 0, 30 minutes, 1 hour, 2.5 hours, 5 hours, and 8 hours. By visual assessment, it can be seen in Figure 3.9 that there is no noticeable darkening.

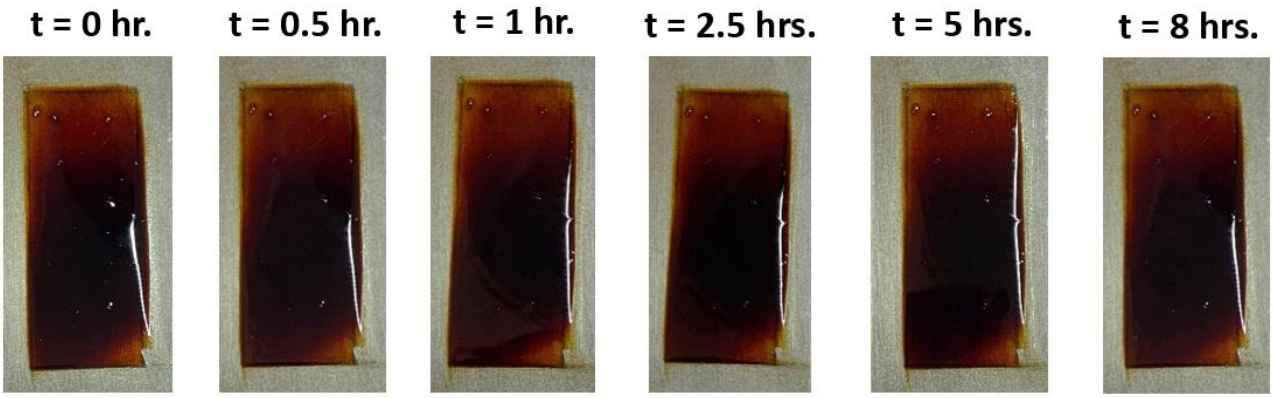

Figure 3.9: Above are testing coupon images at times 0 through 8 hours of constant, uniform heat.

To confirm that our visual assessment was correct, the varnish removal code was used to evaluate the color darkness for each image. Looking at the darkness distribution from the data depicted in the graphical results in Figure 3.10, the varnish region stays nearly consistent. This can be seen from the three distinct varnish peaks in each graph and the consistent left-sided distribution of the data, but not at an increasing rate.

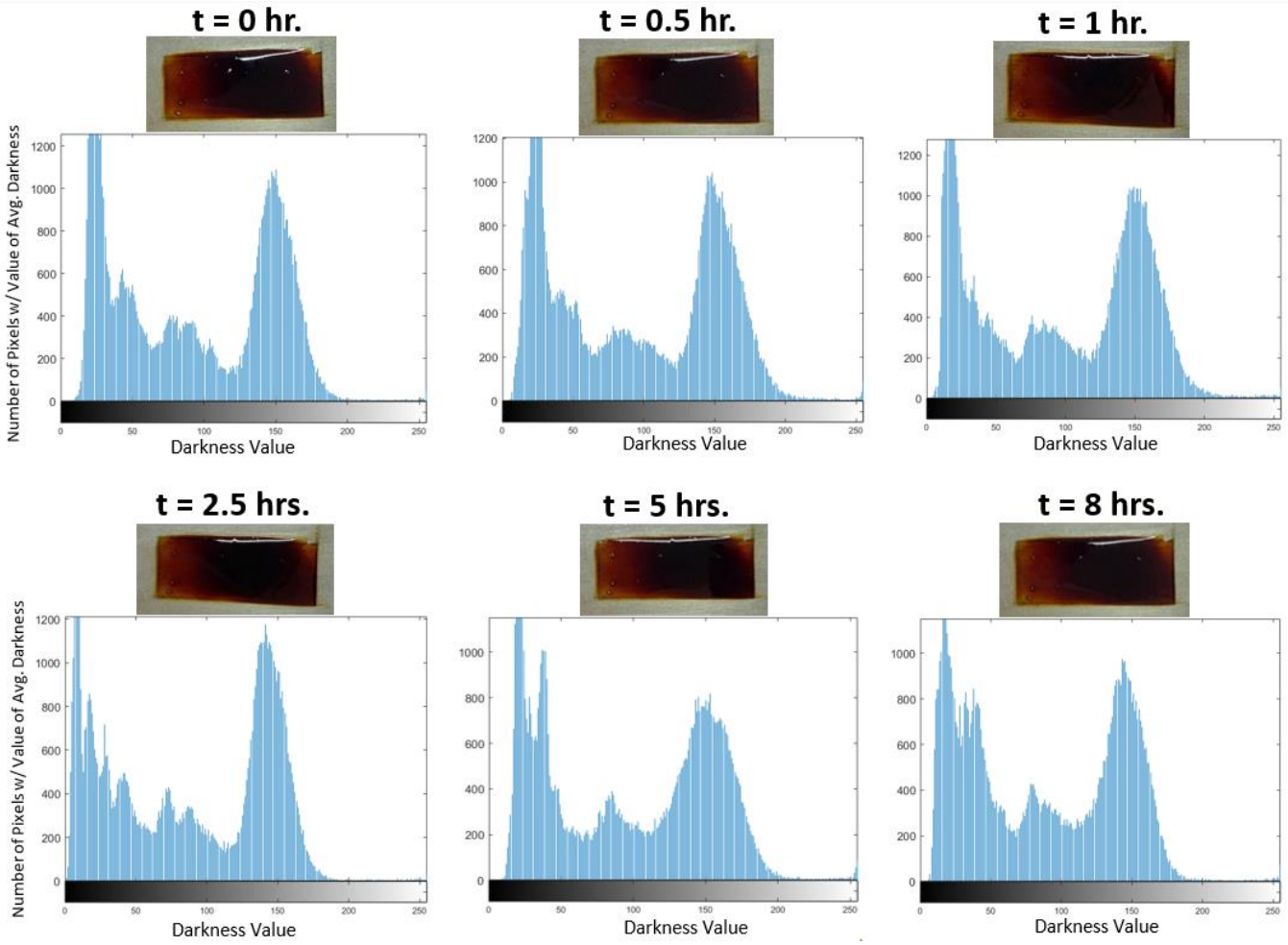

Figure 3.10: Images and associated graphs of varnish darkness vs. the frequency at which this darkness value is seen within each image.

Although this needs further investigation, the preliminary results suggest that thermal fluid degradation may be a partial contributor to varnish darkening, but it is likely not the root cause.

Another likely cause of varnish darkening is absorption of removal fluid into the adhered varnish layers. In order to test the veracity of this concept, a new test was run with pure base oil, with no cleaner additives or heat at a flow rate of 2GPM. The test duration was set for four hours because every fluid that showed the anomaly had manifested this clearly within the data by this

point in both the four-hour and eight-hour testing cycles. Results are seen in the plot in Figure 3.11.

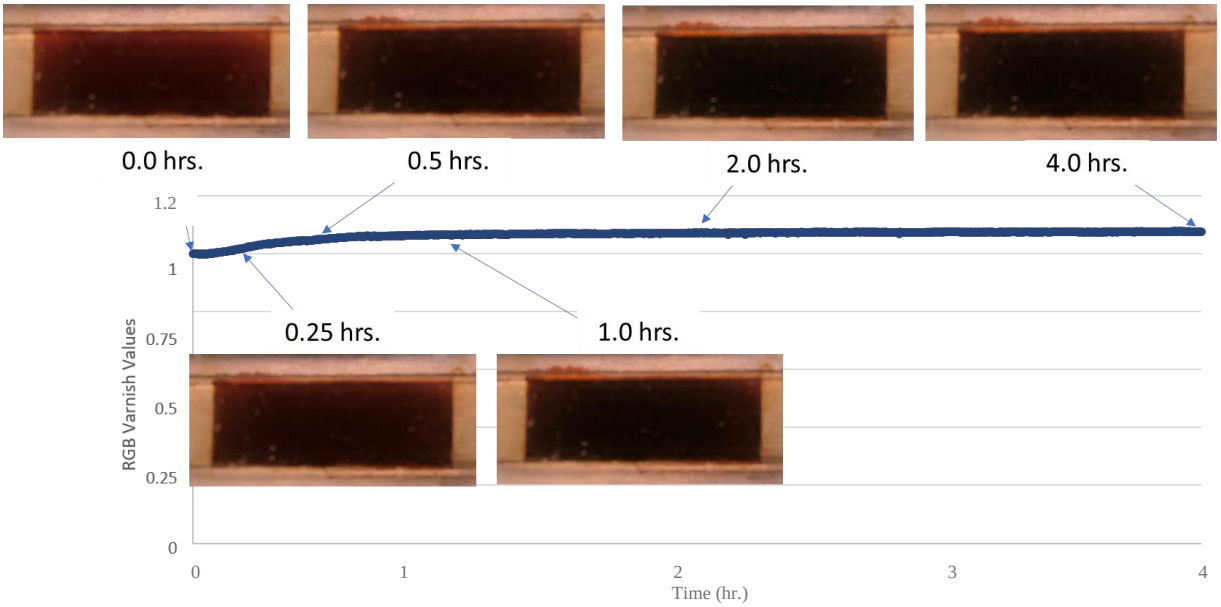

Figure 3.11: Testing images and graphical results from base oil testing at a flow rate of 2 GPM over a 4-hour time period.

After testing and weighing the coupon it was found that no varnish was removed physically from the pre- and post-test weight. However, the varnish darkening was still shown in the images and visual analysis results.

3.2.1 Discussion

After isolating both the temperature and fluid absorption as independent variables in separate tests, we concluded that it is likely that the fluid darkening phenomenon comes from fluid absorption into the coupon. Possible solutions are housing the varnish coupon in a base oil prior to testing to prevent further fluid absorption during testing or using the varnish code to compensate for this on the post-processing end.

Chapter 4: Varnish Removal of Commercial Cleaners

4.1 Introduction

In general, varnish is a byproduct of lubricant degradation during operation that occurs primarily through oxidation of hydrocarbon molecules and can be accelerated by entrained air and water, oil contamination, mechanical stress, high temperatures, electrostatic discharge and metal particles. Lubricant oxidation is known to be the principal cause of oil degradation while in service. [75, 58] Varnish accumulation is also affected by the system materials, environment and the lubricant base oil and additive compositions.[59-62] Varnish can accumulate on metal or wetted surfaces in a turbine lubrication system. This accumulation can lead to severe issues such as sticking of valves, increased bearing temperature, bearing failure, blockage of oil filters, and impeded heat transfer. [63, 64] The adverse effects of varnish are particularly problematic in areas of small tolerances such as servos and control valves. These types of failures can lead to loss of efficiency, requiring replacement of parts or, in extreme cases, catastrophic failure.[65]

Varnish can be mitigated with three different approaches.[66] First, as a preventive approach, lubricants with varnish control properties such as antioxidants, detergents and dispersants can be used to decrease oil oxidation and lower the varnish formation tendency.[67, 33] Unfortunately, improper ratios of base oil to additive or changes in operating temperature or flow rate can cause these additives to have adverse effects on varnish formation.[69, 70] Second, varnish and varnish precursors suspended in the oil can be removed through various types of filtration methods. Filtration methods can be successful in removing lubricant degradation by-products, but they require extended durations for optimal performance and temperatures must be maintained in a range that allows the varnish to remain suspended in the fluid. Further, filtration using media with very small pore sizes can inadvertently remove beneficial additives from the

fluid.[61] Lastly, when varnish accumulation in the system becomes severe, chemical cleaners are often the only option to remove varnish. The chemical cleaning process is conducted either through circulating the mixture of cleaner and in-service oil under normal operational conditions of the equipment, or through external flushing often at high velocity.[71] The chemical cleaners act on the surface deposits and dissolve or suspend them into the fluid. These deposits are then removed from the system by filtration and fluid drain.

A number of chemical cleaners are commercially available which claim to remove varnish from equipment such as turbines and compressors. [74,75] Evaluating the effectiveness and efficiency of different chemical cleaners is challenging because there is currently no standard test method for quantifying varnish removal that enables direct comparison. To partially address this issue, a test system and method were recently developed that model cleaner flow over varnish and enabled visual tracking of the amount of varnish removed.[79] The new test system was demonstrated by comparing the amount and rate of varnish removal of two chemical cleaners.

Here, we extended that investigation to evaluate thirteen different commercially available cleaners with test durations up to forty hours at two different flow rates. Cleaner performance was evaluated qualitatively based on pre- and post-test images of the varnish samples as well as a downstream filter that captured removed varnish particles. Cleaners were also compared quantitatively in terms of mass loss that reflected the total amount of varnish removed and analysis of images of the varnish samples taken during the removal process. The results illustrated that there were dramatic differences between the performance of various commercially available chemical cleaners and emphasized the need for standard tests to enable direct comparison and selection of the best cleaner for a given system.

4.2 Results and Discussion

First, we performed a qualitative comparison of the cleaners based on the appearance of the coupons after tests run at a flow rate of 2.0 GPM. Photographs of the coupons after 8 hours of testing are shown in Figure 4.1, where the top and bottom rows correspond to images take before and after the heptane rinse/drying process, respectively. These images indicate that some cleaners remove varnish more effectively than others. Specifically, quantitative analysis indicates that fluids C1, C2, C3, C4, C9, and C10 removed more varnish than fluids C5, C6, C7, C8, C11, C12, and C13. The photos also suggest that the different fluids remove varnish through different mechanisms. For example, while fluids C2, C3 and C4 all removed varnish, the post-test coupon images for these three cases are very different.

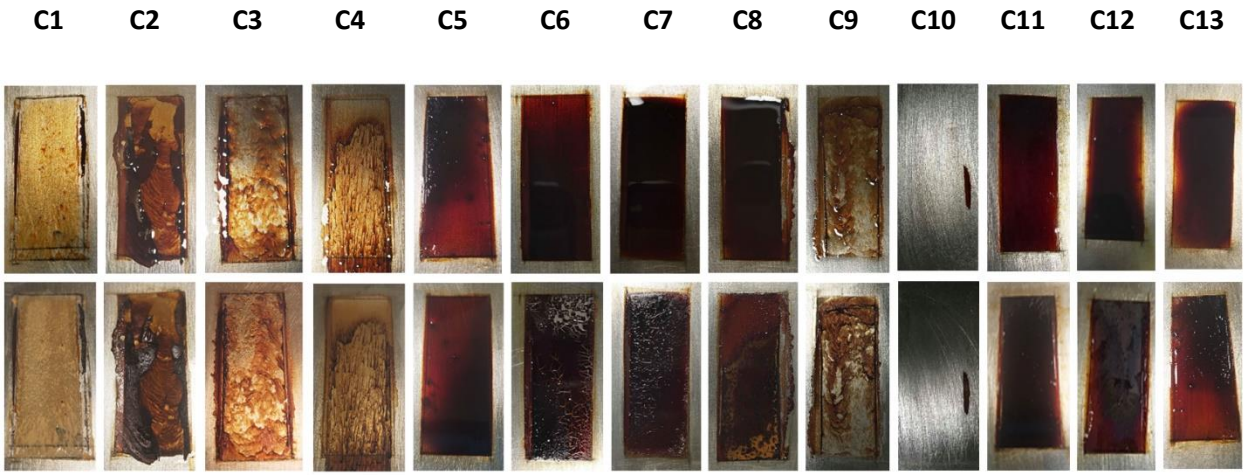

Figure 4.1: Photos of the varnish coupons after testing with nine commercially available cleaners run at 2 GPM for 8 hours taken before (top row) and after (bottom row) heptane rinse and drying. Fluid flow in the test cell was from top to bottom on these images.

Varnish removal can also be analyzed qualitatively based on the varnish particles collected by filter that is immediately downstream from the test cell. Photos of the filter media before and after testing with each fluid are shown in Figure 4.2. The filters from tests with fluids C5, C6, C7 and C8 are similar in appearance to the pre-test filter, reflecting little or no varnish

removal, consistent with the observations in Figure 4.2. Similarly, the filter is brown for fluid C1, C2, C3, C4, C9, and C10 that removed more varnish in Figure 4.2. The filter images support the difference in removal mechanisms suggested by the post-test coupons. From Figure 3, some fluids remove the varnish in larger pieces (e.g. C2, C4 and C9) while others break the material down into smaller particles that dye the filter the color of the varnish (e.g. C1 and C3).

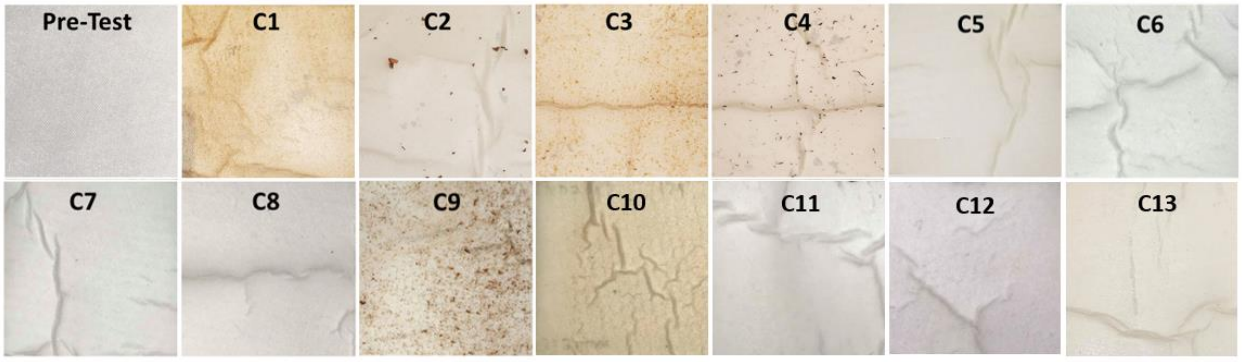

Figure 4.2: Photos of the downstream filter after testing with nine different commercially available cleaners run at 2 GPM for 8 hours. These images correspond to 2.5" x 2.5" squares in the center of the 3" x 5" filters. The upper left image shows a representative filter before testing.

Varnish removal can also be compared quantitatively using the difference in the mass of the coupon before and after testing. This difference was used to calculate a percent varnish removed from tests run at 2.0 GPM in 4- and 8-hour tests. The results are reported in Table 4.1. The percent of varnish removed as measured using this approach ranges from 0 to 95% in the 4-hour tests and 18 to 92% in the 8-hour test. However, the results also suggest that mass loss may not be an accurate approach to measuring varnish removal since, in some cases, the mass loss was greater in the 4-hour test than the 8-hour test. Comparing the mass loss from the 8-hour tests to post-test coupon photos, we observe that very little varnish was removed by fluids C5, C6, C7, C8, C11, and C12 in Figure 4.2, but the mass loss for these fluids ranged from 12% to 47% in

Table 4.1. Since the coupons were massed after the heptane process, it is likely that the heptane process itself removed some varnish, supported by the difference between the pre- and post-heptane coupon images in Figure 4.2. Another limitation of the mass loss calculation is illustrated by fluid C2, for which the coupon image indicated significant removal, but the mass change was relatively small, particularly for the 4-hour test. This is likely attributable to the fact that, although the varnish was pulled away from the coupon, it clumped up and remained on the coupon, such that the change is mass from the start to the end of the test was small.

	Varnish Removal by Mass (%)	
	4-Hour Test	**8-Hour Test**
C1	95.0	92.0
C2	7.10	37.3
C3	51.1	52.6
C4	39.3	76.6
C5	11.6	18.3
C6	37.2	47.0
C7	32.1	31.3
C8	21.7	24.4
C9	81.3	67.6
C10	95.0	98.4
C11	0.0	0.0

C12	0.0	0.0
C13	-	20.7

Table 4.1: Varnish removed by each fluid quantified by the percent change in the mass of the test coupons before and after tests run for 4-hour or 8-hours.

Given the limitations of the mass loss approach of quantifying varnish removal, we used the coupon images taken during testing as a secondary removal metric. Due to the confidential nature of some of these fluids and lack of removal capability of others, only the results for C1-C9 are shown in Figure 4.3 where the data is shown as the quantity of varnish removed not remaining. The lines in Figure 4.3 reflect data from the 8-hour tests and shaded regions capture the difference between the first four hours of the 8-hour tests and the data taken from a 4-hour test. This shaded region therefore approximates the error associated with this test and analysis approach. Based on Figure 4.3, fluid C1 and C10 are the only cleaners that removed nearly all the varnish on the coupon during the 8-hour test. However, fluids C2, C3, C4, and C9 partially remove the varnish, with varnish removals between 20 and 60% after 8 hours.

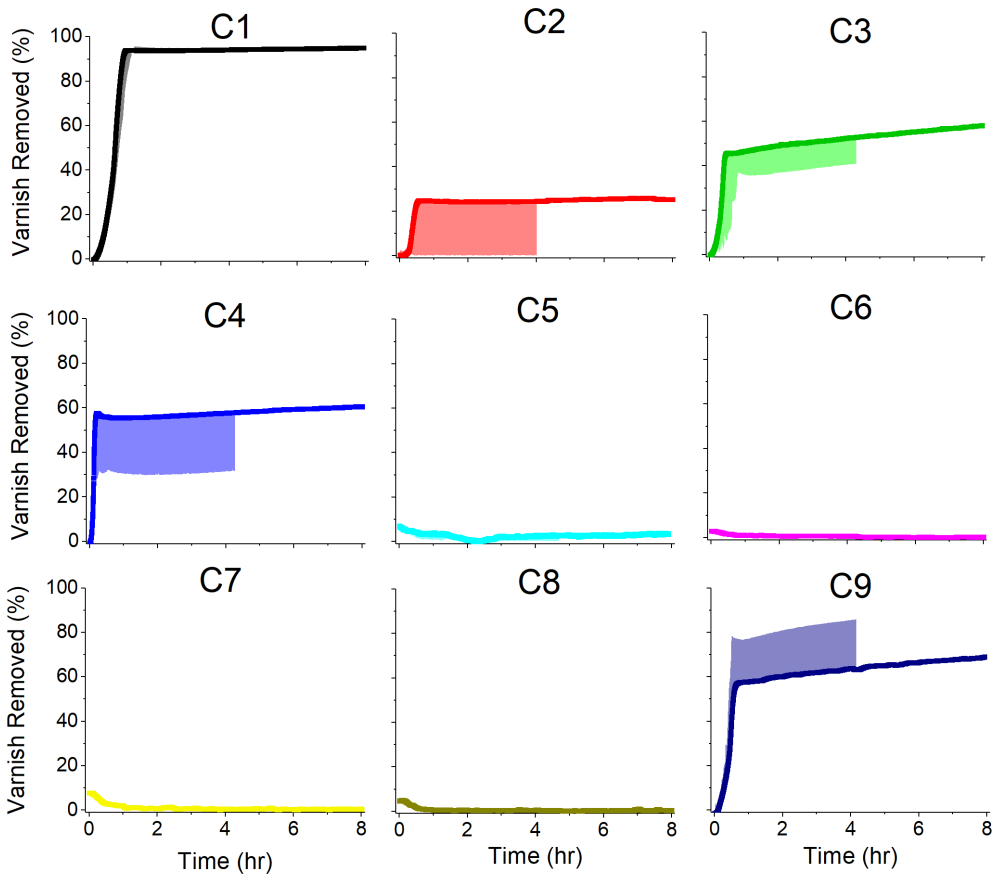

Figure 4.3: Varnish removal as quantified by analysis of images of the varnish coupons taken during testing at 2 GPM. The lines correspond to data taken from 8-hour tests while the shaded regions reflect the difference between data taken from a 4-hour test and the first four hours of the 8-hour tests.

The results of the *in situ* image analysis seen in Figure 4.3 are qualitatively consistent with the observations from the coupon and filter photos in Figures 4.1 and 4.2 as well as the mass loss calculations in Table 4.1. Importantly, all of these removal metrics show that C1 removes most varnish while C5, C6, C7 and C8 remove the least. However, trends are inconsistent between the removal metrics for fluids C2, C3, C4 and C9 that partially remove varnish. Differences are likely attributable to the fact that the image analysis approach is based on an average color change across the varnish region. Specifically, if the varnish clumps up or darkens during the test, the removal based on image analysis may be artificially high.

Based on the above discussion, there are limitations to both the mass-based and image-based varnish removal metrics. Therefore, to best capture the overall removal, we averaged the percent varnish removed using the mass loss and image analysis approaches from the 4-hour test and the image analysis data after 4 hours of the 8-hour test. The results are shown in Figure 5, where the error bars reflect the standard deviation across the three types of data used to calculate the average removal. These results demonstrate that the best performance was achieved with fluid C10, followed by fluid C1, and then fluids C9, C3, and C4. The other fluids removed, on average, less than 12% of the varnish seen in Figure 4.4.

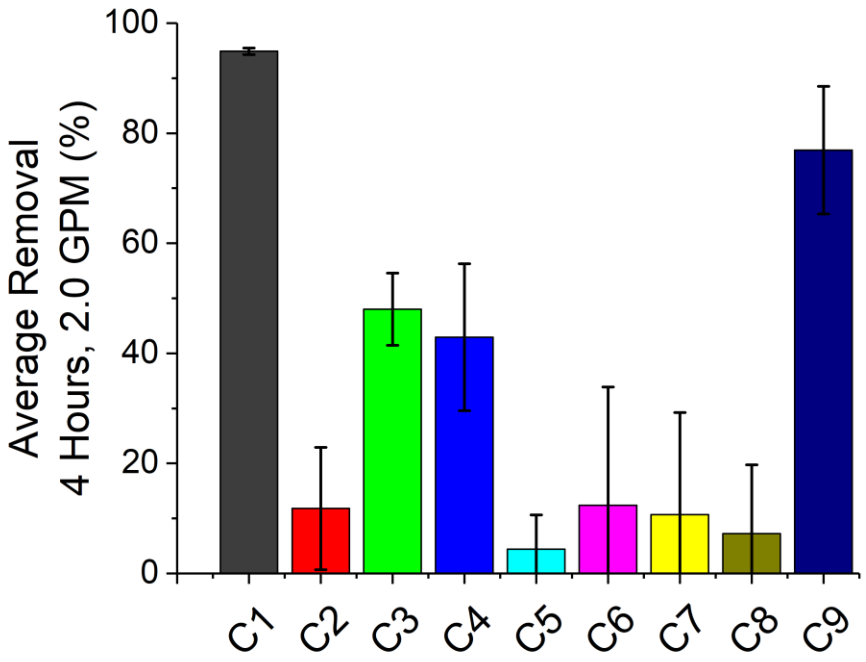

Figure 4.4: Percent varnish removal calculated as an average of the removal taken from a 4-hour test using both the mass loss and image analysis approaches and the first four hours of the 8-hour tests. Error bars reflect the standard deviation.

We next ran tests at a lower flow rate of 0.5 GPM with fluids C1, C2, C3, C5, C6 and C9 only, due to the limited availability of fluids C4, C7 and C8. Each test was run for at least 40 hours and

fluid C3 was tested twice. The varnish removed after 40 hours at 0.5 GPM was quantified using the image analysis approach and the results are shown in Figure 6. At the lower flow rate, only fluid C1 removes any appreciable amount of varnish, with the second-best performance being observed for fluid C9 that removed 8% after 40 hours of testing. These results were confirmed by qualitative agreement with mass loss data, but the mass loss results are not shown because some tests were run for more than 40 hours so a direct comparison could not be made.

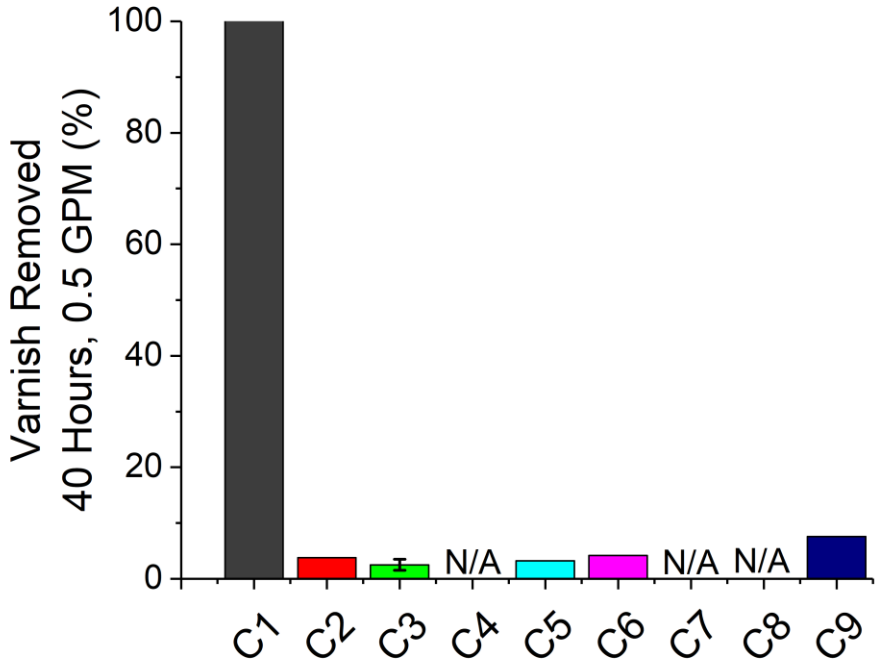

Figure 4.5: Percent varnish removal after 40 hours of testing at 0.5 GPM calculated using image analysis. Each test was run once, except for fluid C3 which was run twice where the difference between the two tests is reflected by an error bar for that fluid.

Lastly, we compared the varnish removal over time at 0.5 and 2.0 GPM for fluids C1, C3 and C9, the three cleaners that removed the most varnish in Figure 5. The results are shown in Figure 7. In this figure, the lines are an average of two tests for fluid C3 at both flow rates, an average of

three tests for fluid C1 at both flow rates, the average of two tests for fluid C9 at 2.0 GPM and the result of a single test for fluid C9 at 0.5 GPM. Some of these tests were run for much longer, but the comparison is reported here for only the first 4 hours of all tests. The results show that varnish is removed sooner and more effectively at the faster flow rate and only fluid C1 removes an appreciable amount of varnish at 0.5 GPM. These results suggest that a higher flow rate improves the efficiency of chemical cleaners, and some cleaners cannot effectively removal varnish at a low flow rate. However, quantifying the effect of flow rate and other operating conditions is the topic of an ongoing study.

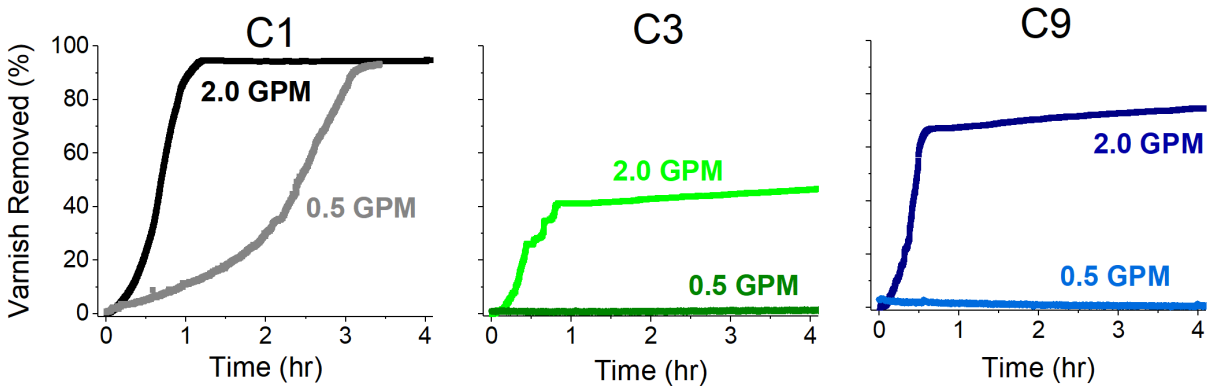

Figure 4.6: Percent varnish removal as a function of time for three of the best performing fluids tested at 0.5 and 2.0 GPM. Varnish is removed sooner at the faster flow rate for all three fluids, but only fluid C1 removes an appreciable amount of varnish at 0.5 GPM after 4 hours.

4.3 Results and Discussion

The performance of nine commercially available chemical cleaners for varnish removal was evaluated using a test system that enabled *in situ* imaging of the removal process. The images were post processed using the color of the varnish to extract a quantitative measure of varnish

removal over time. Image data was complemented by qualitative analysis of the varnish coupons and the downstream filter after testing as well as measurements of the change in mass before and after the test due to varnish removal. Although all approaches of quantifying varnish removal were shown to have limitations, taken together, they enable direct comparison of the performance of the commercial cleaners.

Results demonstrate a wide range of performance is exhibited by the fluids tested, ranging from complete removal after just a few hours of testing to nearly no removal after 40 hours of testing. Further, the findings suggest that different chemical cleaners remove varnish through different mechanisms. Although we have limited information about the chemical composition of these commercial cleaners, our studies above indicate that for some cleaners, e. g. C2, the cleaner components swell and soften the varnish film, such that high speed flow is required to deform and detach the varnish film from the surface, leading to large pieces of varnish on the downstream filter. In contrast, other types of cleaners, e.g. C1, have components that break the varnish film down into small particles which can effectively be removed even under relatively low flow conditions. The direct comparison of nine commercial cleaners performed using our varnish removal test system showed that cleaner C1 has the greatest potential to reliably remove varnish from the lubrication system of industrial equipment due to its efficient varnish removal across a wide range of flow rates and less concern of removed varnish particles blocking downstream filters or valves.

Chapter 5: New Test Cell Modifications

5.1 Design Goal and Parameters

The current varnish rig accommodates only steel coupons as varnish testing samples. Although the coupon method does give an idea of varnish removal capabilities of fluids, it does not accurately portray the geometry of the components that would be found in the types of industrial systems that we are concerned with. So, the open question is how comparable a steel varnish coupon is to the actual removal of varnish within a mechanical system. A goal was set to create a rig modification with the capability of accommodating various three-dimensional parts susceptible to varnish accumulation rather than the flat coupons. Varnish-covered parts under consideration for varnish removal test items ranged from valves to pieces of bearing pads, while still including the steel test coupons used previously. The approach was to design an alternative test cell that could house and hold the parts during testing.

5.2 Prototype Design

The overall goal of this new test cell design is to replicate the effects of fluid running over parts and channels susceptible to varnish accumulation. The samples utilized in design dimensioning were several types of valves, baring pad pieces, and the pre-existing coupons. The samples around which the new test cell was designed are seen in Figure 5.1.

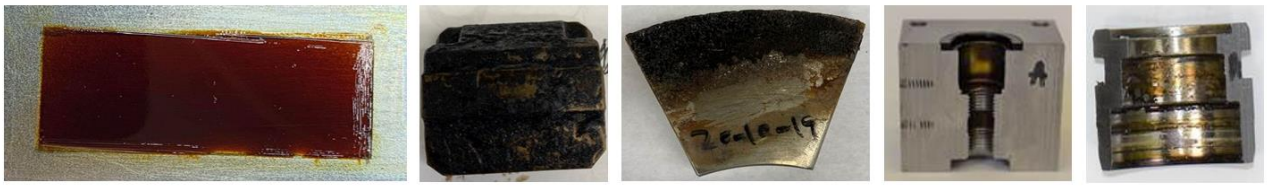

Figure 5.1: Images of the variety of varnish covered parts that were utilized in the 3-D test cell design.

This cell will house a varnish covered test object in the center cavity. The new test cell should be made from 316 stainless steel (16 μm/(m.K)). The test lid should be made from polycarbonate (65-70 μm/(m.K)) with optical quality finish to allow real time data of the varnish removal process as well as vapor polish to protect the lid from wear.

The test cell utilizes a system of supports to allow for a large variety of sizes, shapes, and orientations of various components. The flow through the test cell will immerse the chosen object in fluid and flow it over the adhered varnish layer. An O-ring around the flow area at the top of the cell where the lid meets the steel base which helps contain the fluid within the system.

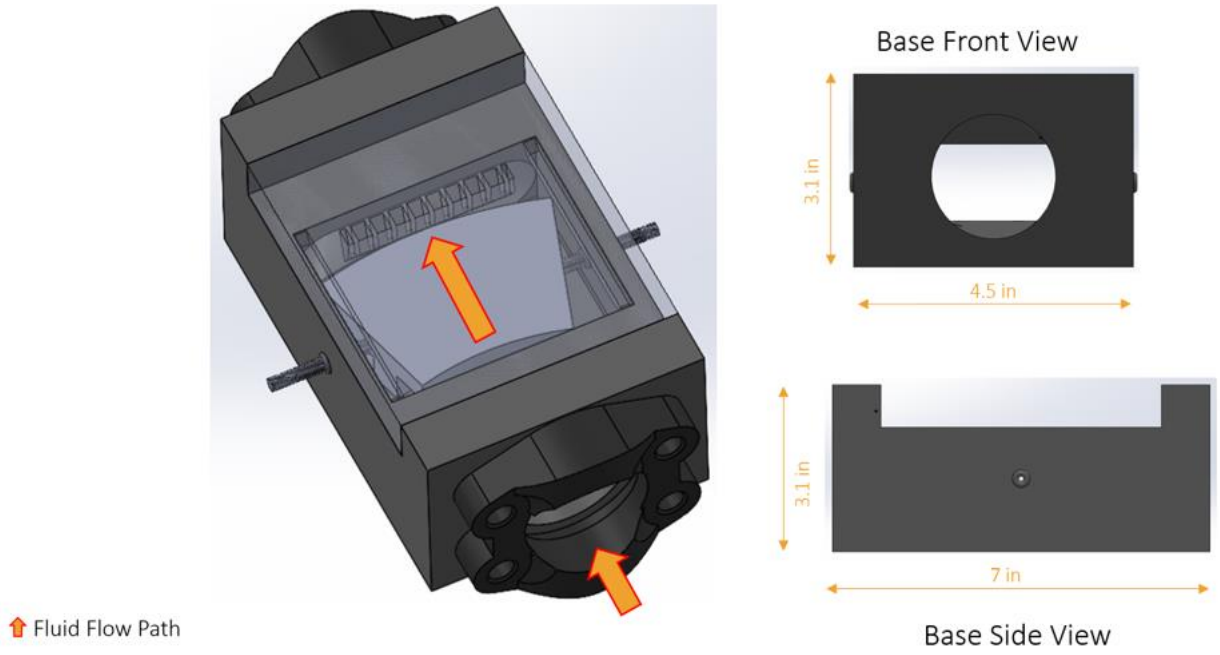

Figure 5.2: A computer aided draft (CAD) depiction of the test cell base and optical quality polycarbonate lid.

The test sample is held against lid by pressure applied from two C-clamps on the outside of the test cell in the same fashion that they are currently employed on the coupon housing seen in Figure 5.3.

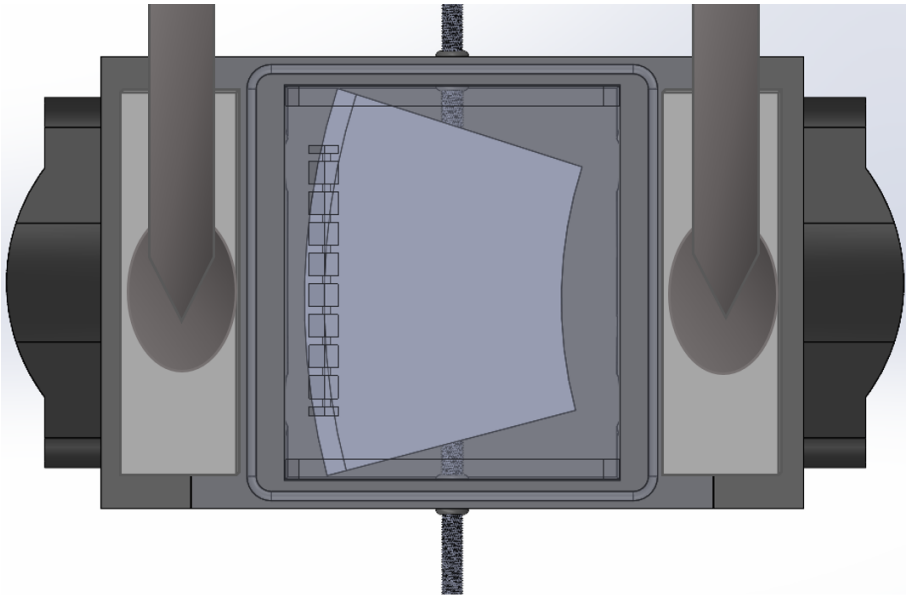

Figure 5.3: A CAD depiction of the test cell base and test lid with c-clamps securing the lid.

Adjustable rubber flats with adhesive to cushion to prevent wear from the part on lid contact and control flow pictured on the underside of the lid in Figure 5.4. The rubber flats are placed contact area between lid and the part to protect the polycarbonate material from damage and prevent the test part from sliding downstream. The fin at the end of the test lid is designed to concentrate flow over the test part and towards the exit port, assist in preventing the part from sliding downstream.

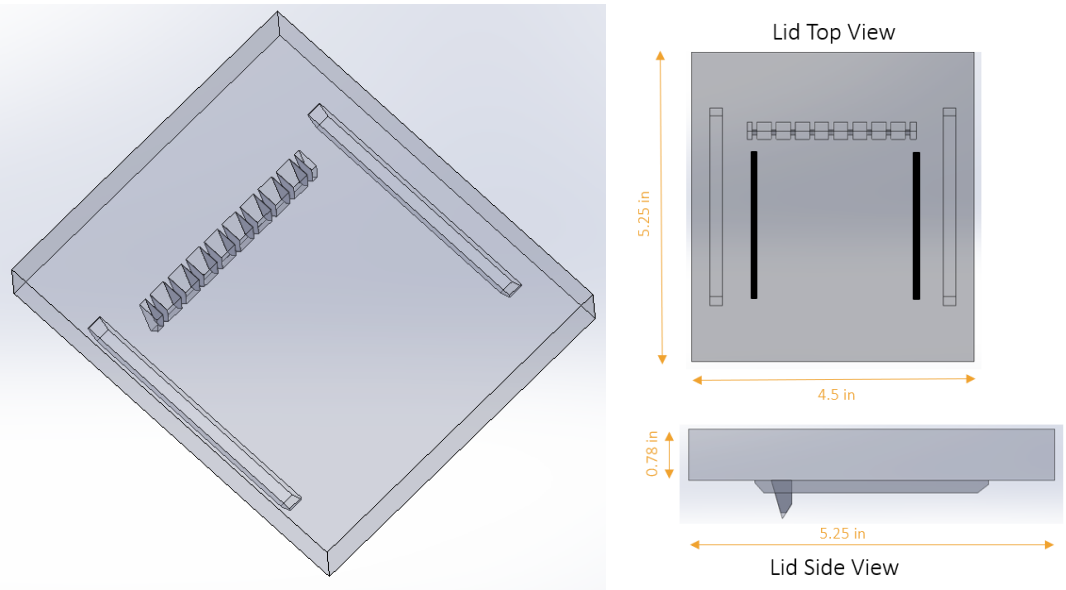

Figure 5.4: CAD depictions of the modified test lid for the 3-D test cell.

The test part is held in place by this clamped lid pressurized by the clamps on the outside of the lid. Some materials are susceptible to corrosion so we must utilize corrosion resistant shims paired with metal inserts of various thicknesses at the bottom of the chamber to help fit the varying part heights previously discussed. The rig utilizes a variety of inserts of different thicknesses and corrosion resistant polymer shims to create the desired depth between the top insert layer, depending on the height of the test part within the system pictured in Figure 5.5.

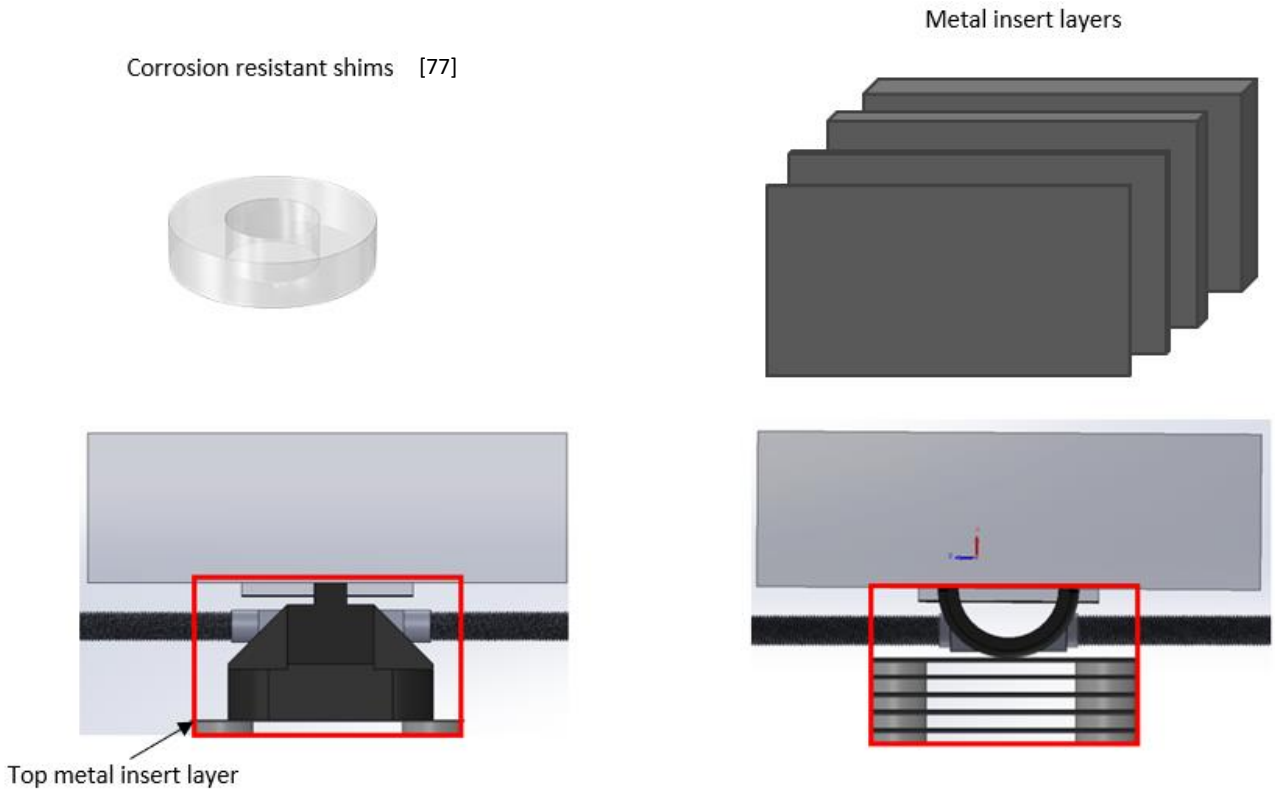

Figure 5.5: CAD assemblies with an example parts held by lid, inserts, shims, and clamping supports.

Supporting clamps with various arm attachments will help hold the parts in place while accommodating different shapes. The threaded rods will allow for the easy change of the attached hands and rod length adjustment for accommodating various sized parts. Figure 5.6 shows how different parts can be fitted within the system. The flow direction of the varnish removal fluid is indicated by the yellow arrow and the test cell chamber size is indicated by the red box.

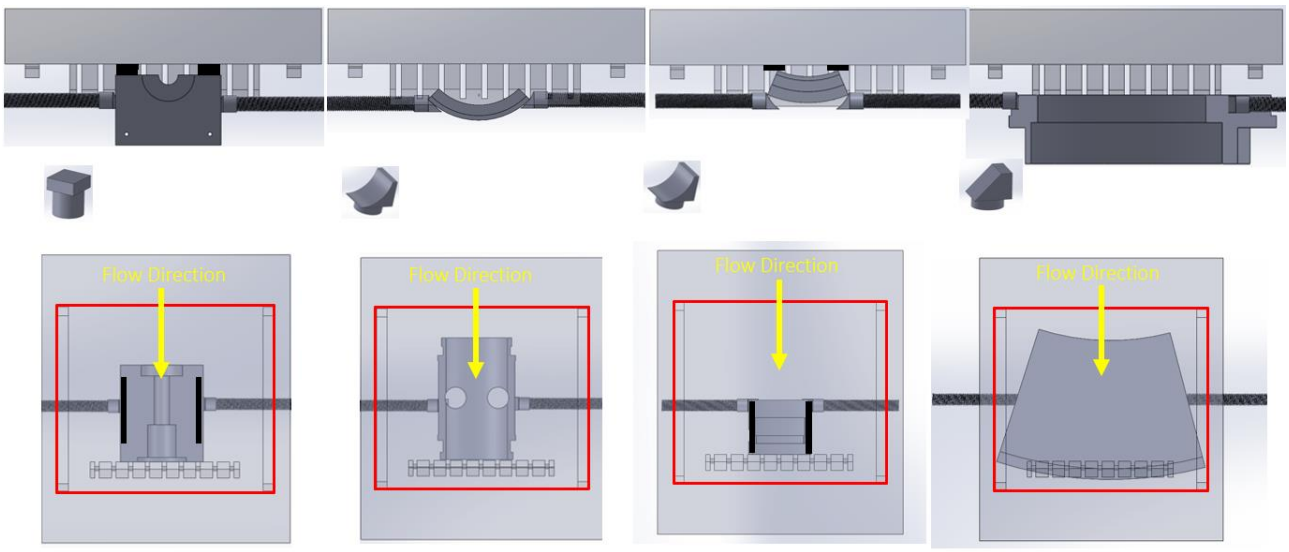

Figure 5.6: CAD assembly with example parts and example hands for attachment onto the ends of the supporting clamps (rod size 0.5 in, thread size UNC ½”-13) based on the associated part type.

The new test cell integrates the piping size used for the rest of the test rig, while concentrating flow through part in the test cell region. The test cell also must transition from the round pipe shape of larger size to a lengthened oval port size to allow for flow through the rectangular region of the cell. The entrance and exit hole of the test cell are cut to accommodate a 1-1/4 in CD-61 vane pump fitting pictured in Figure 5.7 which is the same fitting utilized with the current test cell, the new assembly with the attached fittings can be seen in Figure 5.2.

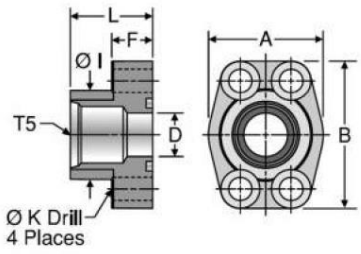

Figure 5.7: Schematic of a CD-61 fitting with associated bolts size UNC 7/16”-14, dim A = 2.6” and B = 3.2”. [49]

The new test cell integrates the current varnish removal rig with the new test cell. Figure 5.8 depicts test region and shows the fluid flow direction as well as giving an idea of how the parts will be fitted together. Due to the taper at the entry point of the test cell from the rest of the system tubing, a “blend section”. The blend section refers to the region in which the cross-sectional flow area changes from circular to an oval-shaped port. The port shape minimizes turbulence through the rectangular center section of the test chamber. The area between the circular flow region and the port flow region must minimize turbulence by creating a smooth flow transition while completely covering the test part to ensure full flow over the varnish covered region of the test part. The new test cell has minimal tapering and allows for most of the flow to go straight into the test cell unincumbered.

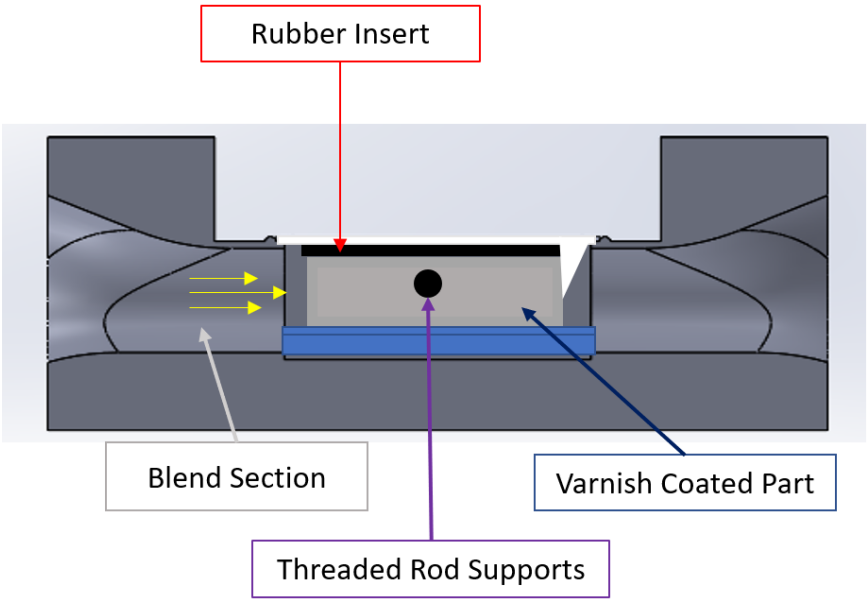

Figure 5.8: Side view of the preliminary test cell design showing the blended section and the location of the test part.

Below is a list of important custom test cell design dimensions seen in Figure 5.9:

- Overall dimensions: 3.2”x7”x2.5” (w l h)
- Port sizing: L = 2.7”, R = 0.62”
- Mounting holes: 7/16-14
- Pipe in/out: Pin = 1.25”

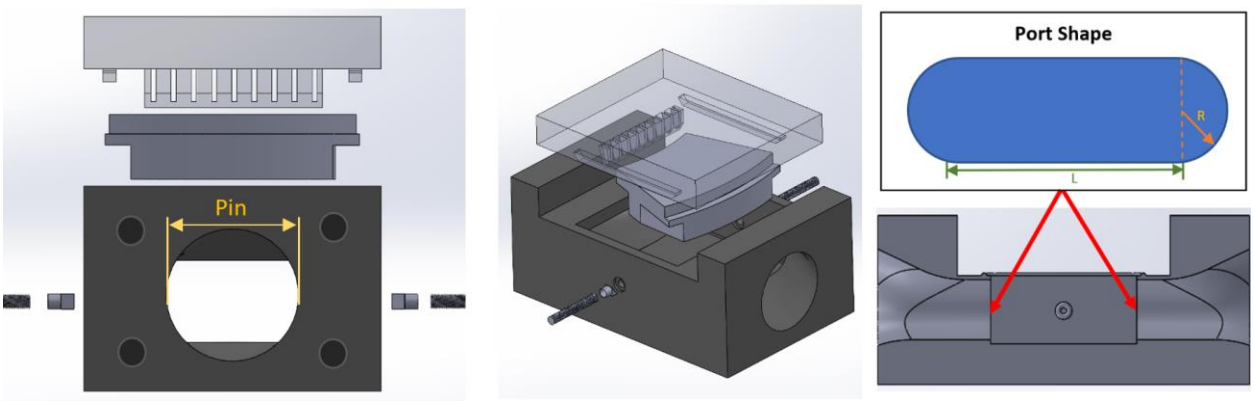

Figure 5.9: Exploded CAD model of the new test cell assembly with dimensioning and specifications.

5.3 Prototype Testing

After establishing the dimensions of our test cell, the next step was simulation of operating conditions. The main focus of our simulation was the change of entry and exit conditions as well as added barriers to laminar flow through the test cell (test part, clamping supports, and fins on lid). Flow simulations were run on the new test cell design using typical testing parameters to confirm that the test cell would perform as expected.

Flow simulations were performed under operating conditions of 90˚C, and at flow rates 0.5 GPM and 4 GPM, the lowest and highest commonly used flow rates in our testing. The

largest part to be tested was then added to the test cell and base assembly shown under the test condition of a 0.5 GPM flow rate in Figure 5.9. Figure 5.10 shows the same, but at 4 GPM

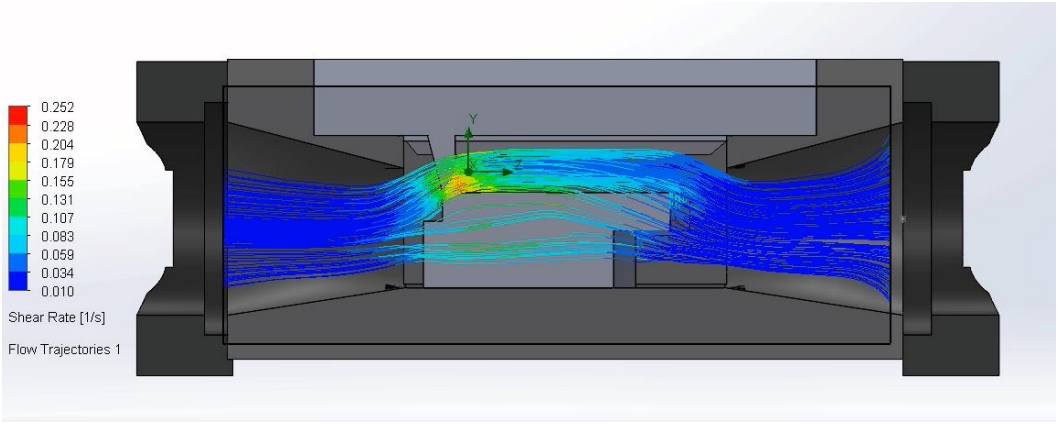

Figure 5.9: Side view of test cell flow modeling at 0.5 GPM test flow rate and 90C testing temperature.

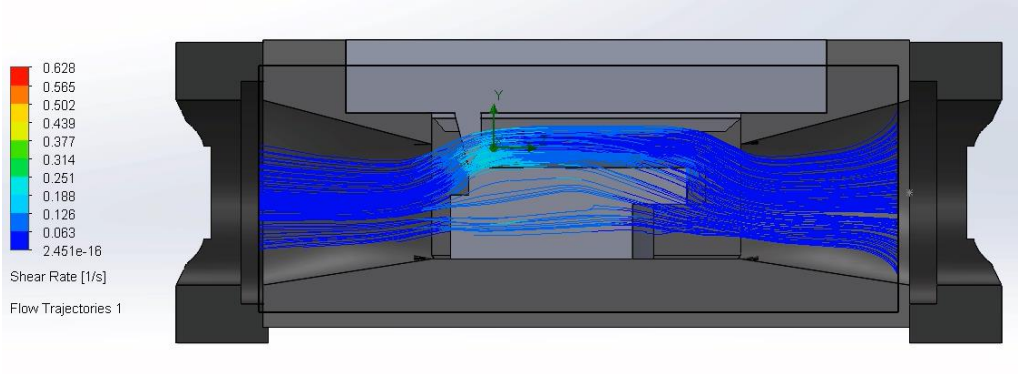

Figure 5.10: Side view of the test cell at 4 GPM flow rate and 90˚C testing temperature.

The simulations above show promising results for the performance of this new test cell, given that only a slight turbulence appeared within the cell. The turbulent areas in Figures 5.9 and 5.10 are the areas of color other than the dark blue laminar entry and exit flow such as the light blue, yellow and red regions in increasing order. The disruption of flow is mostly in the region where the fin is placed, so other options might need to be explored for keeping the part in

place with less flow disruption. Consistent flow is important so we can establish quantifiable and repeatable test data using this test cell.

Once the test lid dimensioning was finalized, the CAD models were sent to a third-party manufacturer. A prototype was made from a 3-D printed plastic polymer to verify the simulated results for leakage and testing viability shown in Figure 5.11. The prototype was made from a less costly material in case adjustments needed to be made to the current design after testing. Most of the other parts, such as the gaskets, clamping support rods and inserts, were also purchased to give a comprehensive idea of the system performance. Evaluation of the prototype is currently underway.

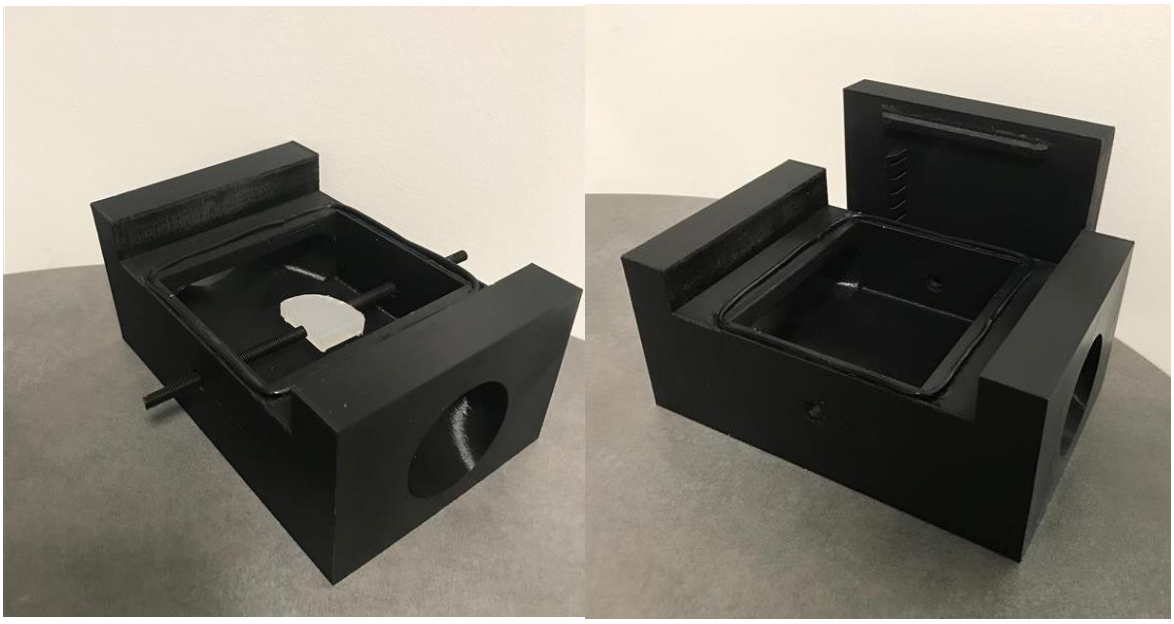

Figure 5.11: Prototype printed by a third-party manufacturer from the CAD model developed in house.

5.4 Results and Discussion

A new test cell was developed to accommodate the testing of real mechanical parts prone to varnish accumulation. Parts explored in this research were valves, bearing pads, and the continued use of test coupons. A design was created using the dimensions of example parts. This

research also included testing of the design using CAD modeling and a flow simulation. A prototype of the test cell was quoted and manufactured using 3D printed plastic. Next steps are currently being taken to determine viability using the test cell prototype and integrate the new test cell with the current test rig.

Chapter 6: Conclusion

6.1 Summary

Oxidation is an unavoidable consequence of lubricated mechanical systems and leads to varnish formation. Varnish is therefore a consistent issue in lubricated mechanical systems. Although varnish buildup can be mitigated, chemical flushes are required once varnish buildup reaches a critical point. Our research is targeted towards improving varnish removing chemical cleaners and evaluating their removal characteristics. Overall, we ran 260 hours of comparative testing for this project. This research allowed us to compare commercial cleaners, refine the test procedure, investigate the cause of discovered testing anomalies, design and prototype a new test cell to accommodate 3D test objects, and identify opportunities for future research. This research also provided a comprehensive characterization of thirteen commercial varnish fluids that will be useful in removal fluid selection and formulation in industry.

6.2 Future Work

6.2.1 Fluid Degradation

Fluid degradation is a natural effect of repeated use of any lubricant. In this research we attempted to determine when degradation begins for a select commercial cleaner and quantify its performance drop over time. Although there are many potential causes of this degradation, it is

clear from this investigation that repeated testing with the other fluids should be performed to fully characterize this phenomenon.

6.2.2 Varnish Darkening

This investigation considered both temperature and fluid absorption as independent variables in separate tests. Based on these tests, we concluded that it is likely that the fluid darkening phenomenon comes from fluid absorption into the coupon. Possible solutions are housing the varnish coupon in a base oil prior to testing to prevent further fluid absorption during testing or using the varnish code to compensate for this on the post-processing end. Both approaches should be explored in future work to improve the test process, particularly for fluids that removal little or moderate amounts of varnish.

6.2.3 New Test Cell Design

Next steps for the new test cell are physical testing with the prototype, including a seal test to ensure that the gaskets and clamps described will perform under operating flow rates. In addition, whether or not the test part is kept in place within the test cell using the method given in this paper should be tested. Then, a final version of the test cell can be manufactured and tested. Further, modifications to the existing testing procedure will need to be made to accompany the new test cell requirements. There may need to be adjustments made to the varnish removal code given the new method of testing. For example, a new lighting format may need to be developed now that there will be possible shading from certain protruding regions of the part.

6.2 Conclusions

Varnish can be detrimental to the performance of mechanical systems. Our research aims to characterize the removal of this varnish film to optimize system efficiency. The research in this paper provides information crucial to the selection of a commercial chemical cleaner and how to use them properly, such as not recycling fluid. The improvements to the test rig will allow for a more comparable testing to what might actually be seen in a chemical flushing environment.

‘

References

[1] Wang, Y., & Wang, Q. J. (2013). *Stribeck Curves BT - Encyclopedia of Tribology* (Q. J. Wang & Y.-W. Chung (eds.); pp. 3365–3370). Springer US. https://doi.org/10.1007/978-0-387-92897-5_148

[2] Ruano, P., Delgado, L. L., Picco, S., Villegas, L., Tonelli, F., Merlo, M., Rigau, J., Diaz, D., & Masuelli, M. (2016). Intech Open, 13. https://www.intechopen.com/books/advanced-biometric-technologies/liveness-detection-in-biometrics

[3] Airey, J., Spencer, M., Greenwood, R., & Simmons, M. (2020). The effect of gas turbine lubricant base oil molecular structure on friction. *Tribology International, 146*, 106052. doi:10.1016/j.triboint.2019.106052

[4] Barman, B. (2002). Behavioral differences between group I and group II base oils during thermo-oxidative degradation. *Tribology International - TRIBOL INT*, *35*, pp 15–26. https://doi.org/10.1016/S0301-679X(01)00073-1

[5] Mang, T. (Ed.). (2014). *PAO (Polyalphaolefine Oil) BT - Encyclopedia of Lubricants and Lubrication*, pp. 1291. Springer Berlin Heidelberg. https://doi.org/10.1007/978-3-642-22647-2_200328

[6] Pirro, D. M., Webster, M., & Daschner, E. (2016). Lubricating Oils. *Lubrication Fundamentals, 3*, pp 35-68. doi:10.1016/s0167-8922(97)80059-4

[7] Canter, N. (2009). Boundary Lubricity Additives. *Tribology & Lubrication Technology.* pp 10-18. https://www.stle.org/images/pdf/STLE_ORG/BOK/LS/Additives/Boundary%20Lubricity%20Additives_tlt%20article_Sept09.pdf

[8] Minami, I. (2017). Molecular science of lubricant additives. *Applied Sciences (Switzerland)*, *7*(5). https://doi.org/10.3390/app7050445

[9] Wang, Y., Liang, X., Shu, G., Wang, X., Bao, J., & Liu, C. (2014). Effect of lubricating oil additive package on the characterization of diesel particles. *Applied Energy*, *136*, pp. 682–691. https://doi.org/10.1016/j.apenergy.2014.09.054

[9] Synthetics, Select. “Oil Viscosity: The Basics.” *AMS Oil*, 2019, www.selectsynthetics.com/part-1--oil-viscosity---the-basics.html.

[10] Robinson, J., Zhou, Y., Bhattacharya, P., Erck, R., Qu, J., Bays, J., & Cosimbescu, L. (2016). Probing the molecular design of hyper-branched aryl polyesters towards lubricant applications. *Scientific Reports*, *6*, 18624. https://doi.org/10.1038/srep18624

[11] Yan, Y. (2019). Tribology and tribocorrosion testing and analysis of metallic biomaterials. Metals for Biomedical Devices, 213–234. https://doi.org/10.1016/B978-0-08-102666-3.00007-9

[13] Adhvaryu, A., Liu, Z., & Erhan, S. Z. (2005). Synthesis of novel alkoxylated triacylglycerols and their lubricant base oil properties. *Industrial Crops and Products*, *21*(1), 113–119. https://doi.org/https://doi.org/10.1016/j.indcrop.2004.02.001

[14] Minami, I. (2017). Molecular science of lubricant additives. *Applied Sciences (Switzerland)*, *7*(5). https://doi.org/10.3390/app7050445

[15] Guegan, J., Kadiric, A., Gabelli, A., & Spikes, H. (2016). The Relationship Between Friction and Film Thickness in EHD Point Contacts in the Presence of Longitudinal Roughness. *Tribology Letters*, *64*(3), 1–15. https://doi.org/10.1007/s11249-016-0768-6

[16] Martini, A., Ramasamy, U. S., & Len, M. (2018). Review of Viscosity Modifier Lubricant Additives. *Tribology Letters*, *66*(2), 58. https://doi.org/10.1007/s11249-018-1007-0

[17] Ver Strate, G., & Struglinski, M. J. (1991). Polymers as Lubricating-Oil Viscosity Modifiers. In Polymers as Rheology Modifiers (Vol. 462, pp. 15–256). American Chemical Society. https://doi.org/doi:10.1021/bk-1991-0462.ch015

[18] Subramanian, D., Wu, K., & Firoozabadi, A. (2015). Ionic liquids as viscosity modifiers for heavy and extra-heavy crude oils. *Fuel*, *143*, 519–526. https://doi.org/https://doi.org/10.1016/j.fuel.2014.11.051

[19] Ghosh, P., & Das, M. (2014). Study of the influence of some polymeric additives as viscosity index improvers and pour point depressants – Synthesis and characterization. *Journal of Petroleum Science and Engineering*, *119*, 79–84. https://doi.org/https://doi.org/10.1016/j.petrol.2014.04.014

[20] Feng, L., Zhang, Z., Wang, F., Wang, T., & Yang, S. (2014). Synthesis and evaluation of alkyl acrylate-vinyl acetate-maleic anhydride terpolymers as cold flow improvers for diesel fuel. *Fuel Processing Technology*, *118*, 42–48. https://doi.org/https://doi.org/10.1016/j.fuproc.2013.08.005

[21] Tang, Z. (2019). A review of corrosion inhibitors for rust preventative fluids. *Current Opinion in Solid State and Materials Science*, *23*(4), 100759. https://doi.org/https://doi.org/10.1016/j.cossms.2019.06.003

[22] Jardine, F., "ENGINE CORROSION-ITS CAUSES AND AVOIDANCE," SAE Technical Paper 250030, 1925, https://doi.org/10.4271/250030.

[23] Ren, G., Zhang, P., Ye, X., Li, W., Fan, X., & Zhu, M. (2021). Comparative study on corrosion resistance and lubrication function of lithium complex grease and polyurea grease. *Friction*, *9*(1), 75–91. https://doi.org/10.1007/s40544-019-0325-z

[24] Aliofkhazraei, M. (2014). *Developments in Corrosion Protection*. IntechOpen. https://books.google.com/books?id=MSqhDwAAQBAJ

[25] Chauhan, D. S., Quraishi, M. A., Ansari, K. R., & Saleh, T. A. (2020). Graphene and graphene oxide as new class of materials for corrosion control and protection: Present status and future scenario. *Progress in Organic Coatings*, *147*, 105741. https://doi.org/https://doi.org/10.1016/j.porgcoat.2020.105741

[26] Papay, A. G. (1998). Antiwear and Extreme-Pressure Additives in Lubricants. *Lubrication Science*, *10*(3), 209–224. https://doi.org/10.1002/ls.3010100304

[27] ASM International (2019). The Effects and Economic Impact of Corrosion. *Corrosion: Understanding the Basics*, 1–20. https://doi.org/10.31399/asm.tb.cub.t66910001

[28] Seddon E., Friend C., Roski J. (2010) Detergents and Dispersants. In: Mortier R., Fox M., Orszulik S. (eds) *Chemistry and Technology of Lubricants*. Springer, Dordrecht. https://doi.org/10.1023/b105569_7

[29] Colyer C.C., Gergel W.C. (1994) Detergents/dispersants. In: Mortier R.M., Orszulik S.T. (eds) Chemistry and Technology of Lubricants. Springer, Boston, MA. https://doi.org/10.1007/978-1-4615-3554-6_3

[30] Abdel-Hameed, H., Ahmed, N., & Nassar, A. (2015). *Some Ashless Detergent/Dispersant Additives for Lubricating Engine Oil*.

[31] Hammond, S., Price, M. A., & Skinner, P. (2003). *Overbased detergent additives*. *2*(12), 4–9. https://patents.google.com/patent/US6599867

[32] Stover, J. (2019). Oil Cleanliness in Wind Turbine Hydraulic Pitch Systems. *Hydraulic System Cleanliness*, (May). doi:10.1520/stp44722s

[33] Coiclough, T. (1987). Role of Additives and Transition Metals in Lubricating Oil Oxidation. *Industrial and Engineering Chemistry Research*, *26*(9), 1888–1895. https://doi.org/10.1021/ie00069a028

[34] Huang, W., Tan, Y., Chen, B., Dong, J., & Wang, X. (2003). The binding of antiwear additives to iron surfaces: quantum chemical calculations and tribological tests. *Tribology International*, *36*(3), 163–168. https://doi.org/https://doi.org/10.1016/S0301-679X(02)00130-5

[35] Spikes, H. (2008). Low- and zero-sulphated ash, phosphorus and sulphur anti-wear additives for engine oils. *Lubrication Science*, *20*(2), 103-136. doi:10.1002/ls.57

[36] Model, M., Braun, R. L., Burnham, A. K., Livermore, L., & Box, P. O. (1990). *Mathematical model of oil generation, degradation, and expulsion*. *4*, 132–146. https://doi.org/10.1021/ef00020a002

[37] Du, Y., Wu, T., & Gong, R. (2017). Properties of water-contaminated lubricating oil: variation with temperature and small water content. *Tribology - Materials, Surfaces & Interfaces*, *11*(1), 1–6. https://doi.org/10.1080/17515831.2017.1279845

[38] Du, Y., Wu, T., & Gong, R. (2017). Properties of water-contaminated lubricating oil: variation with temperature and small water content. *Tribology - Materials, Surfaces & Interfaces*, *11*(1), 1–6. https://doi.org/10.1080/17515831.2017.1279845

[39] M. Taghvaei and S. M. Jafari, "Application and stability of natural antioxidants in edible oils in order to substitute synthetic additives," *J. Food Sci. Technol.*, vol. 52, no. 3, pp. 1272–1282, 2015.

[40] Stadtmiller, W. H., and Andrew N. Smitli. *Aspects of Lubricant Oxidation*. ISBN 0-8031-0482-0, American Society for Testing and Materials, 1986.

[41] Mujahid, A., & Dickert, F. L. (2012). Monitoring automotive oil degradation: analytical tools and onboard sensing technologies. *Analytical and Bioanalytical Chemistry*, *404*(4), 1197–1209. https://doi.org/10.1007/s00216-012-6186-1

[42] Johnson, M., & Livingstone, G. (n.d.). *Identifying varnish and oxidation precursors in lubricant sumps*.

[43] Canter, N. (2007). Spark discharges and varnish formation. *Tribology & Lubrication Technology*, *63*(11), 8–9. https://search.proquest.com/scholarly-journals/spark-discharges-varnish-formation/docview/226972300/se-2?accountid=14515

[44] Fitch, Jim. “Using Oil Analysis to Control Varnish and Sludge.” *Machinery Lubrication*, vol. 59, 18 June 2019, pp. 1–10.

[45] Pumps, G. (n.d.). *applied sciences Analysis of Dimensional Tolerances on Hydraulic and Acoustic Properties of a New Type of Prototypal Gear Pumps*.

[46] Needelman, W. M., & Madhavan, P. V. (1988). *Review of Lubricant Contamination and Diesel Engine Wear*. SAE International . https://doi.org/10.4271/881827

[47] Wong, V. W., & Tung, S. C. (2016). Overview of automotive engine friction and reduction trends–Effects of surface, material, and lubricant-additive technologies. *Friction*, *4*(1), 1–28. https://doi.org/10.1007/s40544-016-0107-9

[48] N. Truong, “Today‘s Varnish Control Technologies,” 2019. [Online]. Available: https://www.machinerylubrication.com/Articles/Print/1111.

[49] D. A. Johnson, “CHARACTERIZING CHEMICAL CLEANERS USED IN REMOVING VARNISH IN GAS TURBINE ENGINES,” 2018.

[50] Revina, D. V, & Novikova N.A., N. G. L. (1981). *Producing a varnish based on coking industry products to protect equipment against corrosion*. https://www.osti.gov/biblio/5522352

[51] CMYK color charts and values. (2003). Retrieved from https://mixam.com/support/cmykchart

[52] Mathanraj, S. (2019). Histograms in Image Processing with Skimage-Python. *Image Processing and Acquisition Using Python, November*, 3-21. doi:10.1201/9780429243370-1

[53] Baibing, Y., Chunming, X. U., Suoqi, Z., Samuel, H. S. U. C., & H, C. K. (2013). *Thermal transformation of acid compounds in high TAN crude oil*. *56*(July). https://doi.org/10.1007/s11426-013-4897-6

[54] Morinaga, M. “Varnish and Sludge, the Hidden Oil Pollutants.” *RRR*, 2016, www.triple-r-europe.com/sludge.

[55] K. Farooq, “Varnish Removal and Control in Turbine Lubrication Systems,” pp. 281–287, 2010.

[57] Fitch, J., Gebarin, S. (2008), "Review of degradation mechanisms leading to sludge and varnish in modern turbine oil formulations," Oxidation and the Testing of Turbine Oils, eds. Migdal, C, Wardlow, A., Ameye, J., (West Conshohocken, PA; ASTM International).

[58] Chen, L., Dong, J., and Chen, G. (1997), "The Study of Tribo-Induced Deposits from a Copper-Containing Antiwear Additive," Tribology Transactions, 40(2), pp 339–345.

[59] Stover, J. (2008). Adsorption: A simple and cost-effective solution to remove varnish. *Practicing Oil Analysis, 10*(3–4).

[60] Von Fuchs, G. H., Diamond, H. (1942), "Oxidation Characteristics of Lubricating Oils," Ind. Eng. Chem., 34(8), pp 928–937.

[61] Zuidema, H. H. (1946), "Oxidation of lubricating oils*,"* Chem. Rev., 38(2), pp 197–226.

[62] Phillips, W. D. (2006), "The high-temperature degradation of hydraulic oils and fluids," J. Synthetic Lubr., 23(1), pp 39–70.

[63] Fan, M., Yang, D., Wang, X., Liu, W., Fu, H. (2014), "$DOSS^{-}$ Based QAILs: As Both Neat Lubricants and Lubricant Additives with Excellent Tribological Properties and Good Detergency*,"* Ind. Eng. Chem. Res., 53(46) , pp 17952–17960.

[64] Yano, A., Watanabe, S., Miyazaki, Y., Tsuchiya, M., Yamamoto Y. (2004), "Study on sludge formation during the oxidation process of turbine oils," Tribol. Trans., 47(1), pp 111-122.

[65] Sniderman, D. (2015), "Varnish contamination in hydraulic & lube oil systems," Tribol. Lubr. Technol., 71(11), pp 24-30.

[66] Kon, T., Honda, T., Sasaki, A. (2020), "Estimation of the Oxidative Deterioration of Turbine Oil Using Membrane Patch Color," Adv. Tribol., 2020, Article ID 1708408, pp 1-8.

[67] VanRensselar, J. (2016), "The unvarnished truth about varnish," Tribol. Lubr. Technol., 72 (11), 26.

[68] Farooq, K. (2010), "Turbine lubrication fluid varnish mitigation," Power Plant Chemistry, 12(4), pp 232–239.

[69] Liu, Z., Wang, H., Zhang, L., Sun, D., Cheng, L., Pang, C. (2016), "Composition and degradation of turbine oil sludge," J. Therm. Anal. Calorim., 125, pp 155-162.

[70] Newley, R. A, Spikes, H. A., Macpherson, P. B. (1980), "Oxidative wear in lubricated contact," J. Lubric. Tech., 102(4), pp 539–544.

[71] Lantz, S., Zakarian, J., Deskin, S., Martini, A. (2017), "Filtration Effects on Foam Inhibitors and Optically Detected Oil Cleanliness," Tribology Transactions, 60 (6), pp 1159-1164.

[72] Santos, J. C. O., Garcia Dos Santos, I. M., Souza, A. G., Sobrinho, E. V., Fernandes, V. J., & Silva, A. J. N. (2004). Thermoanalytical and rheological characterization of automotive mineral lubricants after thermal degradation. *Fuel*, *83*(17–18), 2393–2399. https://doi.org/10.1016/j.fuel.2004.06.016

[73] N. Truong and N. Corporation, "Today ' s Varnish Control Technologies," 2019. [Online]. Available: https://www.machinerylubrication.com/Articles/Print/1111.

[74] Fitch, J. C., & Gebarin, S. (2008). Review of degradation mechanisms leading to sludge and varnish in modern turbine oil formulations. *ASTM Special Technical Publication*, *1489 STP*(8), 54–63. https://doi.org/10.1520/stp45724s

[75] Kaihlanen, K. (2016), "Varnish contamination in hydraulic & lube oil systems*,"* Tribol. Lubr. Techno, 72(11), pp 68-71.

[76] Livingstone, G. J., Thompson, B. T., Okazaki, M. E. (2007) "Physical, performance, and chemical changes in turbine oils from oxidation," J. ASTM Int., 4(1), pp 27–44.

[77] Sasaki, A., Uchiyama, S., Kawasaki, M. (2008) "Varnish formation in the gas turbine oil systems," J. ASTM Int., 5(2), pp 2–7.

[78] Johnson, D. A., Dominguez, E., Montalvo, E., Zhou, Z., Martini, A. (2018), "Quantifying Varnish Removal Using Chemical Flushes," Tribol. Trans., 61 (6), pp 1067-1073.

[79] Carr. (n.d.). Retrieved January 12, 2021, from https://www.mcmaster.com/shims

Appendix

A.1 Matlab Visual Analysis Code

```
(1) %% Initialization
clc; close all; format shortG;

if exist('nfiles')
    ClearAll = input('C to clear all data and re-set rectangles, any
other key to use last rectangles.  ','s');
else
    ClearAll = 'C';
end

if ( upper(ClearAll) == 'C' )
    clearvars -EXCEPT ImageDir;
    if exist('ImageDir')
        ImageDir = uigetdir(ImageDir,'Select Folder With Varnish Test
Image Files');
    else
        ImageDir = uigetdir(pwd,'Select Folder With Varnish Test Image
Files');
    end
    splitdir = split(ImageDir,'\');
    LastDir = splitdir{length(split(ImageDir,'\'))};
    imagefiles = dir([ImageDir,'\','*.jpg']);
(2) % finds all jpgs in the current file
    nfiles = length(imagefiles);     % find how many
    TimeValues = zeros(nfiles,1);
 % create a nfiles x 1 matrix to store time

 %% Store time, assuming first file is at time 0 and file number
indices are DeltaTime apart
    DeltaTime = .002777777;              % Initial time [hr]
    for i = 1:nfiles
        TimeValues(i) = DeltaTime*(i);
    end

(3) %% Crop images as the references for the analysis
% First image should be the most varnished one (earliest in time
sequence)
    A = imread([imagefiles(1).folder,'\',imagefiles(1).name]);
% read image 1
%% Crop images as the references for the analysis
% First image should be the most varnished one (earliest in
time sequence)
```

```
    A =
imread([imagefiles(1).folder,'\',imagefiles(1).name]);
% read image 1
    I = imcrop(A,[Xmin Ymin Width Height]); % crop image to
fit screen
    sCont = 'R';
%Prompts user to select varnish, and steel crop retangles
using drag box
    while ( upper(sCont) == 'R' )
        fprintf(1,'Draw a rectangle around the varnished
area. Make any adjustments. Double-click inside the area
when done.\n');
% Varnish crop 1) drag box 2) double click in box to move
to next crop.
        [Varnish1,rect1] = imcrop(I)
% crop image using drag boxes
        fprintf(1,'Draw a rectangle around the left-side
clean steel area. Make any adjustments. Double-click inside
the area when done.\n');
% Left/Steel Crop  1) drag box 2) double click in box to
move to next crop.
        [steelcropL,rect2] = imcrop(I);

% Display cropped images for inspection
        figure()
        subplot(2,2,1:2); image(Varnish1)
        subplot(2,2,3);   image(steelcropL)

% prompt to contine to test analysis or re-select
rectangles
        prompt = 'R to re-select rectangles, Q to quit, any
other key to continue: ';
        sCont = input(prompt,'s');
        if ( upper(sCont) == 'Q' )
            return;
        end
    end

    AveRawColors = zeros(nfiles,10);

(4) % prompt to continue to test analysis
        prompt = 'R to re-select rectangles, Q to quit, any other key
to continue: ';
        sCont = input(prompt,'s');
        if ( upper(sCont) == 'Q' )
```

```
            return;
        end
    end


%% Conduct image processing by looping over all image files in the
directory
    close All;
    for k = 1:nfiles
        currentfilename =
[imagefiles(k).folder,'\',imagefiles(k).name];               % current
file name
        currentimage = imread(currentfilename);             % current
image % crop image to fit varnish and steel
        I = imcrop(currentimage,[Xmin Ymin Width Height]);  % crop
each image in sequence to fit varnish and steel
        Vcrop = imcrop(I,rect1);                            % crop
image to fit varnish
        Scrop = imcrop(I,rect2);                            % crop
image to fit steel on left

        VarnishColors = reshape(mean(mean(Vcrop)),[1,3]);
        SteelColors = reshape(mean(mean(Scrop)),[1,3]);
        if ( k == 1 )
            SteelColors1 = SteelColors;
        end
        % 1st row is time,
        % rows 2-4 are average varnish colors in the varnish rectangle
        % rows 5-7 are average steel colors in the steel rectangle
        % rows 8-10 are the varnish colors shifted by how much the
steel colors
        % have shifted from the first image
        AveRawColors(k,:) = [TimeValues(i), ...
                             VarnishColors, ...
                             SteelColors, ...
                             VarnishColors - (SteelColors -
SteelColors1) ];
        fprintf(1,['Working on file
%',num2str(floor(1+log10(nfiles))),'d of
%',num2str(floor(1+log10(nfiles))),'d %3.0f%% (%s)\n'], k, nfiles,
100*k/nfiles, imagefiles(k).name) % show progress
    end
end

(5)% Find Max and Min values to use in mapping colors to values from 0
% (steel) to 1 (varnish)
MaxRGB = max(AveRawColors);
MinRGB = min(AveRawColors);
AdjNormColors = zeros(nfiles,3);


% Normalized steel color vector
```

```
NormSteel = [];
for k=1:nfiles
    NormSteel(k,:) = AveRawColors(k,1:2)/norm(AveRawColors(k,1:2));
end
% Color dot product to see how close varnish is to steel
ColorDot = [];
for k = 1:nfiles
    ColorDot(k) = NormSteel(k,1)*AveRawColors(k,8) +
NormSteel(k,2)*AveRawColors(k,9) + NormSteel(k,3)*AveRawColors(k,10);
end
% highest steel*steel value
SteelDot = NormSteel(k,1).*AveRawColors(:,5) +
NormSteel(k,2).*AveRawColors(:,6) + NormSteel(k,2).*AveRawColors(:,7);

% map ColorDot from 0 (at cleanest, Steel*Steel) to 1 (at most
varnished, Steel*StartingVarnish)
MinDot = min(ColorDot); % most varnished, mapping to 1
MaxSteelDot = max(SteelDot); % cleanest, mapping this to 0
DotSlope = (0-1)/(MaxSteelDot-MinDot);
DotInt = 0 - DotSlope*MaxSteelDot;
NormColorDot = DotSlope*ColorDot + DotInt;

(6) % graphing
figure(2);
plot(TimeValues(1:nfiles),NormColorDot,'m-d');
grid on;
title('Normalized Varnish Dotted with Steel');
xlabel('time (hours)');
ylabel('mapped dot product');
ylim([0,1]);

figure(3);
plot(TimeValues(1:nfiles),ColorDot,'m-d');
grid on;
title('Varnish Dotted with Steel');
xlabel('time (hours)');
ylabel('dot product');


fid = fopen('DotVarnish.txt','w');
fprintf(fid,'Image file\ttime\tRaw Varnish Red\tRaw Varnish Green\tRaw
Varnish Blue\tRaw Steel Red\tRaw Steel Green\tRaw Steel Blue\tDot
Product\n');
for k = 1:nfiles
    fprintf(fid,'%s\t%f\n', ...
        imagefiles(k).name, ...
        NormColorDot(k));
end
fclose(fid);
```

A.2 Results by Fluid

A.2.1 C1

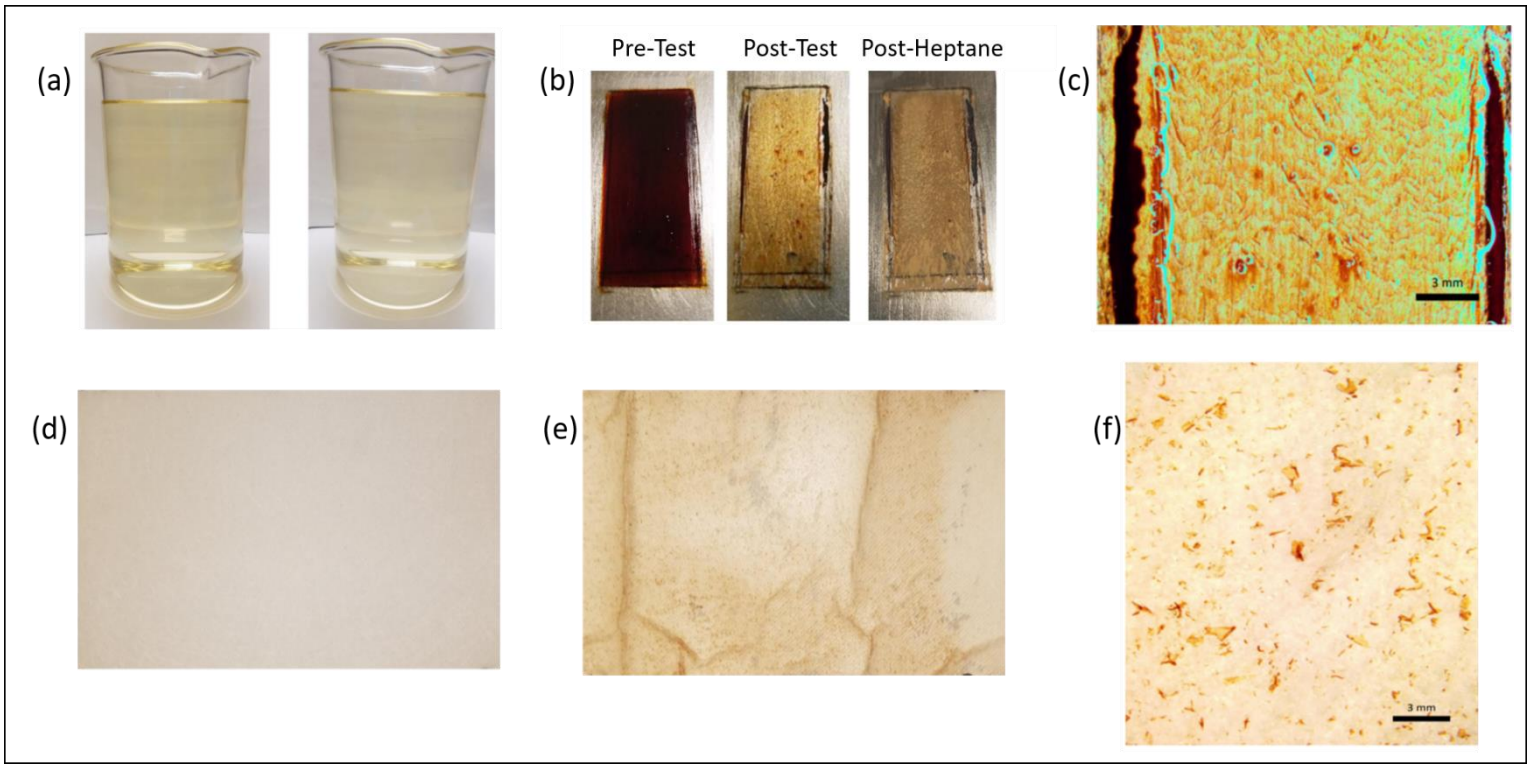

Figure A.1: (a)Pre-Test & Post Test fluid. (b)Pre-Test &Post-Test coupons. (c)Post-Test coupon at 10X magnification. (d) Pre-Test filter untouched by fluid. (e)Post-Test filter. (f)Post-Test filter at 10X magnification.

The first set of images gives qualitative information about the various fluids and their removal properties. In Figure A.1(a) the images of Pre-Test and Post-Test varnish removal fluid show that is has a clear color with a slight yellow tint. Not much changes in the fluid composition from the pre to the post-test image. The Pre-Test varnish on the coupon, in Figure 5(b), presents as the normal rectangular deposit and has normal coloring/composition. The Post-Test and Post-Heptane images show significant removal of the dark deposit of varnish. However, the fluid does not remove the varnish down to the level of the steel, it leaves behind a thin film of varnish still adhered to the coupon. This is corroborated by the microscope image of the coupon, Figure 5(c), which shows that parts of the thin film are thicker than others, but there is still a distinct varnish deposit on the coupon. When comparing A.1(d) and (e), the Pre and Post-Test images of the oil filter that is downstream of the test cell for analysis and to prevent the

spread of varnish particles throughout the system. The filter is designed to mimic the actual downstream filter in a system and particles size and amounts captured in the post test images assist in the characterization of various removal fluids and their properties.

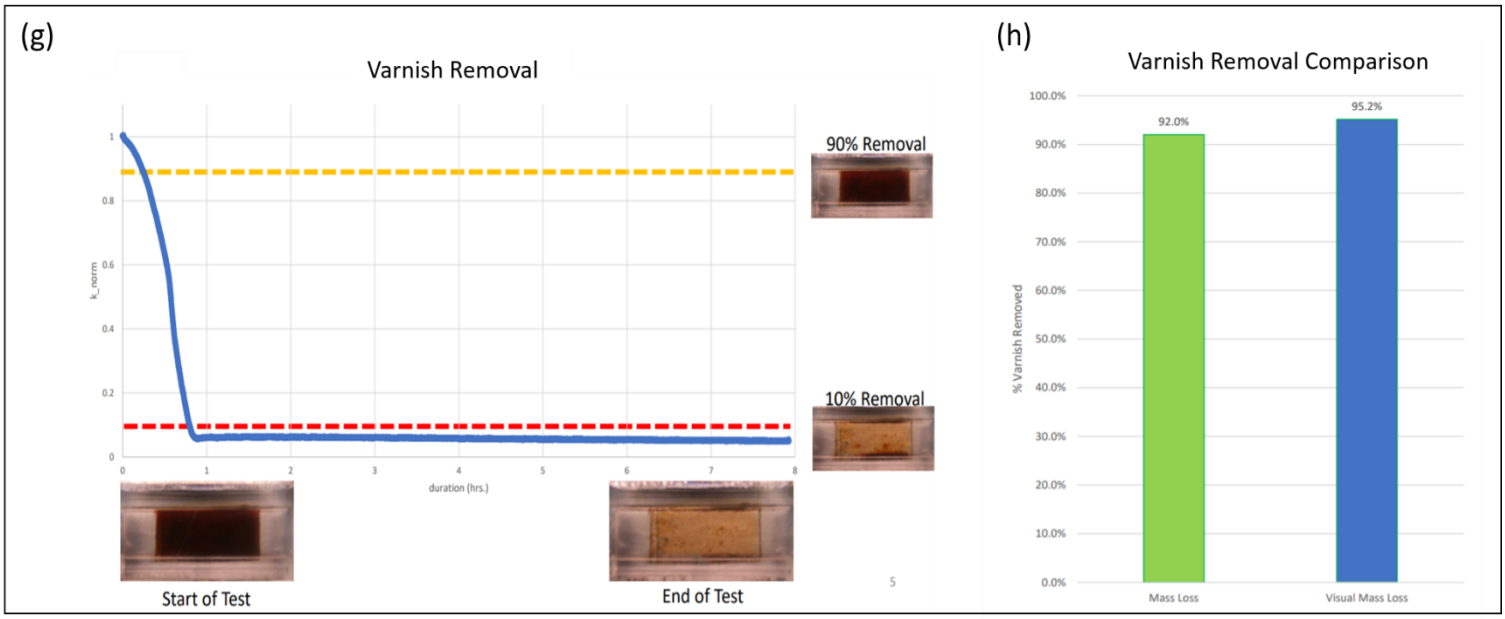

Figure A.2: Varnish Removal (g) Percent varnish removed vs. time plot. (h) Comparison of visual analysis data and actual measured mass loss.

The set of graphs in Figure A.2 (g) give quantitative data about both the fluid's removal capability and a comparison between the visual mass loss data generated utilizing our in-house visual analysis program. We track both the time to 90% removal, the time that it takes for the fluid to remove 10% of the varnish on the coupon, as well as the 10% removal. In Figure A.2 The y-axis of the removal vs. time graph represents the amount of varnish that remains on the coupon as it is being removed in situ. This is calculated using our visual analysis software. As can be seen from Fluid 1 is what is considered to be a good remover because it removes more than 90% of the original quantity of varnish on the coupon. This can now be compared with the start of test and end of test images below the graph for a more tangible view of what the results of a good remover will be, which does not necessitate full removal. The bar graph (h) for the

removal comparison compares the tangible mass loss to the visual mass loss from (g). Because fluid 1 is a good remover and the fluid is rather clear the comparison between the actual mass loss and the visual mass loss is extremely close. Darker fluids make it harder for the code to analyze the camera images as the fluid removes.

A.2.2 C2

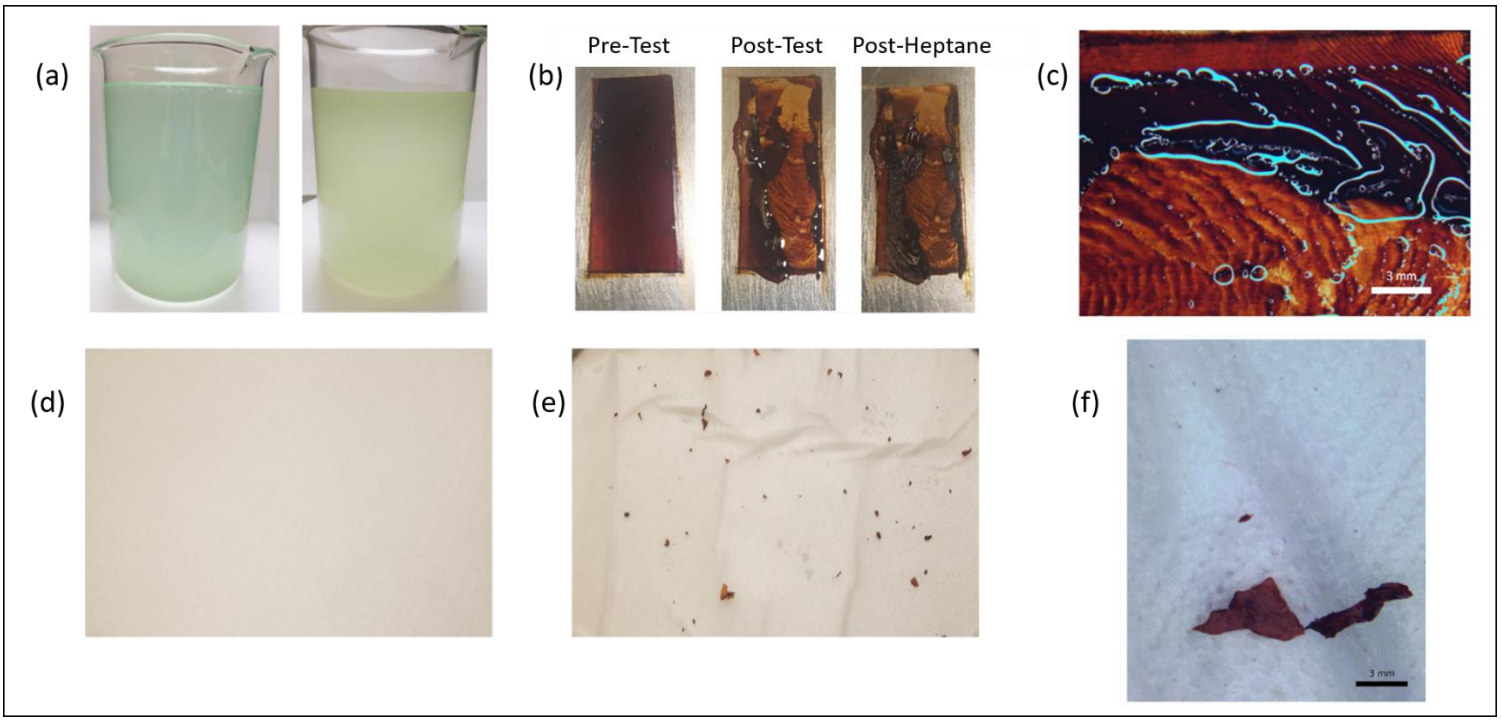

Figure A.3: (a) Pre-Test & Post Test fluid. (b) Pre-Test &Post-Test coupons. (c) Post-Test coupon at 10X magnification. (d) Pre-Test filter untouched by fluid. (e) Post-Test filter. (f) Post-Test filter at 10X magnification.

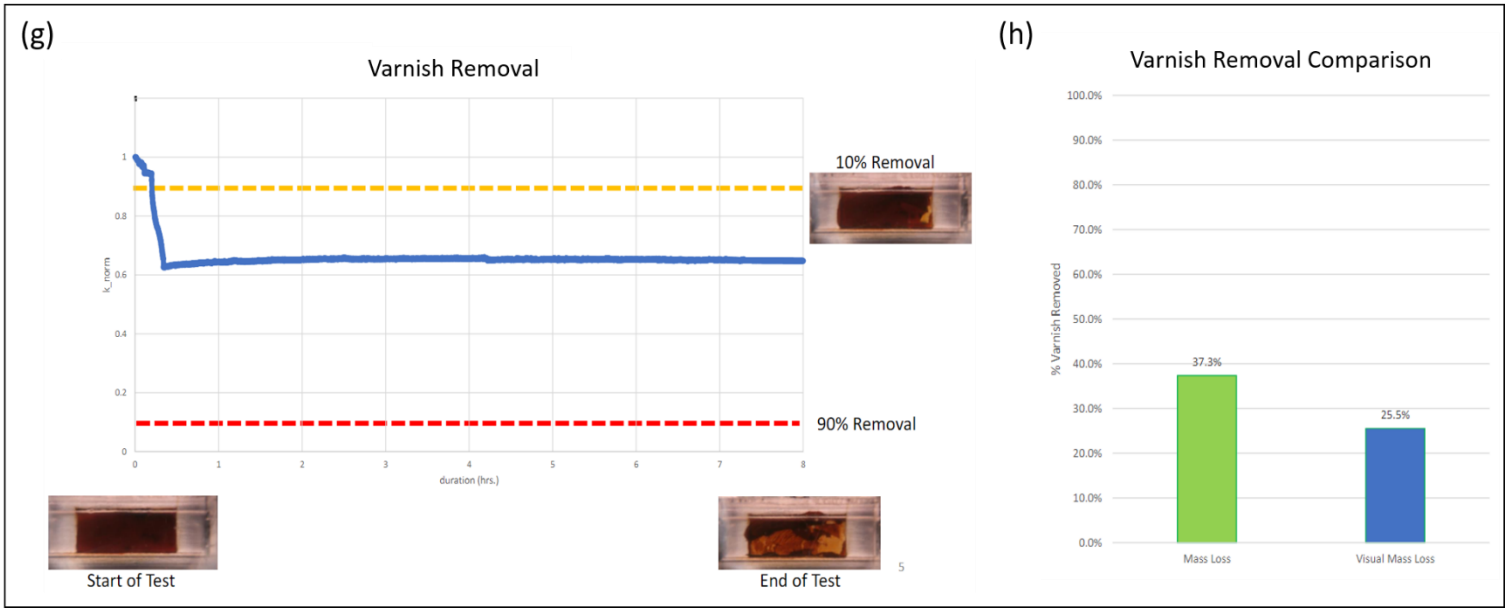

Figure A.4: Varnish Removal (g) Percent varnish removed vs. time plot. (h) Comparison of visual analysis data and measured mass loss.

A.2.3 C3

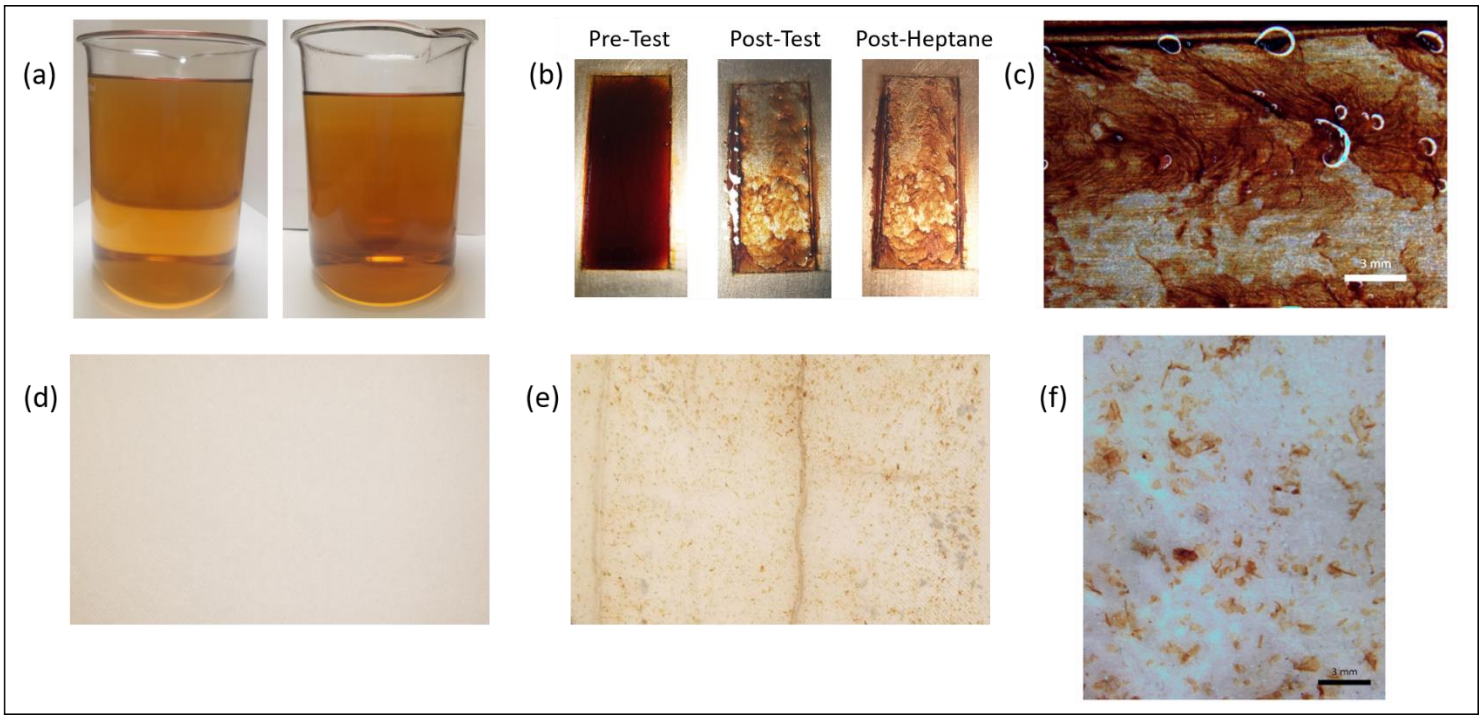

Figure A.5: (a) Pre-Test & Post Test fluid. (b) Pre-Test &Post-Test coupons. (c) Post-Test coupon at 10X magnification. (d) Pre-Test filter untouched by fluid. (e) Post-Test filter. (f) Post-Test filter at 10X magnification.

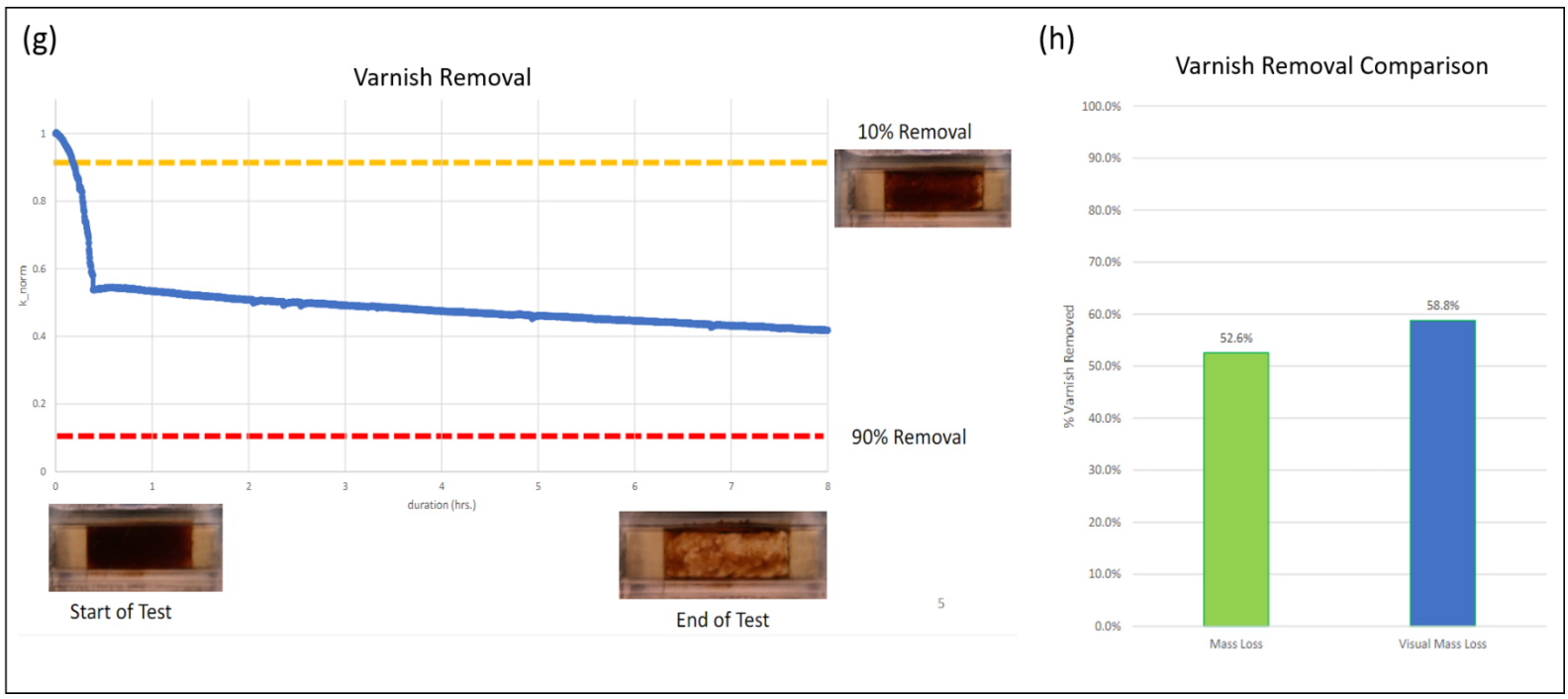

Figure A.6: Varnish removal data (g) Percent varnish removed vs. time plot. (h) Comparison of visual analysis data and actual measured mass loss.

A.2.4 C4

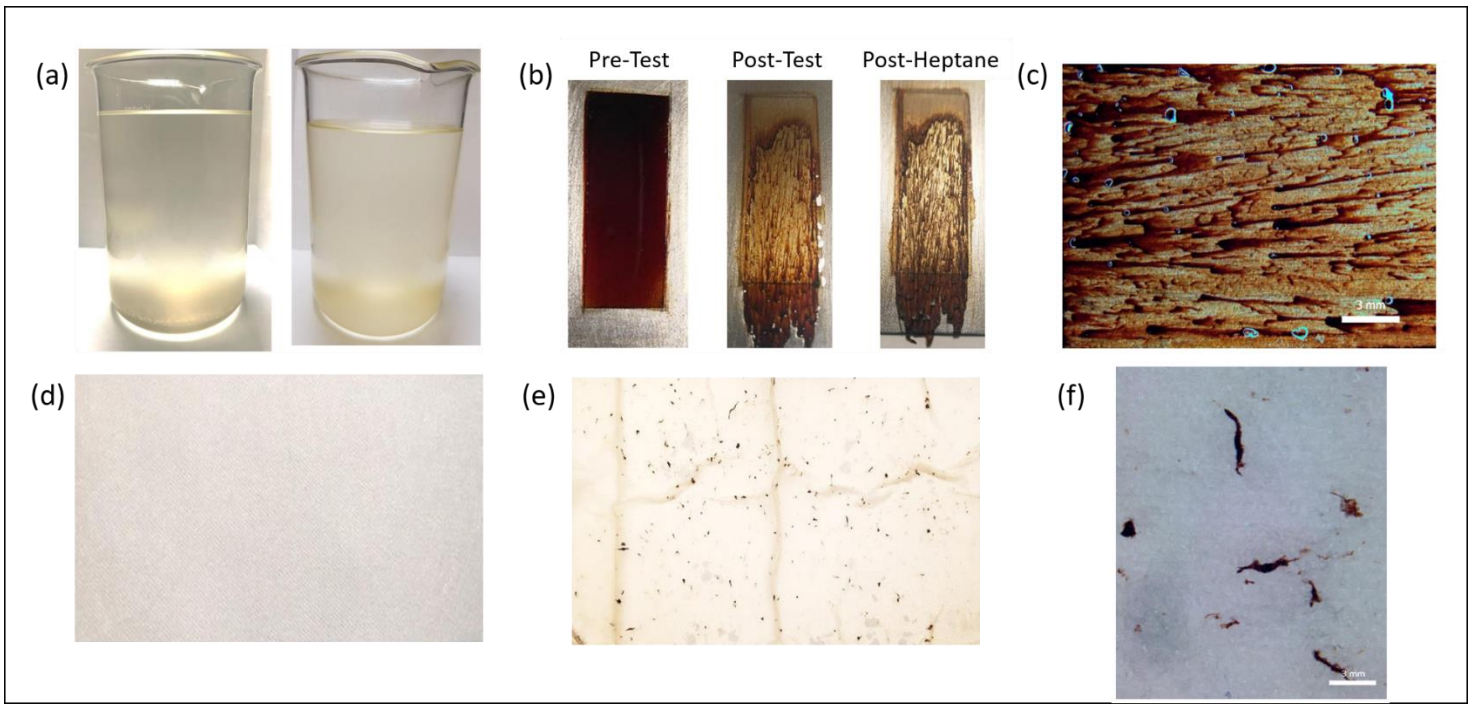

Figure A.7: (a) Pre-Test & Post Test fluid. (b) Pre-Test &Post-Test coupons. (c) Post-Test coupon at 10X magnification. (d) Pre-Test filter untouched by fluid. (e) Post-Test filter. (f) Post-Test filter at 10X magnification.

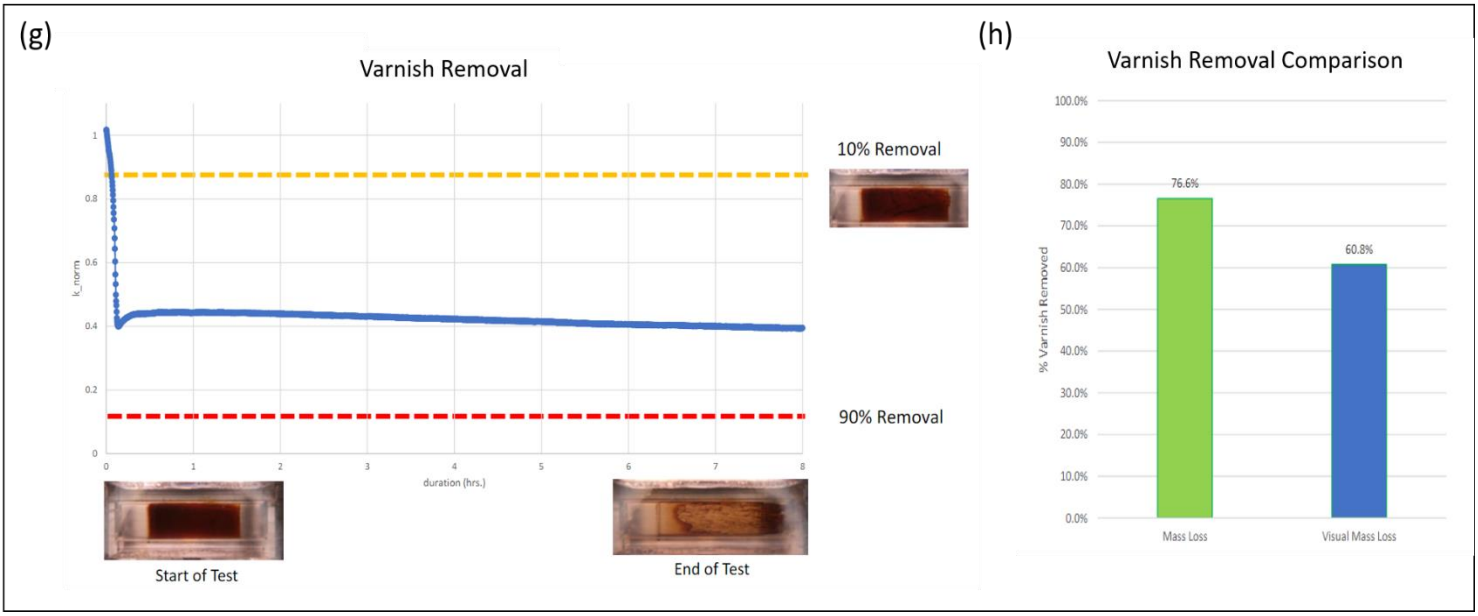

Figure A.8: Varnish removal data (g) Percent varnish removed vs. time plot. (h) Comparison of visual analysis data and actual measured mass loss.

A.2.5 C5

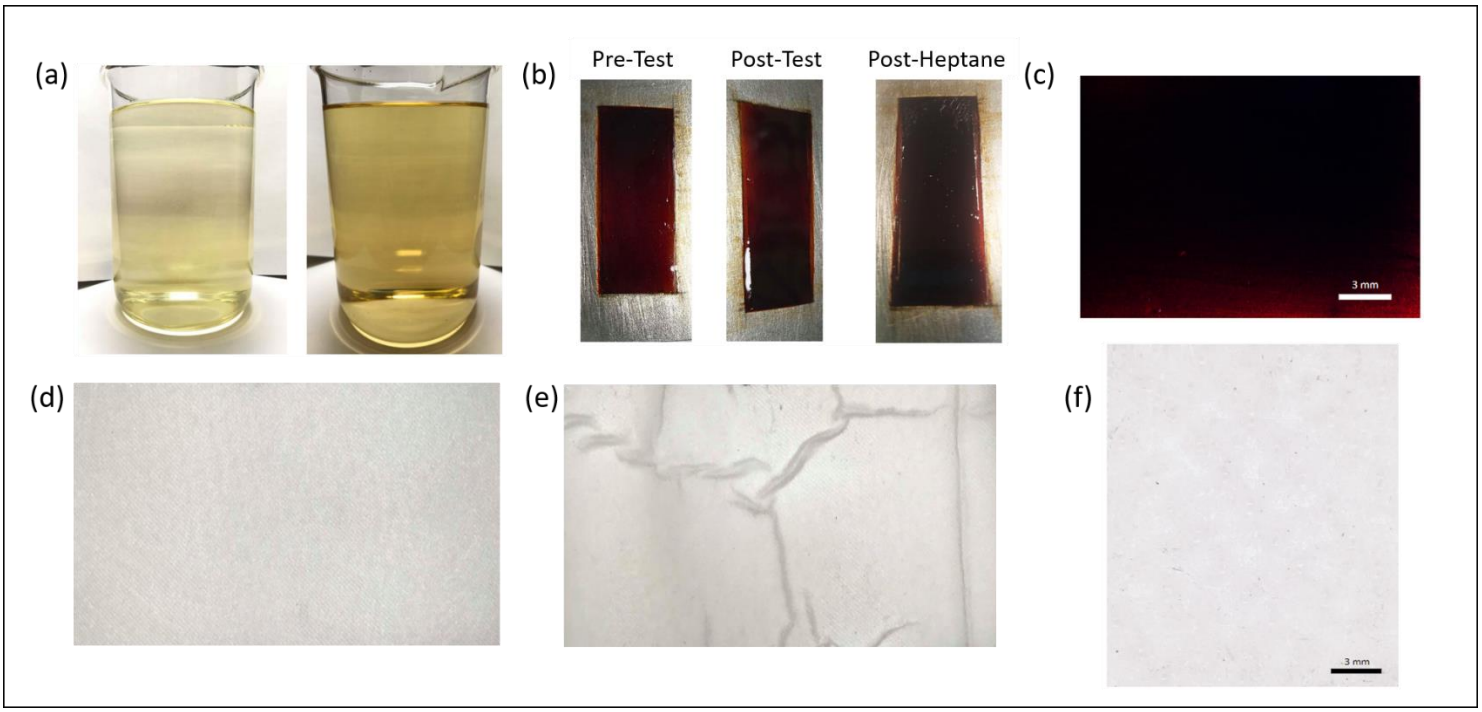

Figure A.11: (a) Pre-Test & Post Test fluid. (b) Pre-Test &Post-Test coupons. (c) Post-Test coupon at 10X magnification. (d) Pre-Test filter untouched by fluid. (e) Post-Test filter. (f) Post-Test filter at 10X magnification.

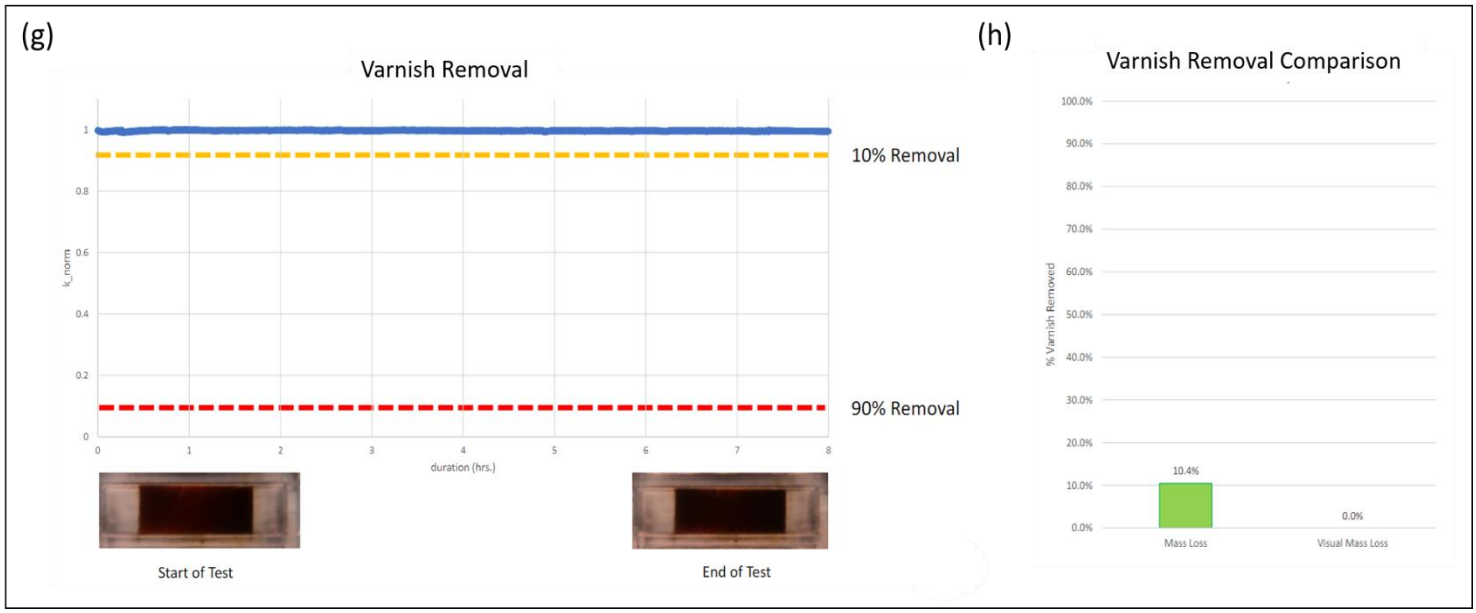

Figure A.12: Varnish removal data (g) Percent varnish removed vs. time plot. (h) Comparison of visual analysis data and actual measured mass loss.

A.2.6 C6

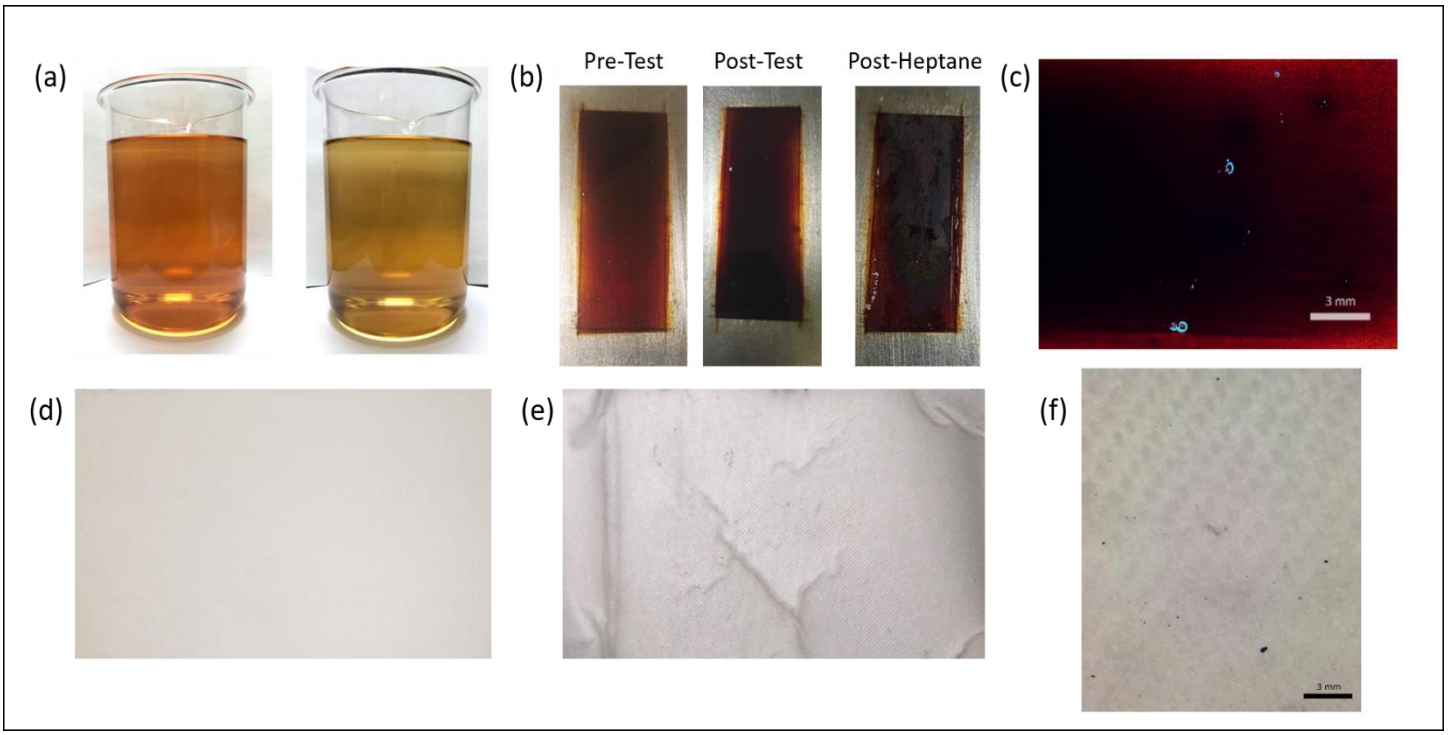

Figure A.13: (a) Pre-Test & Post Test fluid. (b) Pre-Test &Post-Test coupons. (c) Post-Test coupon at 10X magnification. (d) Pre-Test filter untouched by fluid. (e) Post-Test filter. (f) Post-Test filter at 10X magnification.

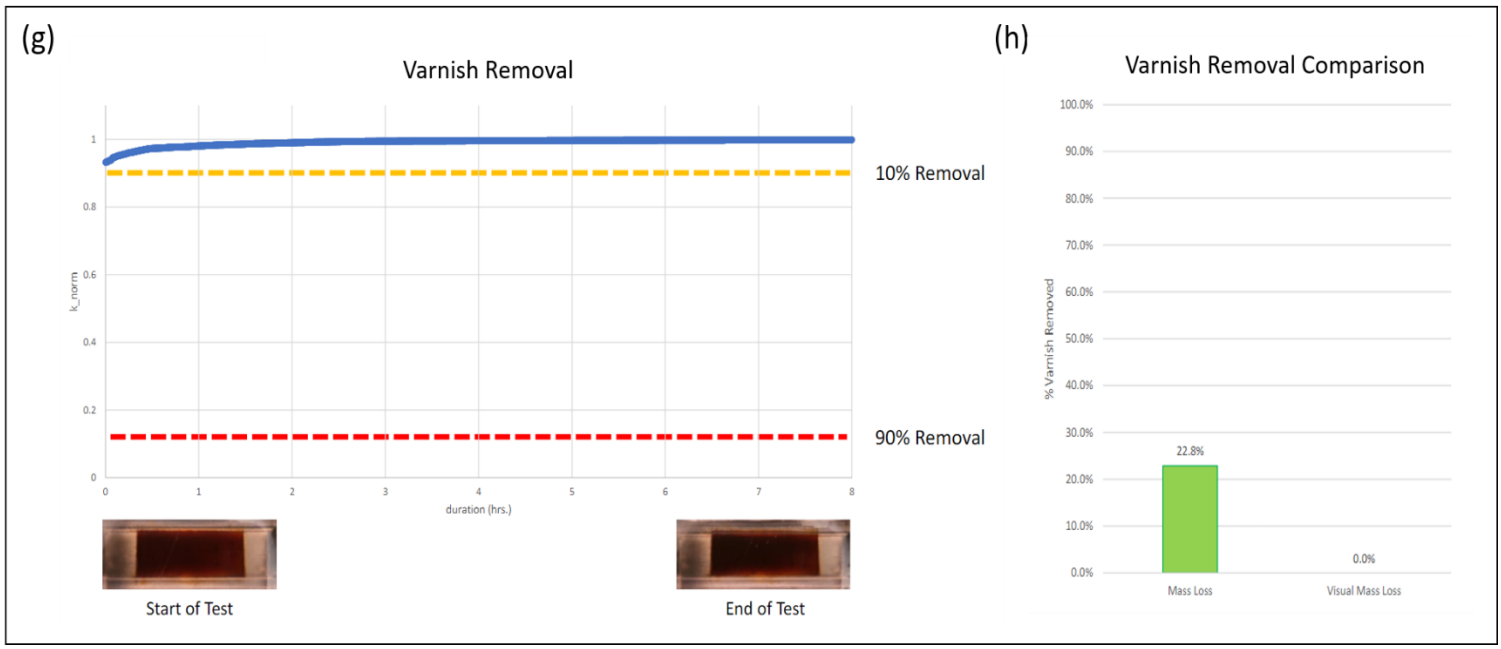

Figure A.14: Varnish removal data (g) Percent varnish removed vs. time plot. (h) Comparison of visual analysis data and actual measured mass loss.

A.2.7 C7

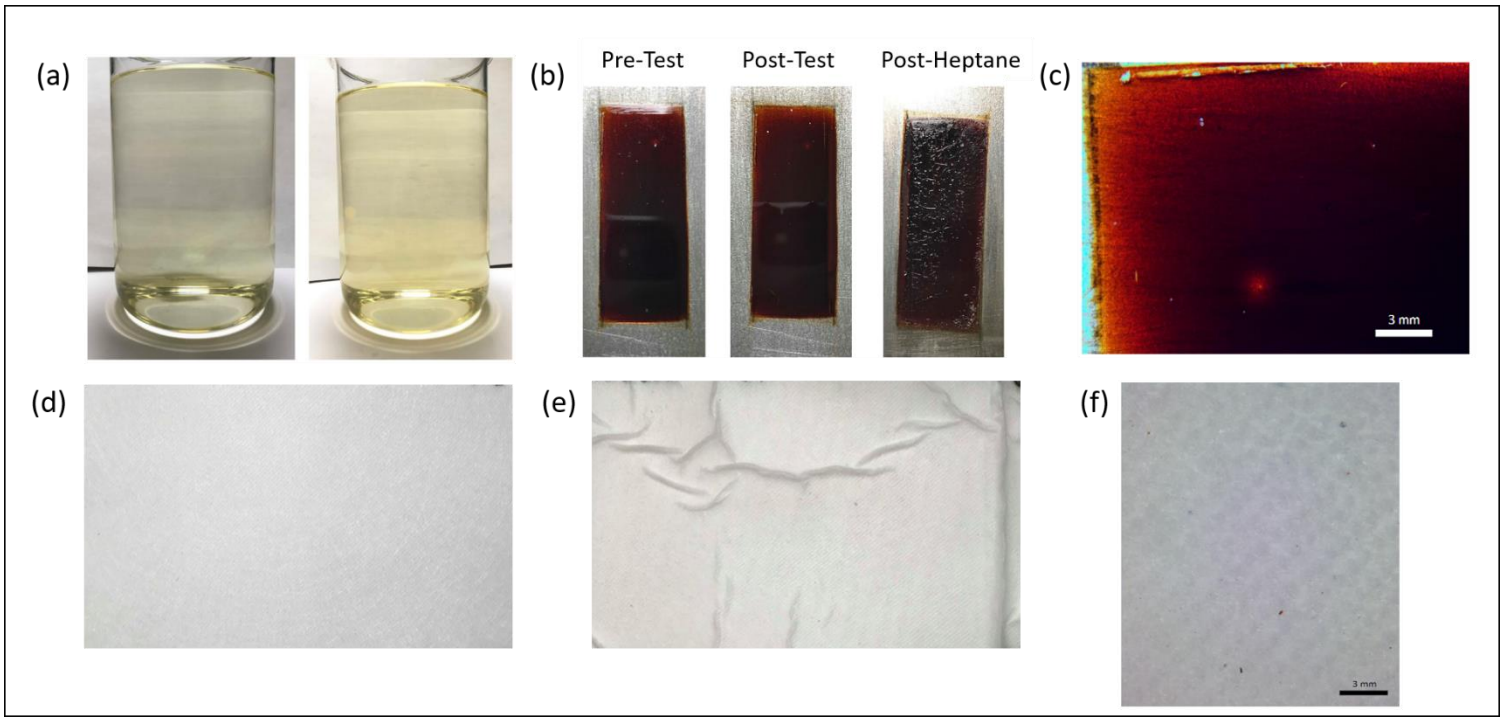

Figure A.19: (a) Pre-Test & Post Test fluid. (b) Pre-Test &Post-Test coupons. (c) Post-Test coupon at 10X magnification.

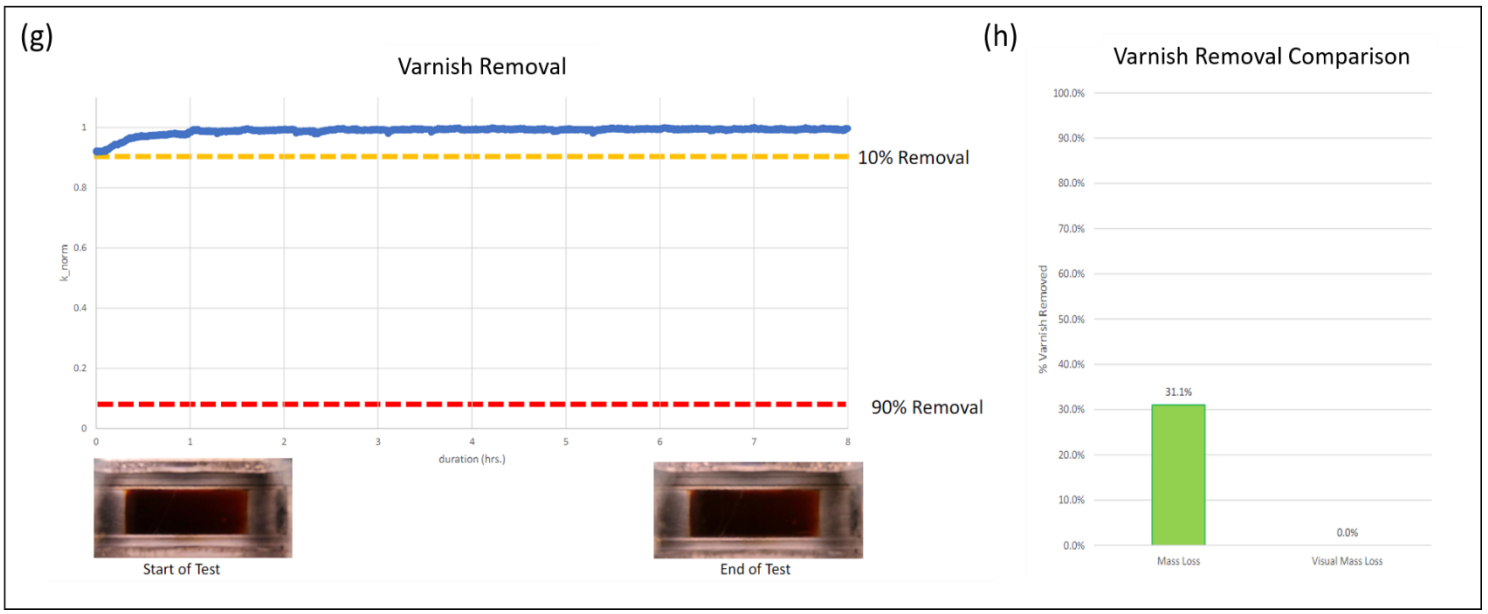

(d) Pre-Test filter untouched by fluid. (e) Post-Test filter. (f) Post-Test filter at 10X magnification.

Figure A.20: Varnish removal data (g) Percent varnish removed vs. time plot. (h) Comparison of visual analysis data and actual measured mass loss.

A.2.8 C8

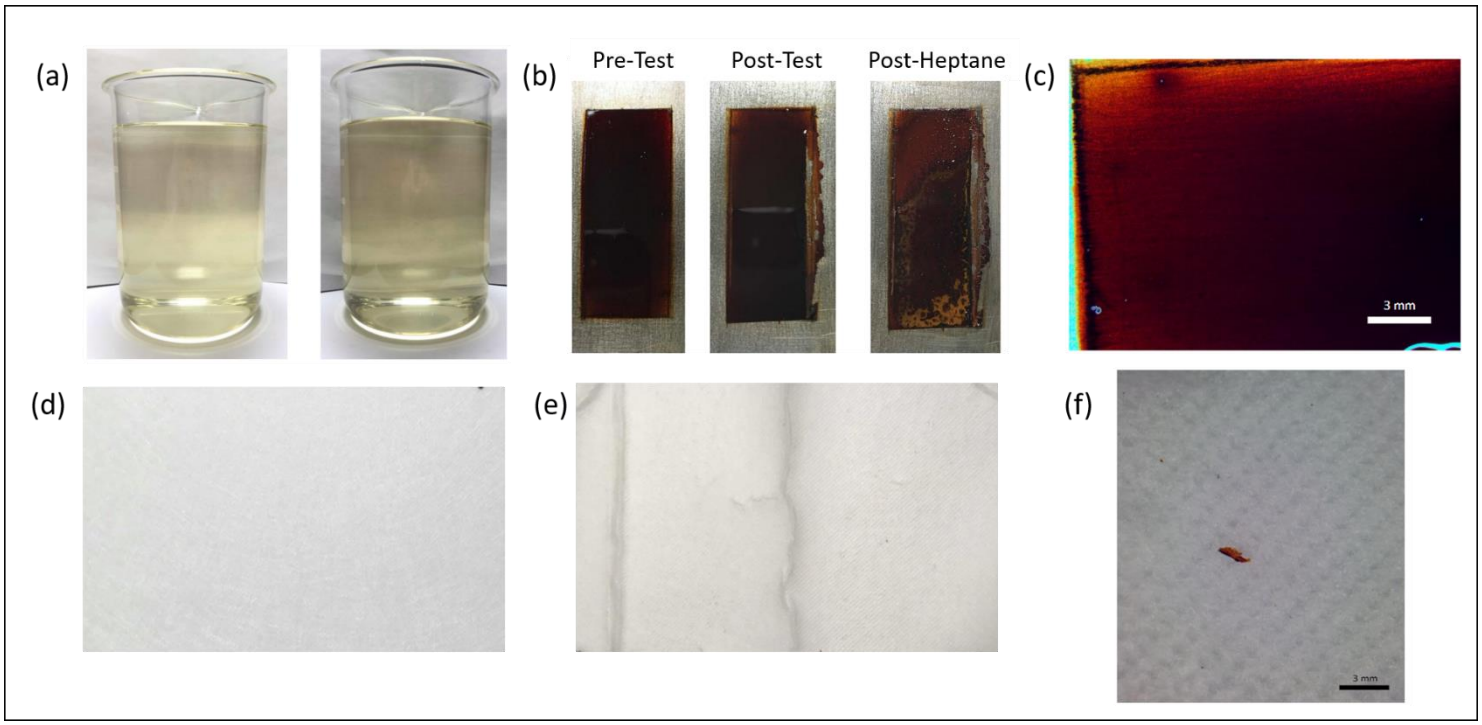

Figure A.21 (a) Pre-Test & Post Test fluid. (b) Pre-Test &Post-Test coupons. (c) Post-Test coupon at 10X magnification. (d) Pre-Test filter untouched by fluid. (e) Post-Test filter. (f) Post-Test filter at 10X magnification.

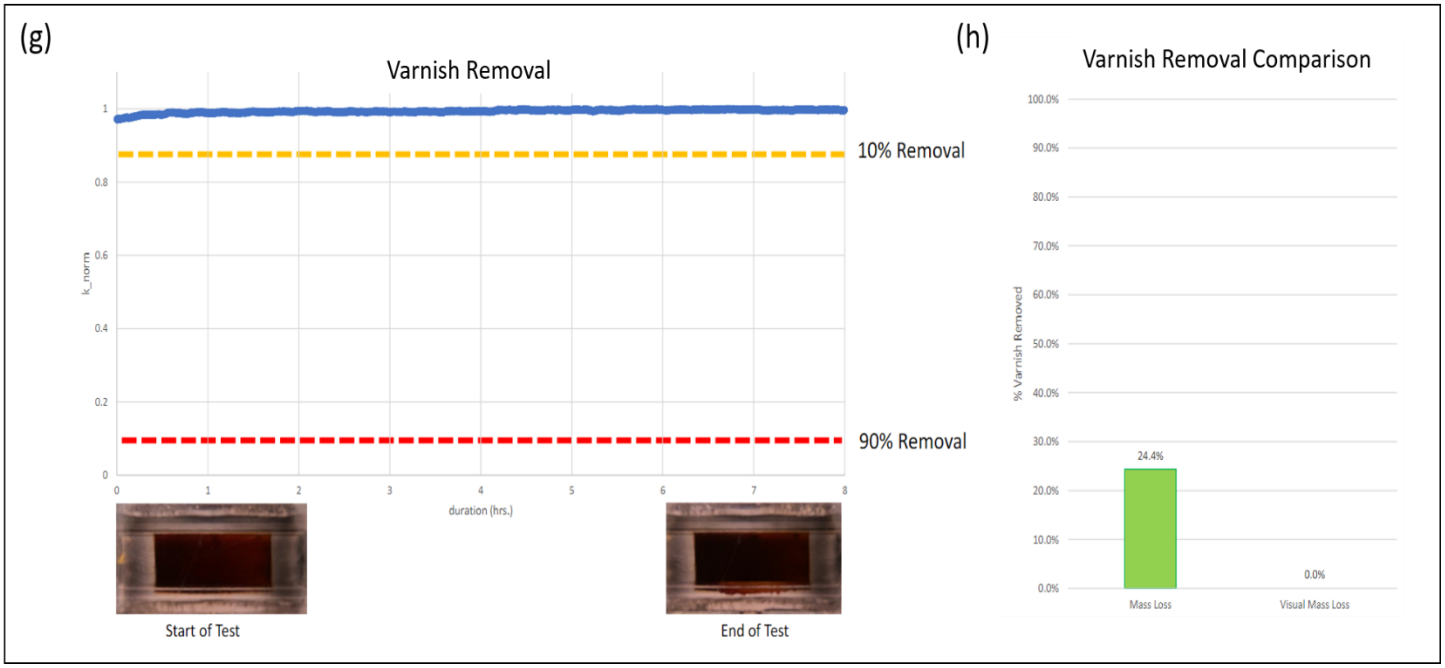

Figure A.22: Varnish removal data (g) Percent varnish removed vs. time plot. (h) Comparison of visual analysis data and actual measured mass loss.

A.2.9 C9

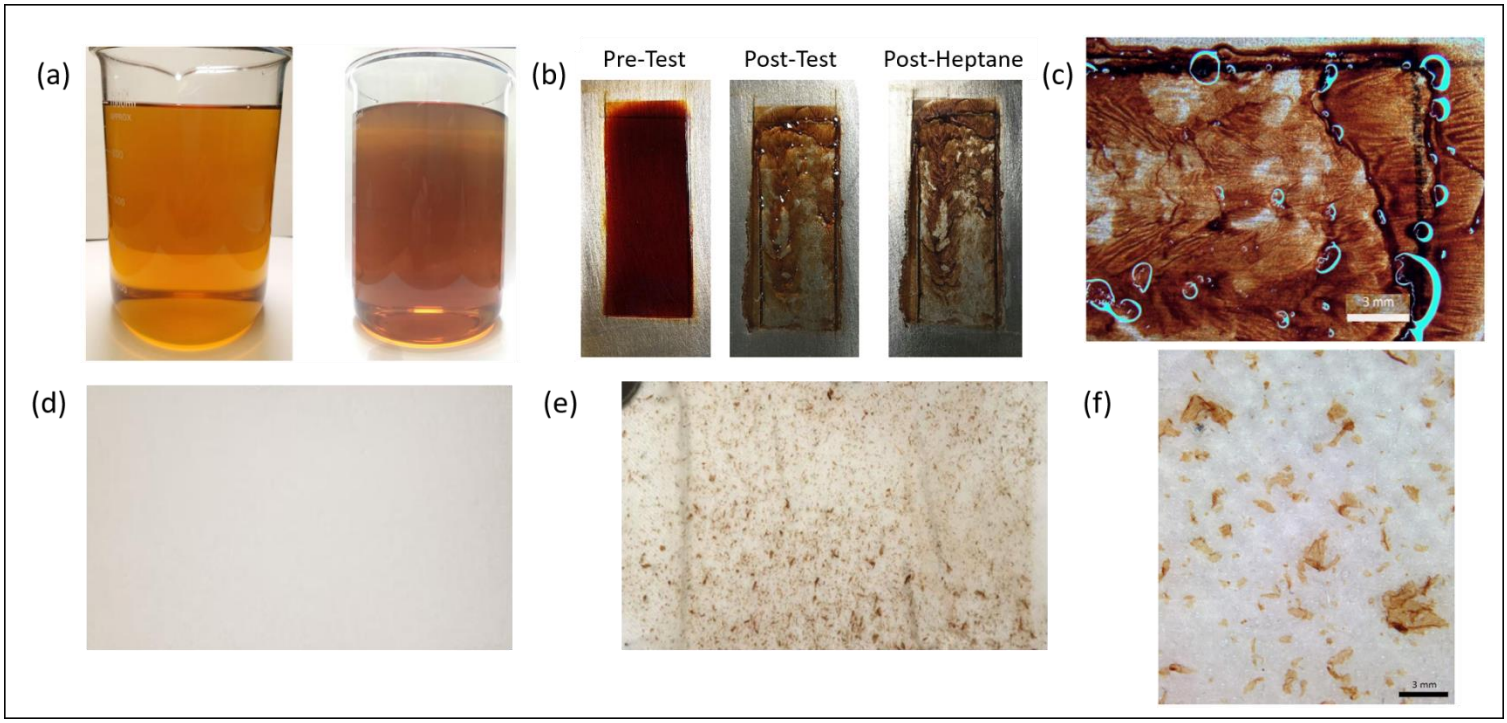

Figure A.23 (a) Pre-Test & Post Test fluid. (b) Pre-Test &Post-Test coupons. (c) Post-Test coupon at 10X magnification. (d) Pre-Test filter untouched by fluid. (e) Post-Test filter. (f) Post-Test filter at 10X magnification.

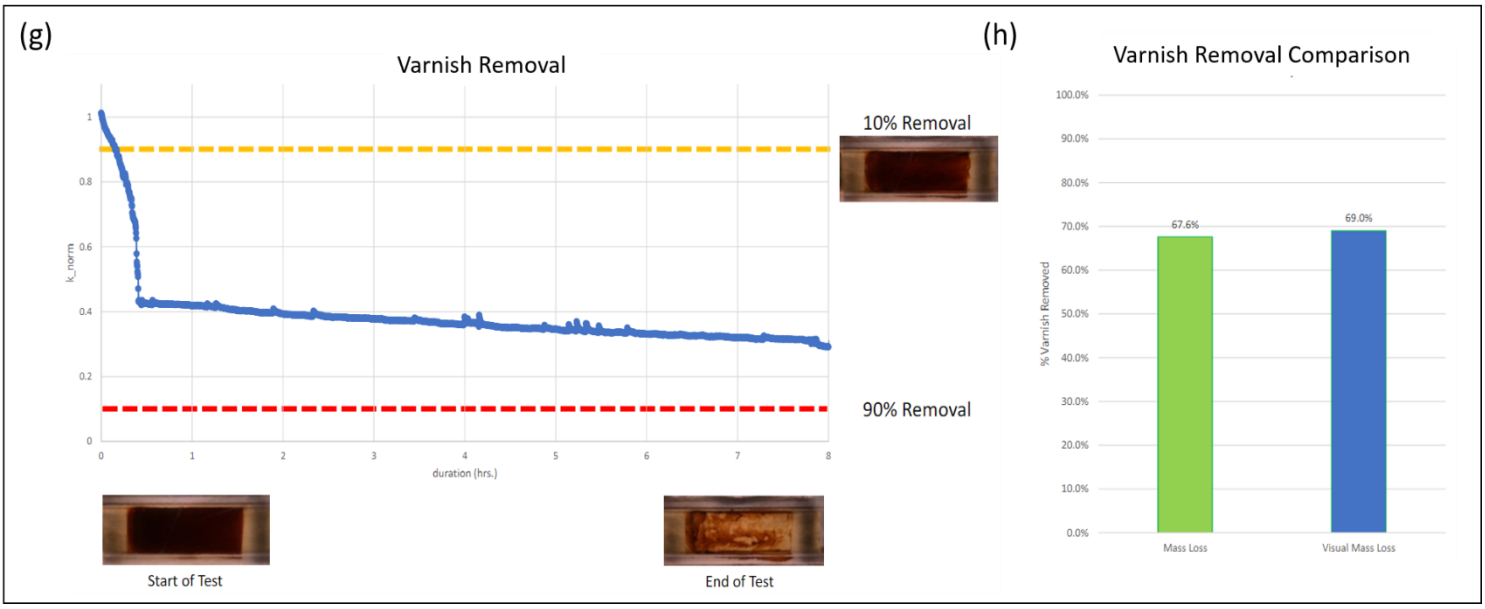

Figure A.24: Varnish removal data (g) Percent varnish removed vs. time plot. (h) Comparison of visual analysis data and actual measured mass loss.